

BUCKLING, POSTBUCKLING AND PROGRESSIVE FAILURE ANALYSES OF
COMPOSITE LAMINATED PLATES UNDER COMPRESSIVE LOADING

A THESIS SUBMITTED TO
THE GRADUATE SCHOOL OF NATURAL AND APPLIED SCIENCES
OF
MIDDLE EAST TECHNICAL UNIVERSITY

BY

ÖMER NAMDAR

IN PARTIAL FULFILLMENT OF THE REQUIREMENTS
FOR
THE DEGREE OF MASTER OF SCIENCE
IN
MECHANICAL ENGINEERING

SEPTEMBER 2012

Approval of the thesis:

**BUCKLING, POSTBUCKLING AND PROGRESSIVE FAILURE ANALYSES
OF COMPOSITE LAMINATED PLATES UNDER COMPRESSIVE
LOADING**

Submitted by **ÖMER NAMDAR** in partial fulfillment of requirements for the degree of **Master of Science in Mechanical Engineering Department, Middle East Technical University** by,

Prof. Dr. Canan ÖZGEN
Dean, Graduate School of **Natural and Applied Sciences** _____

Prof. Dr. Süha ORAL
Head of Department, **Mechanical Engineering** _____

Prof. Dr. Haluk DARENDELİLER
Supervisor, **Mechanical Engineering Dept., METU** _____

Examining Committee Members

Prof. Dr. Mustafa İlhan GÖKLER
Mechanical Engineering Dept., METU _____

Prof. Dr. Haluk DARENDELİLER
Mechanical Engineering Dept., METU _____

Prof. Dr. Can ÇOĞUN
Mechanical Engineering Dept., METU _____

Prof. Dr. Levend PARNAS
Mechanical Engineering Dept., METU _____

Prof. Dr. Yavuz YAMAN
Aerospace Engineering Dept., METU _____

Date: September 10th, 2012

I hereby declare that all information in this document has been obtained and presented in accordance with academic rules and ethical conduct. I also declare that, as required by these rules and conduct, I have fully cited and referenced all material and results that are not original to this work.

Name, Last name : Ömer Namdar

Signature :

ABSTRACT

BUCKLING, POSTBUCKLING AND PROGRESSIVE FAILURE ANALYSES OF COMPOSITE LAMINATED PLATES UNDER COMPRESSIVE LOADING

Namdar, Ömer

M.S., Department of Mechanical Engineering

Supervisor: Prof. Dr. Haluk DARENDELİLER

September 2012, 134 pages

The aim of this thesis is to investigate buckling, post-buckling behaviors and failure characteristics of composite laminated plates under compressive loading with the help of finite element method and experiments. In the finite element analyses, eigen value extraction method is used to determine the critical buckling loads and non-linear Riks and Newton-Raphson methods are employed to obtain post-buckling behaviors and failure loads. The effects of geometric imperfection amplitude on buckling and post-buckling are discussed. Buckling load, post buckling load-displacement relations, out of plane displacements and end shortening of the plates are determined numerically. Furthermore, the numerical results are compared with experimental findings for two different laminates made of woven fabric and uni-directional tapes where buckling, post-buckling behavior and structural failure of laminated plates were determined. The comparisons show that there is a good agreement between numerical and experimental results obtained for buckling load and post-buckling range. However, 15 % - 22 % differences are predicted between the experimental and numerical results for failure of laminates made of woven fabric whereas the laminates with uni-directional tapes show good agreement.

Keywords: Buckling, Post-buckling, Progressive Failure, Composite Structures

ÖZ

BASMA YÜKLEMESİ ALTINDAKİ TABAKALI KOMPOZİT PLAKALARIN BURKULMA, BURKULMA SONRASI VE İLERYEN KIRILMA ANALİZLERİ

Namdar, Ömer

Yüksek Lisans, Makina Mühendisliği Bölümü

Tez Yöneticisi: Prof. Dr. Haluk DARENDELİLER

Eylül 2012, 134 sayfa

Bu tezde basma yüklemesi altındaki tabakalı kompozit plakaların nümerik analizler ve deneyler yardımıyla burkulma, burkulma sonrası davranışları ve kırılma karakteristiklerinin incelenmesi amaçlanmaktadır. Sonlu eleman analizlerinde, özdeğer çıkarma yöntemi kritik burkulma yüklerini belirlemek için, doğrusal olmayan Riks ve Newton-Raphson yöntemleri burkulma sonrası davranışları ve kırılma başlangıcı yüklerini elde etmek için kullanılmışlardır. Geometrik kusur genliğinin burkulma ve burkulma sonrası davranışlara olan etkisi değerlendirilmiştir. Burkulma yükü, burkulma sonrası yük-deplasman ilişkisi, düzlem dışı deplasmanlar, plakaların boyuna kısaltmaları sayısal olarak belirlenmiştir. Buna ek olarak, dokuma kumaş ve tek yönlü tabakalardan yapılmış farklı iki lamina için burkulma, burkulma sonrası davranış ve yapısal kırılmanın tespit edildiği deneysel bulgular sayısal sonuçlarla karşılaştırılmıştır. Karşılaştırmalar burkulma yükü ve burkulma sonrası alan için elde edilen sayısal ve deneysel sonuçlar arasında iyi bir uyum olduğunu göstermektedir. Ancak, tek yönlü tabakalardan yapılmış laminalar iyi uyum gösterirken dokuma kumaştan yapılmış laminaların kırılmasında sayısal ve deneysel sonuçlar arasında 15 % - 22 % farklılıklar öngörülmüştür.

Anahtar kelimeler: Burkulma, Burkulma Sonrası, İlerleyen Kırılma, Kompozit Yapılar

To My Family

ACKNOWLEDGEMENTS

The author wishes to express his heartfelt gratitude to his supervisor Prof. Dr. Haluk DARENDELİLER for his excellent guidance, advices and encouragements throughout the thesis.

The author would like to thank his family, Emine NAMDAR, Hasan NAMDAR, Sabriye NAMDAR and Ahmet Niyazi NAMDAR for their everlasting support, encouragement and patience throughout the research.

The author would like to offer his special thanks to Serdar ÖFKELİ for his help in manufacturing of composite test specimens.

The author would also like to extend his thanks to Servet ŞEHİRLİ and Mehmet ERİLİ for their supports in performing the experiments.

The author would also like to express his appreciation to METU-BILTİR CENTER for their support during manufacturing of test fixture.

The support and cooperation of the author's colleagues and friends is gratefully acknowledged.

TABLE OF CONTENTS

ABSTRACT	iv
ÖZ	v
ACKNOWLEDGEMENTS	vii
TABLE OF CONTENTS	viii
LIST OF FIGURES	xii
LIST OF SYMBOLS AND ABBREVIATIONS	xvii
CHAPTERS	
1. INTRODUCTION	1
1.1 Composite Materials.....	1
1.1.1 Matrices.....	2
1.1.2 Reinforcements	2
1.1.3 Material Forms	3
1.2 Buckling Phenomena.....	4
1.2.1 Stable Symmetric Buckling	5
1.2.2 Unstable Symmetric Buckling	7
1.2.3 Asymmetric Buckling	9
1.3 Scope of the Thesis.....	10
1.4 Outline of the Thesis	11
2. LITERATURE SURVEY	12
3. BUCKLING OF LAMINATES.....	24
3.1 Stress and Stress Variations of a Laminate	24
3.2 Lamina Stress-Strain Behavior.....	26
3.3 Laminate Stresses, Forces and Moments.....	27
3.4 Buckling of a Laminated Plate	31
3.4.1 Buckling of Specially Orthotropic Plates.....	33
3.4.2 Buckling of Symmetric Angle Ply Laminates	35
4. BUCKLING AND PROGRESSIVE FAILURE ANALYSES BY FINITE ELEMENT METHOD	36

4.1	Finite Element Analysis	36
4.2	Instability Analysis.....	37
4.2.1	Eigen value Buckling Prediction (LANCZOS)	38
4.2.2	Postbuckling Analysis.....	38
4.2.3	Newton-Raphson Method by Viscous Damping	41
4.3	Progressive Failure Analysis	43
4.3.1	Hashin's Failure Criteria.....	44
4.3.2	Damage Evolution Procedure	45
4.3.3	Viscous Regularization Scheme.....	49
4.3.4	Determination of the Energies Dissipated due to Failures.....	50
5.	EXPERIMENTS & MATERIALS	58
5.1	Test Fixture.....	58
5.2	Test Specimens.....	65
5.3	Test Equipment and Procedure.....	66
5.4	Mechanical Properties of Materials.....	66
5.5	Stackings of Laminates.....	68
5.6	Curing of Composite Laminates.....	70
5.7	Cure Cycle of Specimens	71
5.8	Cutting of Specimens	72
6.	COMPARISON OF NUMERICAL AND EXPERIMENTAL RESULTS.....	73
6.1	The Finite Element Model.....	73
6.2	Eigenvalue Buckling Results and Comparison of Elements	78
6.3	Numerical Method Comparison	81
6.4	Effect of Initial Geometric Imperfection.....	83
6.5	Comparison of FE Results and Experiments.....	85
7.	EFFECTS OF PLY ANGLE AND THICKNESS ON BUCKLING AND POSTBUCKLING	101
7.1	Variation of Critical Buckling Load with Ply Angle.....	102
7.2	Effects of Thickness and Ply Angle Variation on Buckling Load and Post- buckling Behavior for UD Laminates	103
7.3	Effects of Thickness and Ply Angle Variation on Buckling Load and Post- buckling Behavior for Fabric Laminates.....	114

7.4 Comparisons of Critical Buckling Loads	124
8. CONCLUSIONS.....	127
REFERENCES.....	131

LIST OF TABLES

TABLES

Table 1. Boundary conditions for Finite Strip	51
Table 2. Energies Dissipated due to Failure Modes for UD and Fabric laminae.....	57
Table 3. Summary of Specimen Properties.....	66
Table 4. Mechanical Properties of Prepreg Laminae	67
Table 5. Strength Values of Laminae.....	68
Table 6. Stiffness matrix of UD laminate	69
Table 7. Stiffness matrix of Fabric laminate.....	69
Table 8. Boundary Conditions of Model [39].....	74
Table 9. Critical Buckling Load of Laminates.....	78
Table 10. Failure loads of specimens and differences between FE results.....	97
Table 11. Buckling and failure loads of angle ply $[\theta/-\theta]_S$ UD laminates.....	106
Table 12. Buckling and failure loads of angle ply $[\theta/-\theta]_{2S}$ UD laminates	109
Table 13. Buckling and failure loads of angle ply $[\theta/-\theta]_{4S}$ UD laminates and specimens	113
Table 14. Buckling and failure loads of angle ply $[\theta/-\theta]_S$ Fabric laminates	117
Table 15. Buckling and failure loads of angle ply $[\theta/-\theta/\theta/-\theta/\theta]_S$ Fabric laminates and specimens	121
Table 16. Buckling and failure loads of angle ply $[\theta/-\theta]_{4S}$ Fabric laminates.....	124

LIST OF FIGURES

FIGURES

Figure 1. Typical 2D weave patterns [2].....	4
Figure 2. Flat plate loaded in compression [3].....	5
Figure 3. Stable symmetric equilibrium paths [3].....	6
Figure 4. Unstable symmetric equilibrium paths [3]	8
Figure 5. Cylinder under uniaxial compression [3]	9
Figure 6. Equilibrium paths for asymmetric bifurcation [3].....	10
Figure 7. Un-deformed and deformed cross-section of a laminate under the Kirchhoff assumptions [35]	24
Figure 8. In-Plane Forces on a Flat Laminate	27
Figure 9. Moments on a Flat Laminate	28
Figure 10. Geometry of N layered Laminate	29
Figure 11. Angle-Ply Symmetric Laminate	30
Figure 12. Symmetric and Balanced Laminate	31
Figure 13. Basic simply supported buckling behavior [34]	32
Figure 14. Load-Deformation behavior of Buckled Plate [34]	32
Figure 15. Effect of Initial Imperfection in Buckling [34].....	33
Figure 16. Simply Supported Laminated Rectangular Plate under Uniform Uni-axial Compression [34]	34
Figure 17. Node ordering and Numbering of Integration Points [36]	37
Figure 18. Unstable Static Response [36]	40
Figure 19. Newton-Raphson Method [36]	42
Figure 20. Uni-directions of Lamina [36].....	43
Figure 21. Damage Variable versus Equivalent Displacement [36]	47
Figure 22. Equivalent Stress-Equivalent Displacement Curve [36]	48
Figure 23. Finite Element Model of Finite Strip.....	51
Figure 24. Loading and Ply directions for all Failure Modes	52
Figure 25. Assumption of Dissipated Energy due to Failure	53

Figure 26. Equivalent Stress versus Equivalent Displacement for Fiber Tension of UD Lamina.....	54
Figure 27. Equivalent Stress versus Equivalent Displacement for Fiber Compression of UD Lamina	54
Figure 28. Equivalent Stress versus Equivalent Displacement for Matrix Tension of UD Lamina.....	55
Figure 29. Equivalent Stress versus Equivalent Displacement for Matrix Compression of UD Lamina	55
Figure 30. Equivalent Stress versus Equivalent Displacement for Fiber Tension of Fabric Lamina	56
Figure 31. Equivalent Stress versus Equivalent Displacement for Fiber Compression of Fabric Lamina.....	56
Figure 32. Test Fixture of Thesis Study.....	59
Figure 33. Boundary Conditions of Plate Edges.....	60
Figure 34. Providing co-linearity between Load Actuator and Plate with the help of Test Fixture	61
Figure 35. Knife Edges of Test Fixture.....	62
Figure 36. Panel Geometry and Boundary Conditions	63
Figure 37. The 10 mm gap between L-section blocks and knife edges.....	64
Figure 38. Front view of Test Fixture with Fabric Specimen	65
Figure 39. Temperature versus Time graph of Cure Cycle.....	71
Figure 40. Pressure versus Time graph of Cure Cycle.....	72
Figure 41. Finite Element Model of Laminates	73
Figure 42. Constrained node region and lines on the FE model	75
Figure 43. Unconstraint region in the FE model.....	76
Figure 44. Ply stacking of Fabric laminate	77
Figure 45. Ply stacking of UD laminate.....	77
Figure 46. Out-of-plane displacement shape of UD laminate for the first mode.....	79
Figure 47. Out-of-plane displacement shape of FABRIC laminate for the first mode	79
Figure 48. Load-deformation behavior of UD plates for fully and reduced integration shell elements.....	80

Figure 49. Load-deformation behavior of FABRIC plates for fully and reduced integration shell elements.....	81
Figure 50. Load-deformation behavior of UD plates for Riks and Newton-Raphson Stabilize Methods.....	82
Figure 51. Load-deformation behavior of Fabric plates for Riks and Newton-Raphson Stabilize Methods.....	83
Figure 52. Buckling of UD plates with increasing initial shape imperfections	84
Figure 53. Buckling of FABRIC plates with increasing initial shape imperfections	85
Figure 54. Load versus out-of-plane displacement curves of UD specimens and FEM Results.....	87
Figure 55. Load versus end-shortening displacement curves of UD specimens and FEM Results.....	88
Figure 56. Failure of UD-1 Specimen.....	89
Figure 57. Failure path of UD-1.....	90
Figure 58. First ply failure of UD plate in matrix compression at load step $P=82.979$ kN (Layer 1)	91
Figure 59. Fiber compression failure index with respect to Hashin's criterion at load step of first ply failure (Layer 1).....	92
Figure 60. Matrix compression failure index of UD laminate at load step of first fiber compression failure (Layer 1).....	92
Figure 61. Fiber compression failure index of UD laminate at load step $P=82.932$ kN (Layer 1).....	93
Figure 62. Damage evolution of UD laminate (Layer 1) after failure initiation (left side: matrix compression, right side: fiber compression)	94
Figure 63. Load versus out-of-plane displacement curves of FABRIC specimens and FEM Results.....	95
Figure 64. Load versus end-shortening displacement curves of FABRIC specimens and FEM Results.....	96
Figure 65. First ply failure of fabric laminate in matrix compression at load $P=90.877$ kN (Layer 1)	98
Figure 66. Fiber compression failure index of fabric laminate at load $P=90.877$ kN (Layer 1).....	98

Figure 67. Matrix compression failure index at load $P=91.437\text{ kN}$ (Layer 1).....	99
Figure 68. Fiber compression failure index of fabric laminate at load $P=91.437\text{ kN}$ (Layer 1).....	99
Figure 69. Damage evolution of fabric laminate in Layer 1 after failure initiation (left side: matrix compression, right side: fiber compression)	100
Figure 70. Variation of critical buckling loads of angle ply $[\theta/-\theta]_{4S}$ UD laminates and $[\theta/-\theta/\theta/-\theta/\theta]_S$ Fabric laminates.....	102
Figure 71. Variation of critical buckling loads of angle ply $[\theta/-\theta]_S$, $[\theta/-\theta]_{2S}$, $[\theta/-\theta]_{4S}$ UD laminates.....	103
Figure 72. Load versus out-of-plane displacements of angle ply $[\theta/-\theta]_S$ UD laminates	104
Figure 73. Load versus end-shortening displacements of angle ply $[\theta/-\theta]_S$ UD laminates	105
Figure 74. Load versus out-of-plane displacements of angle ply $[\theta/-\theta]_{2S}$ UD laminates	107
Figure 75. Load versus end-shortening displacements of angle ply $[\theta/-\theta]_{2S}$ UD laminates	108
Figure 76. Load versus Out-of-Plane displacements of angle ply $[\theta/-\theta]_{4S}$ UD laminates	110
Figure 77. Out-of-plane displacement shape of $[45/-45]_{4S}$ UD laminate	111
Figure 78. Out-of-plane displacement shape of $[60/-60]_{4S}$ UD Laminate.....	111
Figure 79. Load versus end-shortening displacements of angle ply $[\theta/-\theta]_{4S}$ UD laminates	112
Figure 80. Variation of critical buckling loads of angle ply $[\theta/-\theta]_S$, $[\theta/-\theta/\theta/-\theta/\theta]_S$, $[\theta/-\theta]_{4S}$ Fabric laminates	114
Figure 81. Load versus out-of-plane displacements of angle ply $[\theta/-\theta]_S$ Fabric laminates	115
Figure 82. Load versus end-shortening displacements of angle ply $[\theta/-\theta]_S$ Fabric laminates	116
Figure 83. Load versus out-of-plane displacements of angle ply $[\theta/-\theta/\theta/-\theta/\theta]_S$ Fabric laminates	118

Figure 84. Out-of-plane displacement shape of $[45/-45/45/-45/45]_S$ Fabric laminate	119
Figure 85. Out-of-plane displacement shape of $[60/-60/60/-60/60]_S$ Fabric laminate	119
Figure 86. Load versus end-shortening displacements of angle ply $[\theta/-\theta/\theta/-\theta/\theta]_S$ Fabric laminates	120
Figure 87. Load versus out-of-plane displacements of angle ply $[\theta/-\theta]_{4S}$ Fabric laminates	122
Figure 88. Load versus end-shortening displacements of angle ply $[\theta/-\theta]_{4S}$ Fabric laminates	123
Figure 89. Variation of critical buckling loads of angle ply $[\theta/-\theta]_S$ UD laminates and $[\theta/-\theta]_S$ Fabric laminates	125
Figure 90. Variation of critical buckling loads of angle ply $[\theta/-\theta]_{2S}$ UD laminates and $[\theta/-\theta/\theta/-\theta/\theta]_S$ Fabric laminates	125
Figure 91. Variation of critical buckling loads of angle ply $[\theta/-\theta]_{4S}$ UD laminates and $[\theta/-\theta]_{4S}$ Fabric laminates	126

LIST OF SYMBOLS AND ABBREVIATIONS

Q_{ij}	: Reduced Stiffness Matrix
T	: Transformation Matrix
A_{ij}	: Extensional Stiffnesses
B_{ij}	: Bending-Extensional Stiffnesses
D_{ij}	: Bending Stiffnesses
δ_w	: Lateral Displacement
P_{ref}	: Reference Load
P_{cr}	: Critical Buckling Load
C_d	: Damaged Elasticity Matrix
d_f	: Fiber Damage Variable
d_m	: Matrix Damage Variable
d_s	: Shear Damage Variable
δ_{eq}^0	: Initial Equivalent Displacement
δ_{eq}^f	: Final Equivalent Displacement
\dot{d}_v	: Viscous Damage Variable
E_{11}	: Longitudinal Young's Modulus
E_{22}	: Transverse Young's Modulus
G_{12}	: In-Plane Shear Modulus
ν_{12}	: Poisson's Ratio
X_T	: Longitudinal Tensile Strength
X_C	: Longitudinal Compression Strength
Y_T	: Transverse Tensile Strength
Y_C	: Transverse Compression Strength
S	: In-Plane Shear Strength

CHAPTER 1

INTRODUCTION

1.1 Composite Materials

The use of composite structures increase gradually in aerospace, automotive and energy industries since composite materials have many advantages like lightweight and high strength characteristics. As a result of that, composite structures are required to analyze to obtain optimum weight and stiffness values. The design criteria which have been specified to attain the structural safety of composite structures must be ensured by the manufacturers. One of these design criteria is buckling for the composite structures.

Investigation of the post-buckling behaviors of the composite panels is an important issue to observe strength and stiffness characteristics of composite materials. When a certain load applied to a plate, buckling may be observed and plate becomes unstable before the stresses on the plate reach to material allowable. Furthermore, post-buckling behavior and material failure at the end of post-buckling should be investigated, if buckling of plate is permissible until to a particular load level.

Composite Materials have been preferred in many parts of structural area instead of metallic materials. The structural performance of a composite material depends on its composition, orientation, fiber shape, matrix and fiber material properties and quantity of bondings between fiber and matrix. There are many different composite material and manufacturing type in the industry and all of these materials have advantages or disadvantages. Composite materials must be chosen by taking into consideration of these advantages or disadvantages in the design phase of structure [1].

The laminates which are produced by combining two or more types of fiber and matrix material for obtaining specific performance requirements are called as hybrid systems. Single fiber-matrix combination is a well accepted configuration for hybrid laminates and prepregs, fabrics, woven roving, chopped fibers can be used to combine hybrid reinforcement [1].

1.1.1 Matrices

Reinforcements are binded together by using matrix material and load is transferred between fibers. Furthermore, environmental moisture, chemical corrosion and oxidation are prevented by matrix material. Also, matrix holds together the fibers and keeps fibers in the proper orientation and position. Organic, metallic, carbon and ceramic materials are used as matrix material in the industry. However, metal, carbon and ceramic matrices have not used as much as organic matrices due to high cost of the applications. Researches and development stages are proceeded but recently they are not widely used in airframe structures [1].

Organic Matrices are divided in to two categories. These are thermosets such as epoxy, polyester, phenolics, bismaleimide, polyimides and thermoplastics such as polyethylene, polystyrene, polypropylene, polyetheretherketone, polyetherimide, polyethersulfone, polyphenylene sulfide [1].

Epoxy resins are the major material for low temperature applications and provide good hot/wet performance, chemical resistance and superior dimensional stability. Matrix material of composite structure is the most widely chosen from epoxy family in the advanced composite industry. Glass, carbon/graphite, aramid, boron and the other reinforcements are held together by using epoxy matrices [1].

1.1.2 Reinforcements

Composite materials consist of matrix and reinforcement materials. Reinforcement materials compose the strength and stiffness characteristics of composite structure.

Reinforcement materials, which are used in the composite industry, can be written as fiberglass, kevlar, polyethylene, carbon/graphite, ceramic fibers [1].

Carbon fibers have high strength and stiffness properties. When carbon fibers are combined an effective matrix material, high performance structures can be obtained. Carbon fiber reinforced composites are stronger and stiffer than the metallic parts which have same weight with carbon fibers. As a result of that, stiff and light-weight structure can be designed by using carbon fiber reinforced composite materials. In addition, carbon fiber composites are available as prepreg, molding compound and the other product forms [1].

1.1.3 Material Forms

Dry or preimpregnated forms of fiber/matrix combinations provide many advantages in design and manufacturing. Also, dry forms do not contain matrix, so, matrix material must be applied to forms during the lay-up process. On the other hand, prepreg forms include matrix material and do not require any extra matrix application [1].

Unidirectional Tapes are preimpregnated laminae which have longitudinal fibers. The mechanical properties of transverse direction are considerably lower than longitudinal properties due to weakness of matrix material. Therefore, fiber orientations of unidirectional laminate should be arranged conscientiously to respond the entire longitudinal and transverse load [1].

Woven Fabrics are expensive pre-forms than the unidirectional tapes but the cost of manufacturing and layup labor requirement decrease the total cost. Furthermore, complex geometry applications and geometric positioning of the woven fabrics are better than the unidirectional tapes. Weave types and number of yarns per area identify the fabrics and several of them can be summarized as unidirectional fabrics, plain weave, twill, satin weave (Figure 1). In unidirectional fabrics, the reinforcement fibers are aligned in one direction and these reinforcement fibers are

held together with the help of tie yarns which are non-structural materials. In plain weave fabrics, the reinforcement warp yarn woven over the one reinforcement fill yarn and this process is repeated consistently. This fabric has considerably stable, less flexible construction and suitable for the flat structures. In satin weave fabrics, the reinforcement warp yarn woven over the several reinforcement fill yarns and this process is repeated. The configuration which one warp yarn woven over four fill yarn and under pone fill yarn is called as 5-harness satin weave. Satin Weaves have high strength characteristics for both material directions [1].

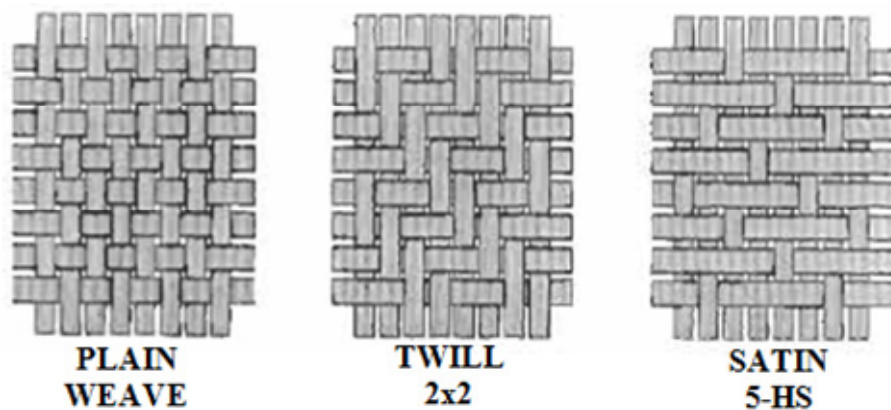


Figure 1. Typical 2D weave patterns [2]

1.2 Buckling Phenomena

The elastic structural stability is defined as the response of the structure under loading and this behavior are expressed in terms of equilibrium paths. Simple structures, under loading, may be defined by a single equilibrium curve but occurrence of many equilibrium paths is possible for the structures which have complex geometries or boundary conditions. For these cases, the critical buckling level can be taken for the point which primary equilibrium path and secondary equilibrium path intersect with each other. When the load is applied to the structure, the primary equilibrium path is observed and it is stable until the bifurcation point is

reached. After the bifurcation point, the structure tries to find new equilibrium path (secondary equilibrium path) since primary equilibrium path has become unstable. Critical buckling load of simple structures (pin-jointed or clamped elastic beam) under compressive loading is determined by using Classical Buckling Theory. However, buckling behavior of complex structures differs with respect to geometries or boundary conditions. These behaviors can be summarized as follows; stable symmetric buckling, unstable symmetric buckling and asymmetric buckling [3].

1.2.1 Stable Symmetric Buckling

In symmetric buckling, the deformation direction of structure, under compressive loading, is unknown. Furthermore, the bifurcation point of the structure, which intersects by secondary equilibrium path, is stable. As shown in Figure 2, simply supported flat plates under compressive load are proper instance to stable symmetric buckling.

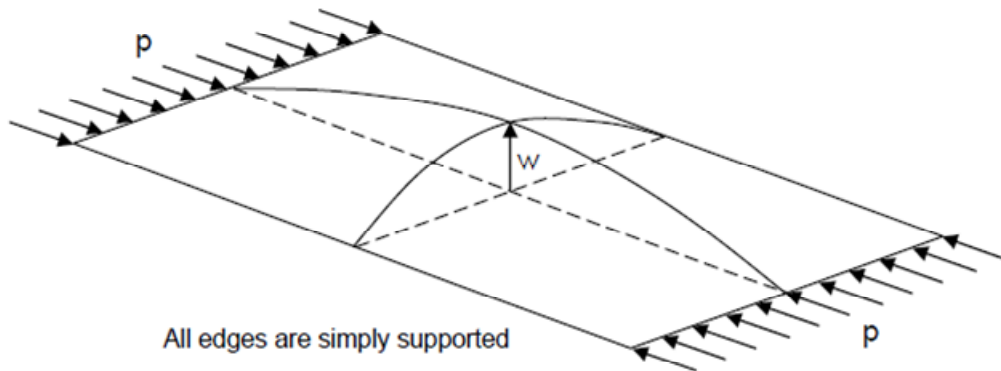


Figure 2. Flat plate loaded in compression [3]

When the load reaches to the critical buckling level, primary equilibrium path becomes unstable and plate starts to deform in accordance with the shape of buckling

mode. After buckling, plate continues to support increasing load at decreased stiffness, so, incremental loading follows secondary equilibrium path as in [3]

Load versus central deflection curve of the simply supported plate under compressive edge loading is shown in Figure 3. Plate can buckle towards the opposite direction. As a result of that, secondary equilibrium path develops for the opposite direction as the symmetric one of the presented path in Figure 3.

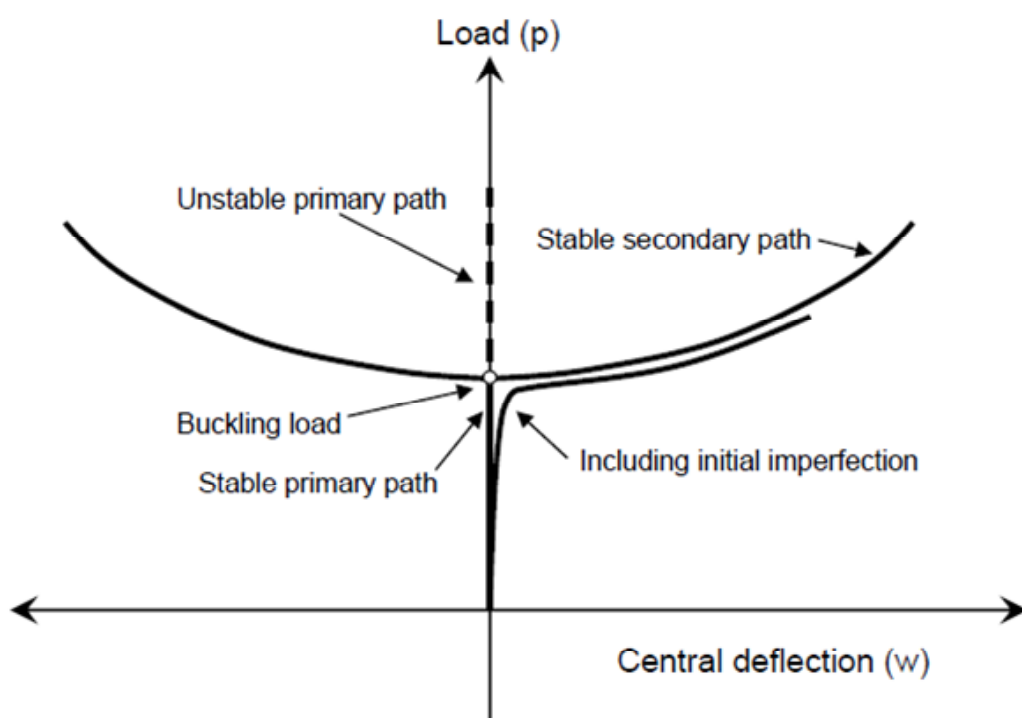


Figure 3. Stable symmetric equilibrium paths [3]

In analytical solutions, flat plates are assumed that they have perfect geometry but in actual case plates include some geometric imperfections originating from manufacturing processes. As shown in Figure 3, sudden bifurcations are observed for the perfect flat plates when the compressive edge load reaches to the critical buckling level however in plates which have initial geometric imperfections the transition

from primary equilibrium path to secondary equilibrium path are smoother than the perfect plates. Furthermore, this smoothness of transition between equilibrium paths increases as the imperfection level of plates increase and initial slope of the load-displacement curve is affected negatively. Therefore, the initial geometric imperfections with small amplitudes as compared to the panel thicknesses are introduced to the finite element models which are used in these analyses [3].

1.2.2 Unstable Symmetric Buckling

In unstable symmetric buckling, it is unknown that the structure, under compressive loading, deforms to which one direction but same buckling shapes and deformation amplitudes are exhibited for either negative or positive buckling directions which are orthogonal to loading direction (Figure 4). For the perfect structures, primary equilibrium path is intersected by a secondary equilibrium path which is unstable. Furthermore, load carrying capacity decreases rapidly and after the bifurcation load versus deflection curve has negative curvature due to instability of secondary equilibrium path unlike stable symmetric buckling [3].

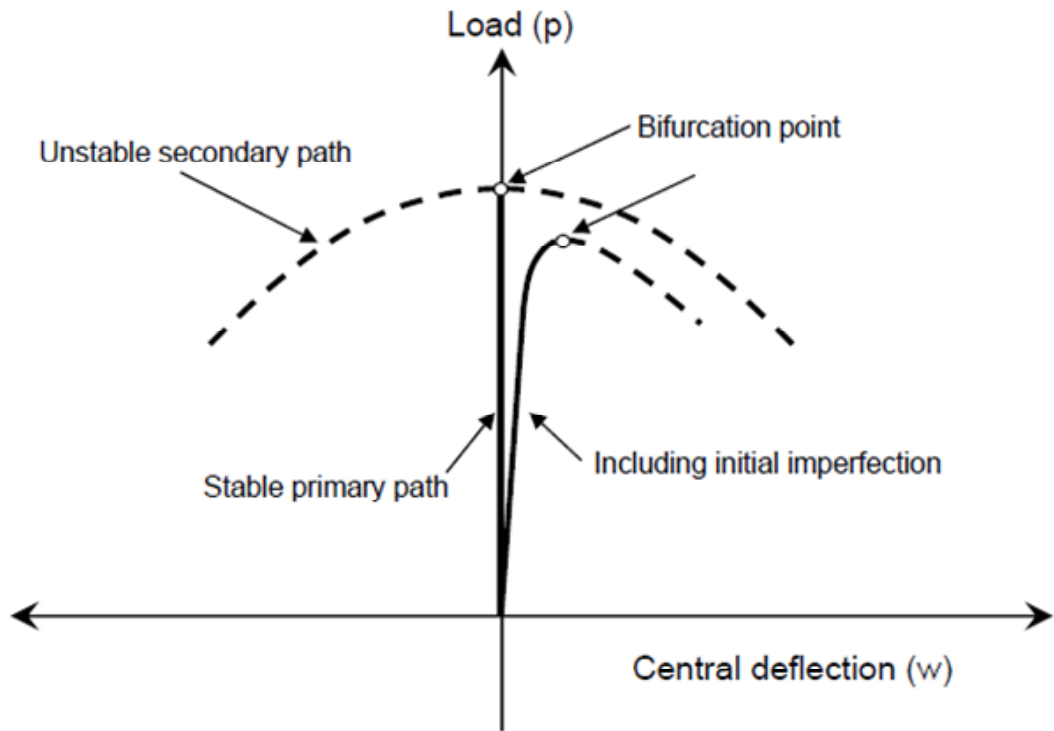


Figure 4. Unstable symmetric equilibrium paths [3]

The effect of imperfections is remarkable for the structure. Unstable symmetric buckling is observed for the cylindrical shells which are loaded uniaxial compressive load [3] (Figure 5).

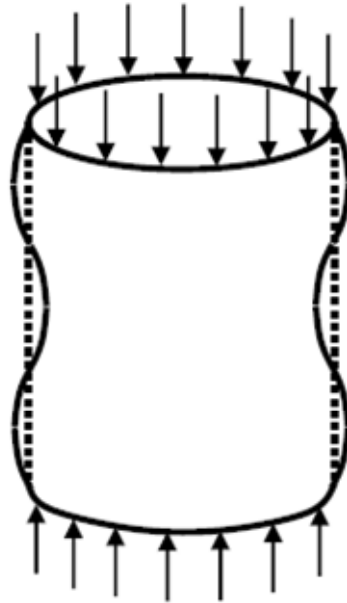


Figure 5. Cylinder under uniaxial compression [3]

1.2.3 Asymmetric Buckling

The structures which have asymmetry in the geometry or loading exhibit asymmetric buckling behavior (Figure 6). That is to say, secondary equilibrium path exhibits unstable or stable behavior in accordance with the buckling direction of structure. Truss structures are proper instance to asymmetric buckling [3].

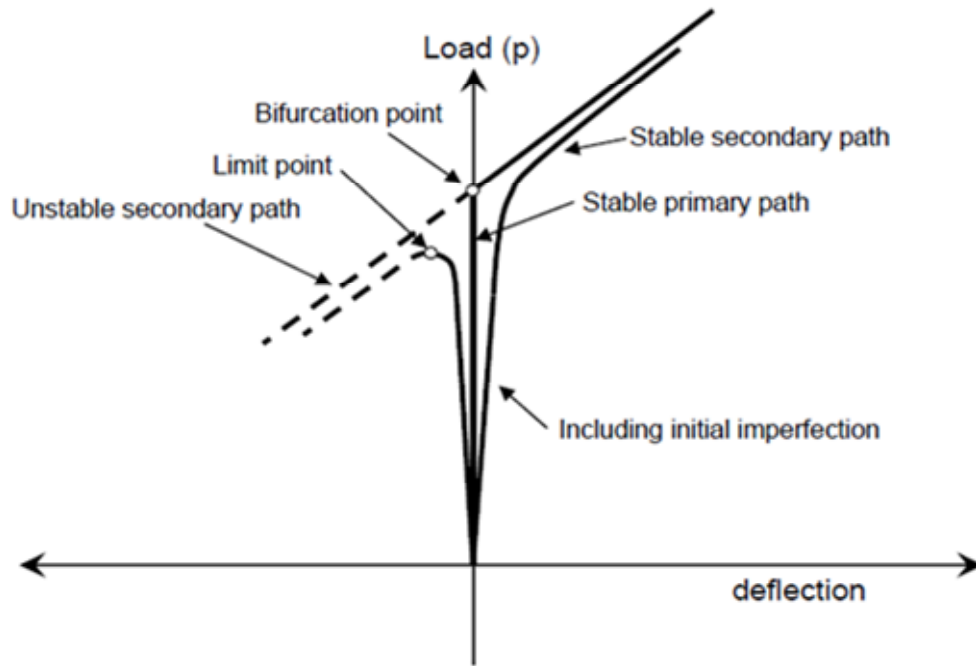


Figure 6. Equilibrium paths for asymmetric bifurcation [3]

1.3 Scope of the Thesis

In this thesis study, buckling, post-buckling and failure characteristics of composite laminated plates made by UD and woven fabric panels under compressive loading have been investigated with numerical analyses and experiments. Finite element analyses have been carried out by using Abaqus v6.10 FEA software. The composite specimens were manufactured by using prepreg forms which consist of thermoset epoxy and carbon/graphite. The specimens have angle-ply symmetric and balanced laminate configuration. Buckling behaviors of the plates are identical with stable symmetric buckling behavior.

1.4 Outline of the Thesis

In Chapter 1, composite materials and buckling phenomena of various structures are introduced.

In Chapter 2, the studies which are related with buckling, post-buckling behaviors and progressive failure analyses of composite laminates are reviewed.

In Chapter 3, analytical solutions of buckling of composite laminated plates are investigated. Furthermore, Classical Lamination Theory, stress-strain relations, forces and moments, specially orthotropic and symmetric angle-ply laminates, mechanical stiffness matrices of composite laminates are presented in this chapter.

In Chapter 4, the methodology of finite element analyses which are performed for buckling, post-buckling and progressive failure analyses is summarized. Eigen value extraction method, non-linear Riks and Newton-Rapson methods are investigated. Furthermore, progressive failure approach and assumption of energies dissipated due to failures are presented.

In Chapter 5, the design and construction of test fixture which is used in experiments is described. Mechanical material properties, dimensions, stacking sequences and curing cycles of test specimens are presented.

In Chapter 6, finite element model, boundary conditions, eigenvalue results, element and method comparisons are presented. The results which are obtained from numerical and experimental findings compared with each other.

In Chapter 7, a number of numerical analyses have been realized to evaluate the effect of ply angle orientations and thicknesses on the composite laminates.

CHAPTER 2

LITERATURE SURVEY

Although the critical buckling loads of the composite materials were investigated extremely, there are a few studies related with the post-buckling behavior and progressive failure analysis of the composite laminates in the literature;

Singh and Kumar [4] performed a study that was related with post-buckling behavior and progressive failure of simply supported symmetric laminates under in-plane shear load with various boundary conditions. A finite element analysis procedure, including first order shear deformation theory and geometric non-linearity, was carried out with the von-Karman sense. Failure of lamina was estimated using 3D Tsai-Hill failure criterion and delamination between two adjacent layers was identified using maximum stress failure criterion. Results showed that the direction of applied shear load, in-plane boundary conditions, ply lay-ups, plate aspect ratios and material properties of lamina effect directly pre-buckling and post-buckling behavior, first-ply failure load, ultimate load and transverse displacements of laminates under in-plane shear load .

Won Kong, Lee, Kim and Hong [5] performed an analytical and experimental study which was related with post-buckling behavior of graphite-epoxy stiffened laminated composite panels under uniaxial compressive load. Non linear finite element method, including progressive failure analysis considering maximum stress criterion, was used in the analysis of panels. Matrix, shear and fiber failures were taken into account in the progressive failure analysis. Out of plane displacements were monitored with the help of Moiré fringe technique and failures were detected by using Piezo-electric film sensors during the experiments. Analytical results, which were obtained from non-linear finite element procedure, were compared with experiments. The results of buckling load, post-buckling behavior and ultimate post-

buckling strength showed overall good performance with the experimental studies. Furthermore, the effects of stacking sequences and stiffener shapes were investigated by means of these parametric studies.

Falzon, Stevens and Davies [6] performed a numerical and experimental study that was related with post-buckling behavior of a blade-stiffened laminated composite panel. Composite blade-stiffened fasteners were analyzed using a new failure mechanism. Failure initiation was observed at the free edge of the post-buckled composite stiffener due to mid-plane delamination. Interlaminar shear stress failure, which was calculated from strain gauge measurements using an approximate analysis based on lamination theory, and observed failure were consistent with each other. The critical shear stress and shear strain that was obtained from three point bending test of the web laminate have been compared with each other. Comparisons showed that the critical shear stress was provided with a good accuracy using approximate analysis based on lamination theory and including edge effects.

Soh, Bian and Chakrabarty [7] developed an approach was related with elastic/plastic buckling analysis of a simply supported anisotropic plate under uniaxial compressive load. Critical buckling loads of carbon epoxy, glass epoxy and boron aluminum plates, called as fiber reinforced composites, were estimated by employing developed theoretical approach. Elastic/plastic theory of composite materials was developed using theory of isotropic materials. Brittle fibrous composites have more complex mechanical behaviors with respect to isotropic materials. Thus, damage in brittle fibrous materials is not suitable for developed theory.

Bisagni [8] analysed buckling and post-buckling behaviors of CFRP cylindrical shells under uniaxial compressive load. Various analysis methods (eigenvalue, non-linear Riks and dynamic analysis) were compared to examine buckling phenomenon. Geometric imperfections were measured using the test specimens and these imperfections were implemented into finite element model. Numerical analyses and experimental results were compared with each other and the effect of imperfect

shape was investigated. The reliability of finite element analyses was correlated with experimental results in the post buckling field.

Loughlan [9] investigated the influence of membrane–flexural coupling on the elastic stability of anti-symmetric angle-ply laminates under compressive loading. Laminates that consist of various ply angles and ply numbers were analyzed to examine effects of the variations of membrane-flexural coupling magnitudes in the laminated composite plates. Finite strip method was used for determination of the coupled compressive buckling solutions. The degree of membrane–flexural coupling decreased because of increasing the ply number in the laminate and plate exhibited orthotropic behavior for the critical stress levels. Ply-angle variation affected sensitively buckling behavior of anti-symmetric angle-ply laminates. Results showed that the optimized ply-angle is less effective in the post-buckling range with respect to post-buckled compressive stiffness.

Caputo, Esposito, Perugini and Santoro [10] performed a numerical and experimental investigation that was related with post-buckling behavior of damaged and undamaged laminated composite skin panels. Damaged model contains impact damage and debonding. The test that was performed for compressive loading up to static failure was observed using transducers and strain gauge for numerical and experimental correlation. Two available commercial finite element softwares were used for numerical approaches that include full transient and static analyses. Numerical and experimental results were compared with each other. Both of ABAQUS and ANSYS analyses showed good performance to predict pre and post-buckling equilibrium paths except some differences on mode jumping phase.

Bisagni and Cordisco [11] performed an experimental study was related with buckling and post buckling behavior of thin walled CFRP shells. Compression and torsion loading were applied separately and in combination by a test equipment using laser scanning system that measures the geometric imperfection for investigating progressive change in deformations. The effect of laminate orientations were identified and results showed that there was no relation between buckling load and

load sequence also, shells can resist to loads in post buckling field without any damage.

Xie and Biggers [12] analyzed post-buckling behavior of composite laminated tailored plates with progressive failure approach. Buckling and ultimate loads of flat and curved plates that have central cutouts were increased using a simple tailoring concept. In-plane restraints on unloaded edges, tailoring and effects of cutouts were investigated and compared with experimental results from literature. Relative improvements were observed on buckling and ultimate load capacities of flat plates with respect to comparisons between tailored and uniform flat plates with the same cutout size. In the curved panels, tailoring concept reduced the sensitivity of imperfections and ultimate loads were greater than the buckling loads unlike the uniform curved panels. Damage initiation locations and damage propagation paths were different in the flat and curved panels. Results showed that tailoring concept provided good improvements on post-buckling behavior, buckling and ultimate load capacity on flat and curved panels.

Camanho, Dávila and Moura [13] proposed a new decohesion element that was capable of crack propagation under mixed-mode loading. The element was placed on interface of solid elements to simulate damage initiation and delamination growth in composite materials. A softening law was implemented into decohesion element in conjunction with a single relative displacement-based damage parameter to pursue the damage state of the elements and to avoid reverting undamaged state of cohesive element during unloading. The inter-laminar fracture toughnesses and strengths were defined using element constitutive equations. The Benzeggagh-Kenane interaction criterion was used to estimate mixed mode delamination propagation. The results, obtained from steady-state delamination growth analysis, were compared with the experimental data. Comparisons between numerical analysis and experiments showed that analysis that was carried out using decohesion element and experimental data agreed well.

Falzon and Hitchings [14] performed an experimental and numerical study which was related with post-buckling behavior of blade-stiffened composite panel under uniaxial compressive load. An unexpected secondary instability was observed during loading afterward initial buckling stage by a dynamic mode shape change. Arc-length-related finite element methods were carried out due to numerical difficulties of standard path-following quasi-static finite element procedures. On the other hand, modified explicit dynamic analysis was presented in this study since difficulties were encountered in arc-length-related highly non-linear analysis. An imperfection, considering 5% of maximum displacement of first eigenvector, was implemented into finite element model. Results showed that estimation of the mode-switch behavior was provided with a good accuracy using modified explicit dynamic analysis.

Hilburger and Starnes Jr. [15] presented an experimental and analytical study which was related with the effect of initial imperfections on the buckling behavior and failure analysis of a thin walled composite cylindrical shell under compressive load. Six different shell-wall laminates two different shell-radius-to-thickness ratios were considered and shell-wall laminates consisted of four different orthotropic laminates and two different quasi-isotropic laminates. Effects of traditional and nontraditional initial imperfections were accounted into numerical analysis. Traditional imperfection consists of geometric mid-surface imperfections and non-traditional imperfections consist of thickness variations, delaminations, loaded edge geometric imperfections, non-uniform applied end loads. Stable, unstable behaviors and material failures were predicted by non linear static, non linear transient and failure analysis. Results showed that a basic generalized imperfection effect of a composite shell can be formulated using considered imperfections; more accurate computations can be carried out using the non linear analysis procedure that is used in this study.

Featherston and Watson [16] performed some tests which were related with buckling behavior of optimized flat fiber reinforced plates were subjected to shear and in plane bending loads and their various combinations. Two side edges of plates were constrained simply supported and other two edges were clamped. Finite element

analyses were carried out to predict buckling behavior since there is no theoretical solution.

Diaconu and Weaver [17] presented an approximation method to analyze post-buckling behavior of infinitely long and un-symmetrically laminated composite plates. Approximate solution was generated by combinations of polynomial transverse displacements that come up with bending due to un-symmetric laminate configurations and a functional representation that was obtained by using Galerkin method for the buckling mode. Non-dimensional parameters were constituted for a simple and clear formulation. The results that were achieved by this solution for uniaxial compressive load along the longitudinal direction were compared with the results that were obtained from non linear FEM analysis for finite length rectangular long plates. Two different simply supported boundary conditions, giving different results, were used in finite element model. Generally, FE analyses over predicted and rarely under predicted the approximate solution with respect to type of considered boundary conditions. Approximate solution that gave average results between two FE analyses was sufficient for initial design purposes.

Falzon and Cerini [18] analyzed behavior of post-buckled composite panels under the influence of mode-jumping using a different finite element procedure. Recent non-linear static finite element procedures that were used in most of finite element codes were investigated and their shortcomings were determined. A quasi-static solution and a pseudo-transient method were combined with each other for constituting more effective approximation. Besides, there was no need to user intervention during the computation process since switching between quasi-static and pseudo-transient method is automated. Arc-length method was used for quasi-static response while a modified explicit dynamic routine was used for pseudo-transient method. Results that were obtained from presented method were compared with experiment and other finite element methods. Comparisons showed that capturing mode jumps were possible using the presented method.

Gal, Levy, Abramovich and Pavsner [19] presented a new simple triangular finite shell element for predicting the buckling behavior of a tested composite panel under uniaxial compressive load. Incremental geometrically non linear analyses were carried out for buckling analysis and tangent stiffness matrices were monitored at each increment. Results were reproduced with respect to an example from the literature and showed good accuracy according to experimental results.

Laurin, Carrere and Maire [20] performed a study that was related with failure of composite laminates. The strengths of quasi-isotropic composite laminates under compressive load were over predicted with respect to current approaches. At first, material multi-scale failure was proposed for different stacking sequences. This model shows failure of laminates which occurs due to material aspects (ply failures without buckling). Secondly, a structural analysis was performed for predicting accurate results under compressive loadings. Buckling loads and post-buckling loads were proposed by a simple method that considers highly non linear material behavior. Results that were produced with respect to these methods showed good agreement with experimental results. Lastly, buckling is not a phenomenon that leads to failure with respect to an application of the present approach on a self-stiffened panel.

Lopes, Camanho, Gürdal and Tatting [21] studied buckling, post-buckling behaviors and progressive failure analysis of composite flat plates that were manufactured by tow placement technology. Tow placement machines are capable to control fiber tows particularly and to place tows onto shape of laminate through recent developments in tow placement technology. Plates that are manufactured by tow placement machines are called as variable stiffness composite panels because of the variation of properties along their surface. High load-carrying capacities of tow-steered panels were identified by the comparison between traditional straight-fiber laminates and tow-steered panels with respect to previous experimental researches. The motivation of paper is to investigate post-buckling, progressive failure and final structural collapse because of fiber or matrix damages. A user-developed subroutine, including continuum damage model, were implemented into ABAQUS FEA

software to simulate damage initiation and stiffness degradation. Non linear static analyses were carried out finite element model including geometric imperfections. The residual thermal stresses, occurring in the curing process, were considered in order to compute the buckling loads of tow-steered panels under compressive edge load. Final failure results were calculated with a small difference between numerical and experimental results. Tow-steered panels have higher strength and damages of them initiates later than straight-fiber laminates.

Camanho, Maimí and Dávila [22] investigated size effects and strengths of notched carbon-epoxy laminates using continuum damage model. Size effects and propagation of fracture process zone were correlated with an experimental program. Material properties and fracture energies were measured at the ply level with respect to standard test methods due to requirements of continuum damage model. The results that were obtained using continuum damage model were compared with the point stress, linear elastic fracture mechanics and strength of materials approaches. Comparisons showed that the continuum damage model predicted size effects of composite laminates subjected to tension with good accuracy. Additionally, continuum damage model provides degradation of the material stiffness during the loading history and it is applicable to analyze general geometries and boundary conditions.

Pevzner, Abramovich and Weller [23] have developed a MATLAB based software code, has called as TEW, that calculates buckling and collapse loads of axially compressed laminated composite stringer-stiffened curved panels. Effective width method that is employed for analysis of isotropic planar stringer-stiffened panels has been adapted to laminated composite stringer-stiffened circular cylindrical panels. Bending buckling, torsional buckling and local buckling of the blade, J-form and T-form stiffeners were investigated using proposed effective width method. Results that were obtained from proposed method were compared with experimental results and with finite element calculations. Proposed method showed good performance with experiments and FE analyses. Furthermore, it can be employed for design and optimization of laminated composite stringer-stiffened curved panels.

Kassapoglou [24] presented a new design concept increasing compression performance of composite plates. Rectangular composite panel that consists of two concentric layups under compressive load has been analyzed using Rayleigh-Ritz approximation. Buckling loads were calculated using energy minimization approach. The results of detailed finite element models and other published finite element solutions were compared with each other and gave good accuracy except panels including twisting-bending coupling since these stiffnesses were not accounted for this method. According to obtained results, much more lightweight panels can be configured by using presented method.

Kere and Lyly [25] studied post-buckling behaviors of CFRP shells under uniaxial compressive load. Computations were carried out using Reissner-Mindlin-Von Karman type shell facet model. The effects of geometric imperfections were implemented into non-linear analyses. Numerical and experimental results were compared with respect to buckling tests found in literature. Results showed that using of diamond shape imperfections gave accurate results with respect to others for CFRP cylindrical shells.

Basu, Waas and Ambur [26] developed an approach that was related with progressive failure analysis of fiber reinforced laminates. Schapery theory was employed to model each of the ply laminate as a non linear elastic degrading based on plane stress assumption. Physics of kink banding that results in micro-buckling and degradation of the axial lamina properties has been taken into account by developed approach. A user defined subroutine that considered fiber micro-buckling and material degradation features was developed and implemented through ABAQUS finite element software. Elastic lamina orthotropic properties, transverse property degradation, ultimate fiber tensile strength of the lamina were identified with laboratory scale and coupon level test data. Flat un-stiffened and notched panels, subjected to axial compression and in-plane shear loading individually, were tested to verify the results that were obtained from finite element analyses. Presented approach showed good performance with respect to comparisons between experiments and numerical solutions.

Bisagni and Walters [27] performed an experimental study that was related with investigation of the damage propagation in flat composite laminates under axial and transverse loadings. A dual actuator testing machine was used to apply axial and transverse loads individually and in combination. Detection of the local displacements, strain fields and damage propagation was carried out using a digital image correlation system. Two test series, consisting two different graphite-epoxy materials, were tested. In the half of specimens, artificial delaminations were generated using teflon films that were inserted into laminate during lay-up for investigating the damage propagation. Results of the experiments were close to the theoretical elliptical curves of the loading interaction. Complex failure initiation and propagation modes were obtained because of loading type and artificial delaminations. Fiber breakages, fiber–matrix shear failures and inter-lamina damages were observed in test specimens.

Liu and Zheng [28] performed progressive failure analysis of composite laminates using continuum damage model. Progressive failure properties of aluminum and carbon fiber/epoxy composite laminates were predicted using energy based stiffness degradation method. Maximum shear stress was taken into consideration for failure criterion of aluminum liner material, Tsai-Wu failure criterion was employed for composite laminates and fiber breakage, matrix cracking, fiber/matrix interface failure were investigated. The arc-length algorithm was developed to carry out progressive failure process using a 3D finite element model. Load-displacement curve and failure strength of laminate that were obtained from presented study were compared with experiments and other existing models. Results showed that the ascendant failure was matrix cracking for composite laminates, rapid increase was noticed in the number of fiber breakage before collapse of structure and any shear failure was not observed in the analysis.

Pineda, Waas, Bednarczyk, Collier and Yarrington [29] presented progressive damage and failure model of fiber reinforced laminated composites. The thermodynamically based Schapery Theory (ST) was employed for investigation of progressive micro damage in matrix failure. Matrix failure was not taken into account using a matrix

failure criterion but it was observed with the evolution of micro-damage. Tensile failure was investigated using maximum strain criterion and compressive failure was taken into account allowing local fiber rotations. Results that were obtained from presented study compared with a model that used Schapery Theory at the lamina level for calculating micro damage. Load versus displacement and local strain results of both model were compared with experimental results of notched laminates under uniaxial tension load. Comparisons showed that presented progressive damage model based on Schapery Theory agreed well with the previous studies.

Meer and Sluys [30] performed progressive failure analysis using continuum damage model and softening plasticity model in composite laminates. In continuum damage model, elastic stiffness of material was decreased gradually after stress components reached allowable values of material. Strains were separated into elastic and plastic parts and plastic strains employed to reduce the strength of the material in softening plasticity model. Mesh dependency was investigated by introducing viscosity term for both failure models. Matrix failures were observed along a finite width that was independent of the element size. Values of viscosities were determined hardly due to complexity of viscosity parameter. Furthermore, continuum damage model showed good performance under the well influence of viscous regularization.

Wagner and Balzani [31] analyzed post-buckling response of composite laminated panels including progressive ply failure. A numerical model, including failure modes fiber fracture, matrix cracking, and fiber–matrix debonding, was used for investigation of post-buckling behavior of the panel. Brittle degradation model was carried out to consider material nonlinearity when damage was detected within a ply by applied failure criterions. Green strains and second Piola–Kirchhoff stresses were employed to take into account geometrical nonlinearity. Numerical results were compared with the experiments for validation of the presented model. Global behavior, amplitudes of the radial displacement and buckling shape of the axially compressed panel were agreed well with the experimental results. Skin-stringer debonding was observed in the experiment differently from numerical model.

Vescovini and Bisagni [32] studied post-buckling analysis of composite panels with elastic restraints under uniaxial compressive load using single-mode solution. The responses of stiffened panels under the influence of local buckling modes were investigated using closed-form solution that takes into account rotational restraints of skin edges due to stiffeners. Marguerre type equations and classical lamination theory were implemented on the panels that are modeled as thin plates. The problem that was defined with a single-mode approximation was expressed in terms of out of plane displacements and Airy stress function. Buckling loads, out of plane displacements and post-buckling behaviors of composite panels were achieved using closed-form solution and compared with finite element solutions. Results that were derived using closed-form solution showed good accuracy with respect to comparisons between the approach and finite element analyses.

Romanowicz [33] presented a numerical approach based on the finite element model that predicted failure of fiber reinforced composites subjected to combined transverse compression and axial tension. Fiber breakage, fiber/matrix debonding and matrix plastic deformation were investigated with respect to constitutive equations. Another feature of presented study is that fracture allowables of the interface and constituent materials influence unidirectional composite failures. Furthermore, proposed micromechanics model determines mechanical behaviors and failures of composites for various biaxial loadings. Results that were obtained from micromechanics approach were compared with analytical data and experimental results that were found in literature. Numerical calculations showed good performance with respect to comparisons between micromechanics model and experimental results.

CHAPTER 3

BUCKLING OF LAMINATES

Buckling analyses have been carried out using Classical Lamination Theory that consists of stress-strain relationships. Challenging 3-D elastic problems can be solved appropriate displacement assumptions and CLT.

3.1 Stress and Stress Variations of a Laminate

As shown in Figure 7, Kirchhoff hypothesis is used for plates on the laminate translational displacements with respect to a specified coordinate system by use of the laminate cross section in the x-z plane [34].

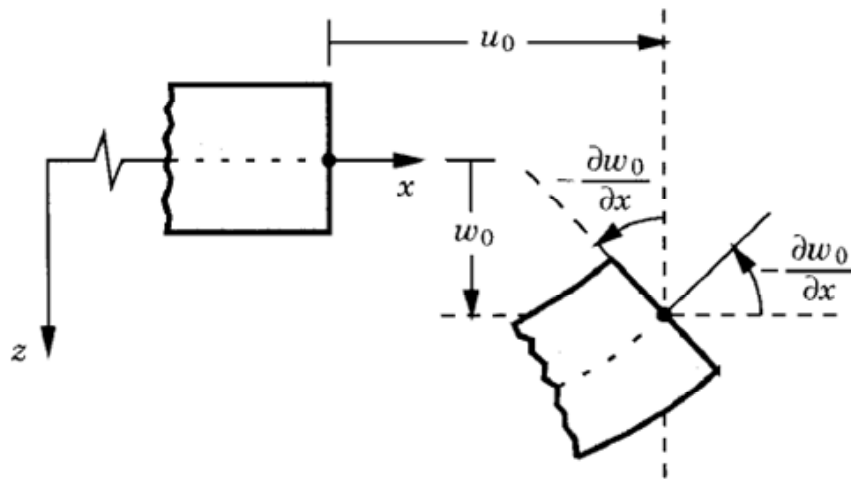


Figure 7. Un-deformed and deformed cross-section of a laminate under the Kirchhoff assumptions [35]

The displacement formulas on x and y direction can be written as follows [34];

$$u = u_0 - z \frac{\partial w_0}{\partial x} \quad (3.1)$$

$$v = v_0 - z \frac{\partial w_0}{\partial y} \quad (3.2)$$

$$w = w_0 \quad (3.3)$$

where u_0 , v_0 and w_0 are the displacements of a point on the surface. When derived displacement equations and linear elastic strain equations have been combined with each other, strain equations of a laminate are obtained [34].

$$\varepsilon_x = \frac{\partial u_0}{\partial x} - z \frac{\partial^2 w_0}{\partial x^2} \quad (3.4)$$

$$\varepsilon_y = \frac{\partial v_0}{\partial y} - z \frac{\partial^2 w_0}{\partial y^2} \quad (3.5)$$

$$\gamma_{xy} = \frac{\partial u_0}{\partial y} + \frac{\partial v_0}{\partial x} - 2z \frac{\partial^2 w_0}{\partial x \partial y} \quad (3.6)$$

or in matrix form;

$$\begin{bmatrix} \varepsilon_x \\ \varepsilon_y \\ \varepsilon_{xy} \end{bmatrix} = \begin{bmatrix} \varepsilon_x^0 \\ \varepsilon_y^0 \\ \gamma_{xy}^0 \end{bmatrix} + z \begin{bmatrix} \kappa_x \\ \kappa_y \\ \kappa_{xy} \end{bmatrix} \quad (3.7)$$

The transverse strains γ_{xz} and γ_{yz} are zero due to Kirchhoff assumption. The mid-surface strains are [34];

$$\begin{bmatrix} \varepsilon_x^0 \\ \varepsilon_y^0 \\ \gamma_{xy}^0 \end{bmatrix} = \begin{bmatrix} \frac{\partial u_0}{\partial x} \\ \frac{\partial v_0}{\partial y} \\ \frac{\partial u_0}{\partial y} + \frac{\partial v_0}{\partial x} \end{bmatrix} \quad (3.8)$$

The mid-surface curvatures are [34];

$$\begin{bmatrix} \kappa_x \\ \kappa_y \\ \kappa_{xy} \end{bmatrix} = - \begin{bmatrix} \frac{\partial^2 w_0}{\partial x^2} \\ \frac{\partial^2 w_0}{\partial y^2} \\ 2z \frac{\partial^2 w_0}{\partial x \partial y} \end{bmatrix} \quad (3.9)$$

3.2 Lamina Stress-Strain Behavior

Stress-strain relations of orthotropic lamina under plane stress condition given below [34];

$$\begin{bmatrix} \sigma_1 \\ \sigma_2 \\ \tau_{12} \end{bmatrix} = \begin{bmatrix} Q_{11} & Q_{12} & 0 \\ Q_{12} & Q_{22} & 0 \\ 0 & 0 & Q_{66} \end{bmatrix} \begin{bmatrix} \varepsilon_1 \\ \varepsilon_2 \\ \gamma_{12} \end{bmatrix} \quad (3.10)$$

Q_{ij} 's are called as reduced stiffnesses that have been composed using components of compliance and stiffness matrices. Reduced stiffnesses can be written in terms of engineering constants [34];

$$\begin{aligned} Q_{11} &= \frac{E_{11}}{1 - \nu_{12}\nu_{21}} & Q_{22} &= \frac{E_{22}}{1 - \nu_{12}\nu_{21}} \\ Q_{12} &= \frac{\nu_{12}E_{22}}{1 - \nu_{12}\nu_{21}} = \frac{\nu_{21}E_{11}}{1 - \nu_{12}\nu_{21}} & Q_{66} &= G_{12} \end{aligned} \quad (3.11)$$

Transformed reduced stiffnesses with respect to any coordinate system are given below [34];

$$\begin{bmatrix} \sigma_x \\ \sigma_y \\ \tau_{xy} \end{bmatrix} = \begin{bmatrix} \bar{Q}_{11} & \bar{Q}_{12} & 0 \\ \bar{Q}_{12} & \bar{Q}_{22} & 0 \\ 0 & 0 & \bar{Q}_{66} \end{bmatrix} \begin{bmatrix} \varepsilon_x \\ \varepsilon_y \\ \gamma_{xy} \end{bmatrix} \quad (3.12)$$

where;

$$[\bar{Q}] = [T][Q][T]^T \quad (3.13)$$

$[T]$ is the transformation matrix for a particular rotation about a transverse normal to the lamina.

3.3 Laminate Stresses, Forces and Moments

Force and moment components acting on a flat laminate can be shown as in Figure 8 and Figure 9;

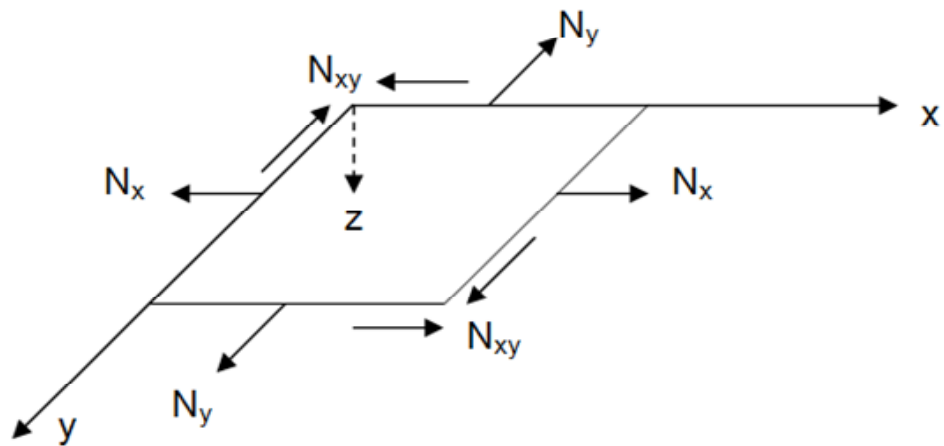


Figure 8. In-Plane Forces on a Flat Laminate

According to CLT, stresses in the k^{th} layer can be determined by using stiffness equations, middle surface strains and middle surface curvatures [34].

$$\begin{bmatrix} \sigma_x \\ \sigma_y \\ \tau_{xy} \end{bmatrix} = \begin{bmatrix} \bar{Q}_{11} & \bar{Q}_{12} & 0 \\ \bar{Q}_{12} & \bar{Q}_{22} & 0 \\ 0 & 0 & \bar{Q}_{66} \end{bmatrix} \begin{bmatrix} \varepsilon_x^0 \\ \varepsilon_y^0 \\ \gamma_{xy}^0 \end{bmatrix} + z \begin{bmatrix} \kappa_x \\ \kappa_y \\ \kappa_{xy} \end{bmatrix} \quad (3.14)$$

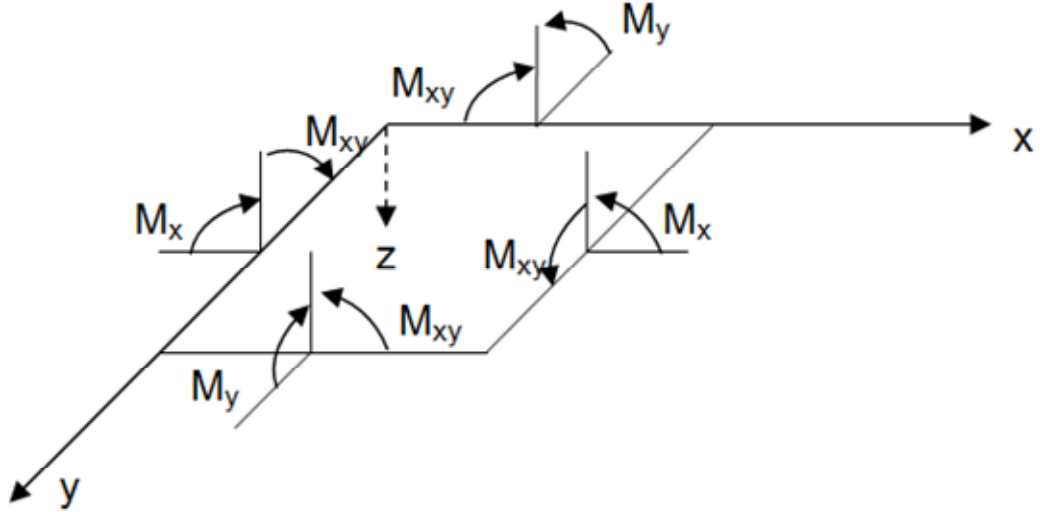


Figure 9. Moments on a Flat Laminate

Loads and moments that are applied onto a laminate can be found by integration of the stresses on each layer of laminate through the thickness. Load and moment formulas of N-layered laminate [34] (Figure 10);

$$\begin{bmatrix} N_x \\ N_y \\ N_{xy} \end{bmatrix} = \int_{-t/2}^{t/2} \begin{bmatrix} \sigma_x \\ \sigma_y \\ \tau_{xy} \end{bmatrix} dz = \sum_{k=1}^N \int_{z_{k-1}}^{z_k} \begin{bmatrix} \sigma_x \\ \sigma_y \\ \tau_{xy} \end{bmatrix}_k dz \quad (3.15)$$

$$\begin{bmatrix} M_x \\ M_y \\ M_{xy} \end{bmatrix} = \int_{-t/2}^{t/2} \begin{bmatrix} \sigma_x \\ \sigma_y \\ \tau_{xy} \end{bmatrix} z dz = \sum_{k=1}^N \int_{z_{k-1}}^{z_k} \begin{bmatrix} \sigma_x \\ \sigma_y \\ \tau_{xy} \end{bmatrix}_k z dz \quad (3.16)$$

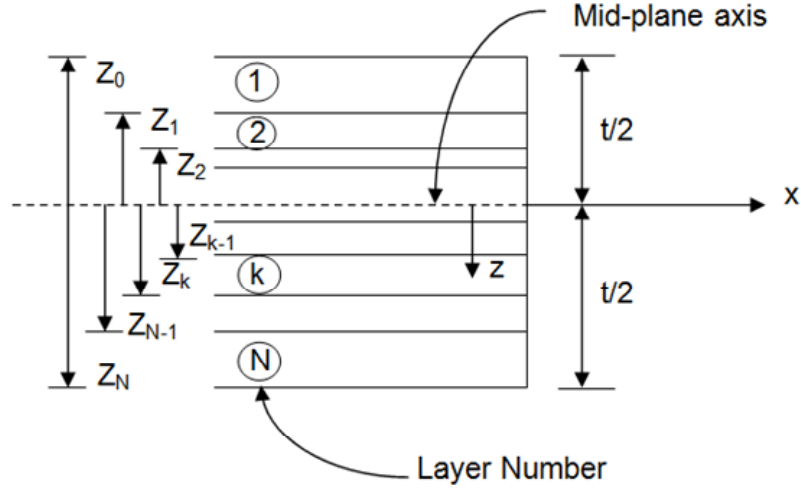


Figure 10. Geometry of N layered Laminate

When the transformed reduced stiffness matrices are combined with load and moment formulas, the following relations are obtained [34].

$$\begin{bmatrix} N_x \\ N_y \\ N_{xy} \end{bmatrix} = \begin{bmatrix} A_{11} & A_{12} & A_{16} \\ A_{12} & A_{22} & A_{26} \\ A_{16} & A_{26} & A_{66} \end{bmatrix} \begin{bmatrix} \varepsilon_x^0 \\ \varepsilon_y^0 \\ \gamma_{xy}^0 \end{bmatrix} + \begin{bmatrix} B_{11} & B_{12} & B_{16} \\ B_{12} & B_{22} & B_{26} \\ B_{16} & B_{26} & B_{66} \end{bmatrix} \begin{bmatrix} \kappa_x \\ \kappa_y \\ \kappa_{xy} \end{bmatrix} \quad (3.17)$$

$$\begin{bmatrix} M_x \\ M_y \\ M_{xy} \end{bmatrix} = \begin{bmatrix} B_{11} & B_{12} & B_{16} \\ B_{12} & B_{22} & B_{26} \\ B_{16} & B_{26} & B_{66} \end{bmatrix} \begin{bmatrix} \varepsilon_x^0 \\ \varepsilon_y^0 \\ \gamma_{xy}^0 \end{bmatrix} + \begin{bmatrix} D_{11} & D_{12} & D_{16} \\ D_{12} & D_{22} & D_{26} \\ D_{16} & D_{26} & D_{66} \end{bmatrix} \begin{bmatrix} \kappa_x \\ \kappa_y \\ \kappa_{xy} \end{bmatrix} \quad (3.18)$$

where;

$$\begin{aligned} A_{ij} &= \sum_{k=1}^N (\bar{Q}_{ij})_k (z_k - z_{k-1}) \\ B_{ij} &= \frac{1}{2} \sum_{k=1}^N (\bar{Q}_{ij})_k (z_k^2 - z_{k-1}^2) \\ D_{ij} &= \frac{1}{3} \sum_{k=1}^N (\bar{Q}_{ij})_k (z_k^3 - z_{k-1}^3) \end{aligned} \quad (3.19)$$

A_{ij} are extensional stiffnesses, B_{ij} are bending-extension coupling stiffnesses and D_{ij} are bending stiffnesses in equations given in 3.19. A_{16} and A_{26} are related with shear-extension coupling and D_{16} and D_{26} are related to bend-twist coupling. Bending-extension coupling stiffness defines the occurrence of forces and moments simultaneously even if laminate is under uniaxial loading. Hence, when an extensional load is applied to a laminate that has B_{ij} stiffnesses, not only extensional deformations occur but also bending and twisting deformations take place [34].

Emergence of coupling stiffnesses differs with respect to composite lay-up configurations. Symmetric laminate is the composite material where plies of laminate are a mirror image about the geometrical mid-plane [34]. Example of symmetric laminate stacking sequence can be shown in Figure 11;

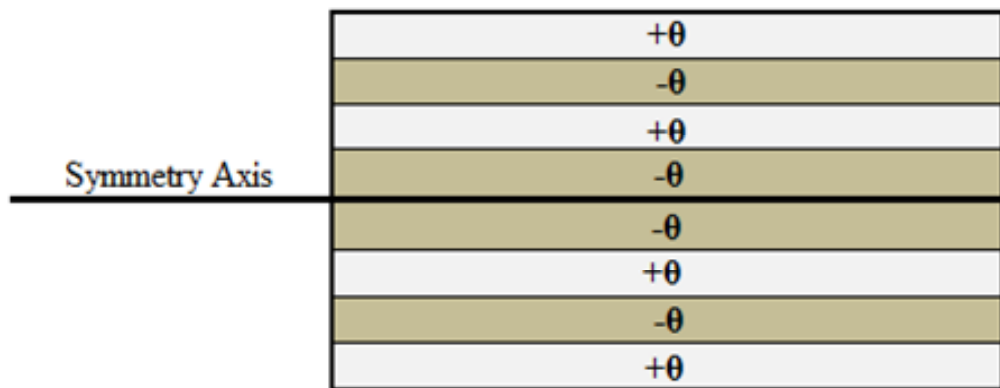


Figure 11. Angle-Ply Symmetric Laminate

Balanced laminate is defined when for each $+\theta$ ply in the lamina there is an equally thick $-\theta$ ply in the laminate excluding 0 and 90 degree plies with same material properties [34]. To obtain an in-plane orthotropic material behavior, laminate should be balanced. A balanced laminate example is given in Figure 12;

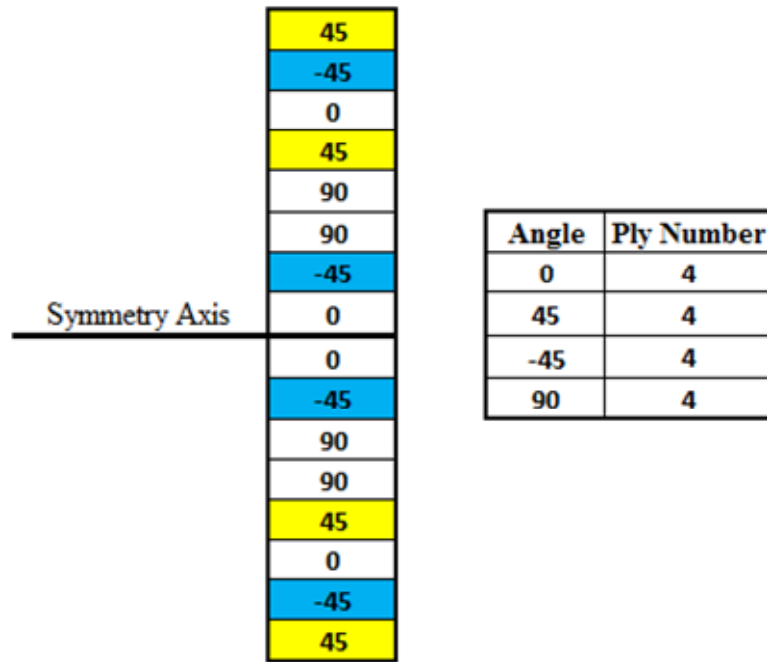


Figure 12. Symmetric and Balanced Laminate

Symmetric, balanced or unsymmetrical laminate configurations effect macro mechanical behavior of laminate directly. The behavior of bending or buckling differs with respect to a laminate that is balanced, symmetric or unsymmetrical.

3.4 Buckling of a Laminated Plate

When buckling develops on a composite laminated plate, the out of plane deformations occur with respect to transverse direction of the laminate as shown in Figure 13. These deformations are observed in the shape of sine waves. Furthermore, number of sine waves increase or decrease with respect to plate length in the load direction and plate geometry, boundary conditions, bending and coupling stiffnesses effect substantially buckling behavior and deformations [34].

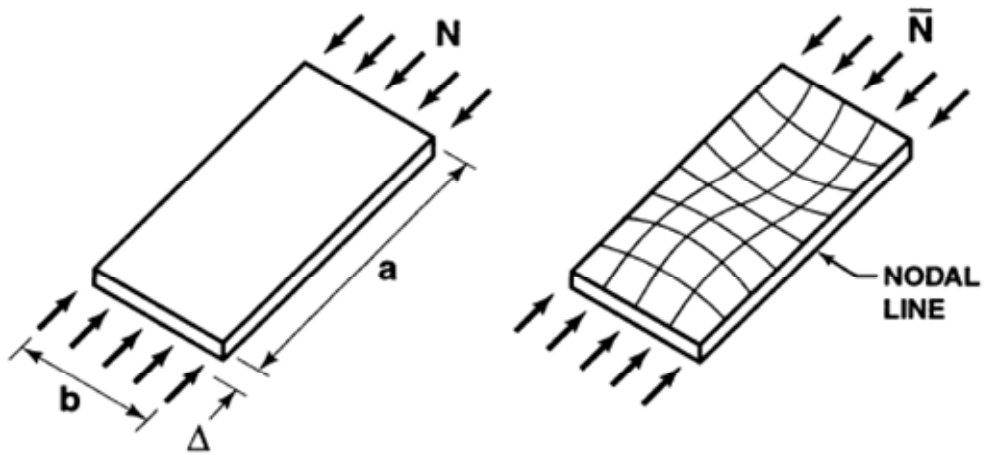


Figure 13. Basic simply supported buckling behavior [34]

The load deformation behaviors of composite plates are different than columns. At first, the loaded plate shortens in load direction and buckles at critical buckling level. After critical buckling load level, plate deformation bifurcates from flat to buckled shape [34]. However, plate continues to resist increased load but it has low stiffness due to buckled shape as shown in Figure 14.

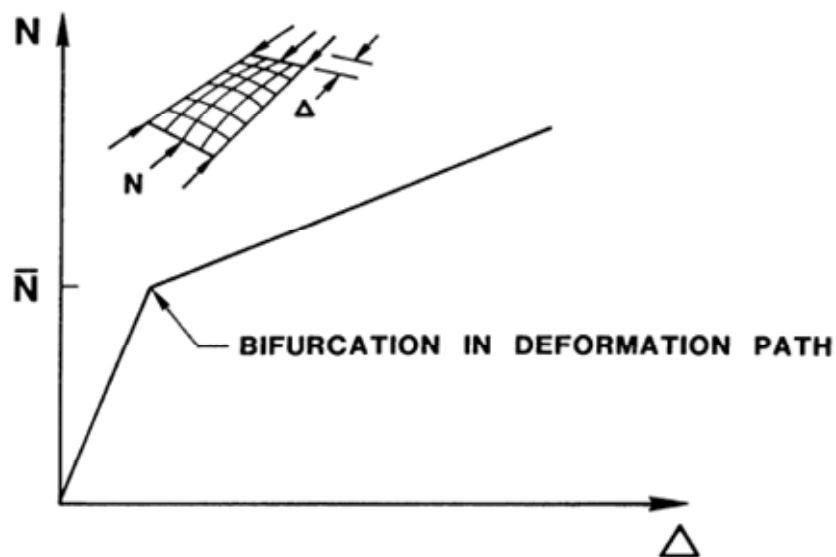


Figure 14. Load-Deformation behavior of Buckled Plate [34]

Initial imperfections change buckling behavior of composite laminated plates. The transition from flat to buckled shape is too sharp in the load deformation curve for a perfect flat plate but this sharp transition becomes smoother with increasing initial imperfections as shown in Figure 15.

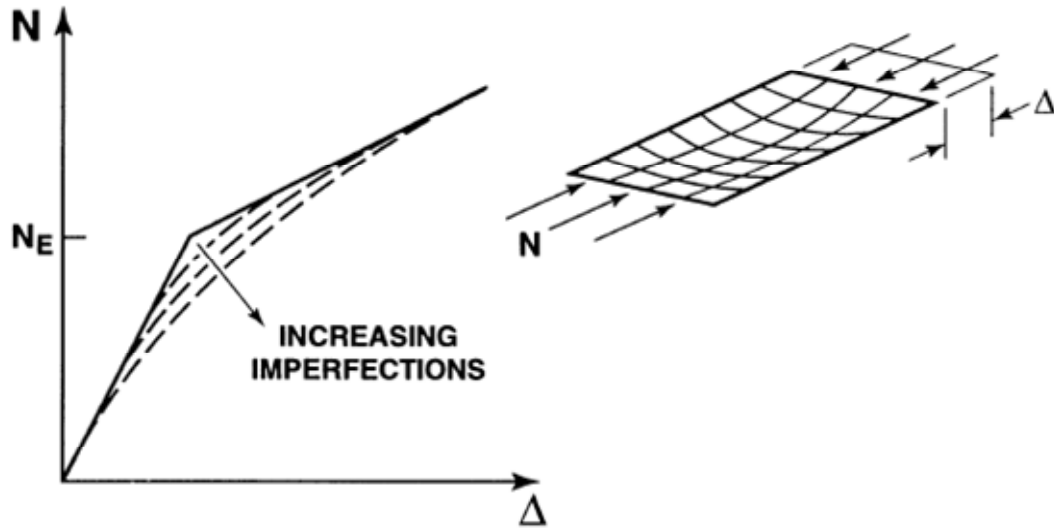


Figure 15. Effect of Initial Imperfection in Buckling [34]

3.4.1 Buckling of Specially Orthotropic Plates

The laminate that has single layer or lots of specially orthotropic layers that are arranged symmetrically with respect to middle surface of laminate is called as specially orthotropic laminate. There are no coupling stiffnesses in stiffness matrix of this laminate. The laminate stiffnesses only include A_{11} , A_{12} , A_{22} , A_{66} , D_{11} , D_{12} , D_{22} and D_{66} . The differential equation that provides the buckling load for flat plate can be written as follows [34];

$$D_{11} \frac{\partial^4 w}{\partial x^4} + 2(D_{12} + 2D_{66}) \frac{\partial^4 w}{\partial x^2 \partial y^2} + D_{22} \frac{\partial^4 w}{\partial y^4} + \bar{N}_{xx} \frac{\partial^2 w}{\partial x^2} = 0 \quad (3.20)$$

Simply supported edge boundary conditions for the plate shown in Figure 16 are given in following expressions [34];

$$\begin{aligned}
 x = 0, a; \quad w = 0 \quad M_x = -D_{11} \frac{\partial^2 w}{\partial x^2} - D_{12} \frac{\partial^2 w}{\partial y^2} = 0 \\
 y = 0, b; \quad w = 0 \quad M_y = -D_{12} \frac{\partial^2 w}{\partial x^2} - D_{22} \frac{\partial^2 w}{\partial y^2} = 0
 \end{aligned}
 \tag{3.21}$$

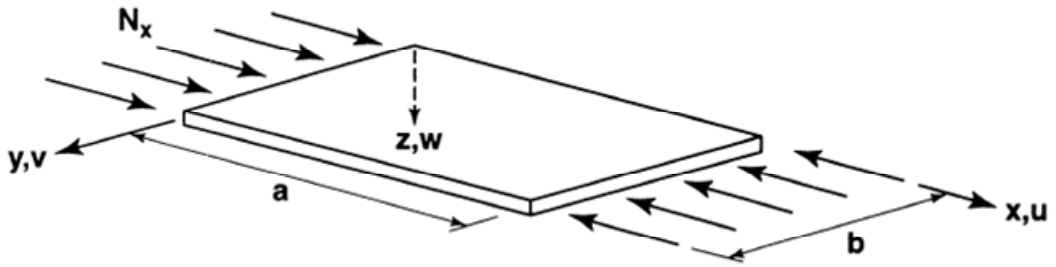


Figure 16. Simply Supported Laminated Rectangular Plate under Uniform Uni-axial Compression [34]

The lateral displacement formulation can be written as follows [34];

$$w = A_{mn} \sin \frac{m\pi x}{a} \sin \frac{n\pi y}{b}
 \tag{3.22}$$

m and n refers to number of buckle half wavelengths in the x - and y - directions. The governing buckling load equation is provided by substitution of lateral displacement formulation [34];

$$\bar{N}_X = \pi^2 \left[D_{11} \left[\frac{m}{a} \right]^2 + 2(D_{12} + 2D_{66}) \left[\frac{n}{b} \right]^2 + D_{22} \left[\frac{n}{b} \right]^4 \left[\frac{m}{a} \right]^2 \right]
 \tag{3.23}$$

To obtain smallest buckling load of plate, n can be taken as 1.

3.4.2 Buckling of Symmetric Angle Ply Laminates

Symmetric angle ply laminates do not include bending-extension coupling stiffnesses but also bend-twist coupling stiffnesses D_{16} and D_{26} occur in laminate stiffness matrix unlike specially orthotropic laminates. The differential equation of angle ply symmetric laminate is [34];

$$D_{11} \frac{\partial^4 w}{\partial x^4} + 4D_{16} \frac{\partial^4 w}{\partial x^2 \partial y^2} + 2(D_{12} + 2D_{66}) \frac{\partial^4 w}{\partial x^2 \partial y^2} + 4D_{26} \frac{\partial^4 w}{\partial x^2 \partial y^2} + D_{22} \frac{\partial^4 w}{\partial y^4} + \bar{N}_{xx} \frac{\partial^2 w}{\partial x^2} = 0 \quad (3.24)$$

Simply supported edge boundary conditions for the plate shown in Figure 16 are given in following expressions [34];

$$\begin{aligned} x = 0, a: \quad \delta w = 0 \quad \delta M_x &= -D_{11} \frac{\partial^2 w}{\partial x^2} - D_{12} \frac{\partial^2 w}{\partial y^2} - 2D_{16} \frac{\partial^2 w}{\partial x y^2} = 0 \\ y = 0, b: \quad \delta w = 0 \quad \delta M_y &= -D_{12} \frac{\partial^2 w}{\partial x^2} - D_{22} \frac{\partial^2 w}{\partial y^2} - 2D_{26} \frac{\partial^2 w}{\partial x y^2} = 0 \end{aligned} \quad (3.25)$$

There is no solution of angle ply symmetric laminate's differential equation due to occurrence of bend-twist couplings D_{16} and D_{26} . Therefore, the solution of the differential equation, given in 3.24, is obtained by using various numerical methods [34].

CHAPTER 4

BUCKLING AND PROGRESSIVE FAILURE ANALYSES BY FINITE ELEMENT METHOD

4.1 Finite Element Analysis

In the analysis of buckling of composite laminated plates which have 460 mm x 350 mm dimensions and various thicknesses, a commercial finite element software Abaqus v6.10 has been used. The general methodology of the post-buckling analyses can be summarized as follows. At first, the critical buckling load and mode shape for the first buckling modes of laminates have been obtained by employing the Linear Eigen Value Extraction method (LANCZOS). Secondly, the initial geometric imperfections with small amplitudes as compared to the panel thickness (0.1-5%), which are determined using the first mode shapes obtained from LANCZOS analyses, have been implemented into FE model for the non-linear analyses. Lastly, the progressive failure analysis has been carried out to investigate the damages on the laminates due to buckling by using Newton-Raphson method.

Element Selection is an important parameter for finite element analysis. Computation time, accuracy of results, required mesh density differs with respect to element which is chosen. Considering these factors, buckling analysis of composite laminates have been carried out by using shell elements S4 and S4R.

S4 is a fully integrated three dimensional finite membrane strain shell element which has four-node and four integration points and it is suitable for large-strain analysis. On the other hand, S4R four-noded, quadrilateral, stress/displacement shell element with reduced integration and large-strain formulation and finite membrane strains, large rotations are taken into account by this element. Therefore, this element is also

suitable for non-linear large displacement analysis as S4 elements. The only difference between these elements is the number of integration points [36].

Reduced integration is computation of element stiffness by using lower order formulation (Figure 17). When reduced integration element is used, fine mesh and distributed loads are required to block hourglass effect. Fully integrated elements do not require hourglass control and give more accurate results with respect to reduced integration elements but computation time of this element is greater 4 or 5 times than reduced integrated ones [36]. Full integration and reduced integration elements were compared with each other and introduced in section 6.2.

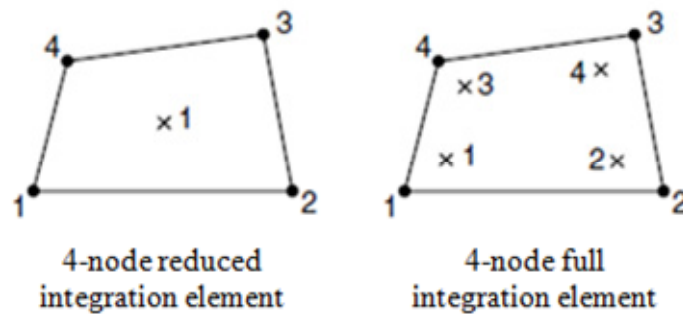


Figure 17. Node ordering and Numbering of Integration Points [36]

4.2 Instability Analysis

Buckling or collapse behavior can occur in geometrically non-linear problems. In this thesis study, instability analyses have been carried out using various analysis procedures. These are eigen value buckling prediction (linear perturbation procedure), Riks method (arc-length) and Newton-Raphson method that is applied an energy dissipation fraction to prevent divergence of the solution [36].

4.2.1 Eigen value Buckling Prediction (LANCZOS)

Eigen value buckling prediction is a linear perturbation procedure which provides critical buckling loads and imperfection sensitivity of structures. Eigen value analysis is performed by solving following equation [36];

$$(K_0^{NM} + \lambda_i K_{\Delta}^{NM})v_i^M = 0 \quad (4.1)$$

where, K_0^{NM} is the stiffness matrix of initial state of FE model, K_{Δ}^{NM} is the initial stress and load stiffness matrix with respect to applied reference load, λ_i is the eigen values v_i^M is the eigenvectors or buckling mode shapes, M and N are the degree of freedom of the FE model and i is the number of buckling mode.

To determine the eigen values, a reference load and required boundary conditions have been applied to FE model. The magnitude of this load is insignificant since load is scaled by the eigen values. Eventually, when eigen values obtained from Lanczos analysis are multiplied with the reference load applied to the model, the critical buckling load of the structure at the specified buckling mode is obtained [36].

$$\lambda_i P_{ref} = P_{cr} \quad (4.2)$$

As seen in equation 4.2, critical buckling load at the i^{th} buckling mode can be found. In this thesis study, critical buckling load of first mode has been taken into consideration since it is the lowest one for composite laminated flat plates but a quite number of buckling modes can be obtained using LANCZOS analysis procedure [36].

4.2.2 Postbuckling Analysis

An eigen value analysis does not inform on post-buckled deformation of laminated plate under increasing loading. Therefore, non-linear static analysis is required to investigate post-buckling response of structure. Two methods have been considered

in this study to investigate the post-buckling analysis: Riks method and Newton-Raphson method by viscous damping.

Newton-Raphson method is prone to fail under load or displacement control for the problems which include highly non-linear behavior like buckling or collapse. In a classical buckling problem, when the load reaches the critical buckling point, Newton-Raphson method fails during the transition between primary equilibrium path and secondary equilibrium path. Therefore, Riks Method is offered for unstable and collapse analysis. However, Riks Method is an expensive analysis procedure on account of computation time and convergence rate. Furthermore, many convergence problems are observed during the analysis that were carried out by using Riks Method, when progressive failure and material stiffness degradation procedures are taken into account for the post-buckling analyses of laminated plates [36].

4.2.2.1 Riks Method

Riks method is a non-linear procedure that is employed for instability analysis and requires incremental solution [36]. Stable and unstable post-buckling behaviors can be solved using Riks Method. In some of non-linear static analyses for instability problems load/deformation path varies as seen in Figure 18. The modified Riks method solves efficiently these types of problems.

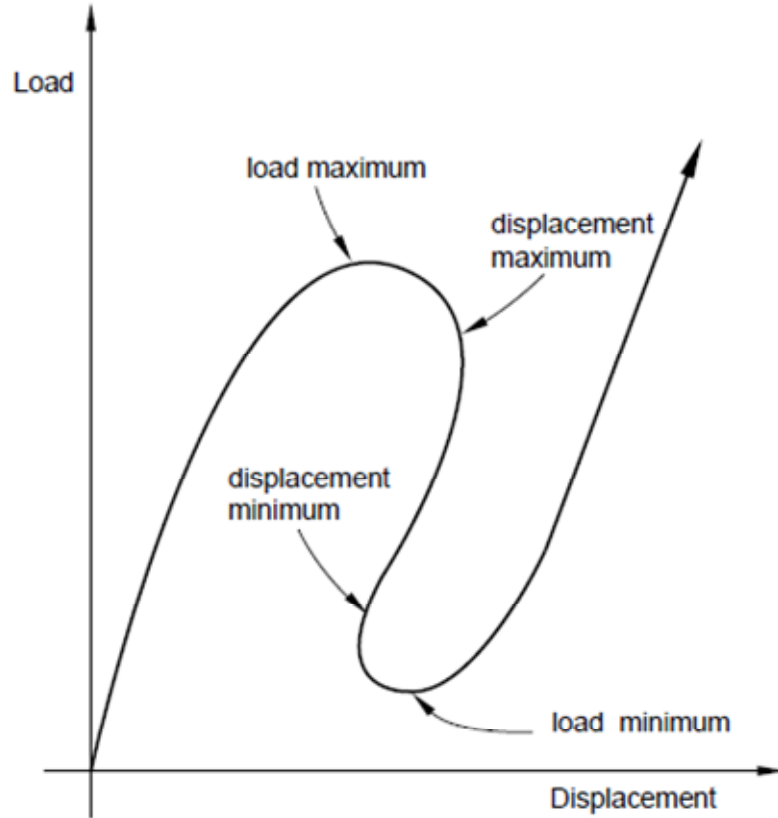


Figure 18. Unstable Static Response [36]

In Riks method, static equilibrium path is followed by using arc-length. The solution starts at any time for the actual load state and displacement λP^N and u^N respectively. Solution path is defined with the equilibrium points that are shown by the vector (\bar{u}^N, λ) in this scaled space and the finite element formula of the structure is given below [36];

$$K_i^{NM} u_i^M = P_i^N \quad (4.3)$$

where, N, M are degrees of freedom of FE model, P_i^N is the loading pattern at i^{th} time, λ is the load magnitude parameter, u_i^M is the displacement at i^{th} time, K_i^{NM} is the tangent stiffness of FE model at i^{th} time.

Load increment of Riks Step is adjusted with respect to previous increment of the analysis. Load proportionality factor increases or decreases in accordance with convergence rate. Riks method starts to analyze the model by an applied initial load P_0 which is determined by user. After the first step of analysis, Riks step determines a reference load P_{ref} that is adjusted from initial dead load and software starts to analyze next step of analysis with modified total load. The loading of model is proportional and current load magnitude is defined with respect to following Formula [36];

$$P_{total} = P_0 + \lambda(P_{ref} - P_0) \quad (4.4)$$

Newton's numerical methods have been employed to solve the non-linear equations by Abaqus/Standard. A %1 extrapolation of strain increment is used by Riks Method. The initial load proportionality factor has been calculated by using an initial increment Δl_{in} which is defined by user [36]. The formula of initial load proportionality factor $\Delta \lambda_{in}$ is;

$$\Delta \lambda_{in} = \frac{\Delta l_{in}}{l_{period}} \quad (4.5)$$

l_{period} is total arc-length scale factor and value of $\Delta \lambda_{in}$, which is calculated by using Δl_{in} and l_{period} , is taken into account at first iteration of Riks analysis. For next iterations, λ is calculated automatically and this automatic incrementation can be controlled using Δl_{max} and Δl_{min} [36].

4.2.3 Newton-Raphson Method by Viscous Damping

For solving non-linear problems, generally Newton-Raphson based algorithms have been used at most of commercial non-linear finite element software (Figure 19). The commercial finite element software provides an analysis procedure which stabilizes unstable quasi-static problems by introducing artificial damping into the model.

Quasi-static problems can be solved by including automatic stabilization with damping factor [36].

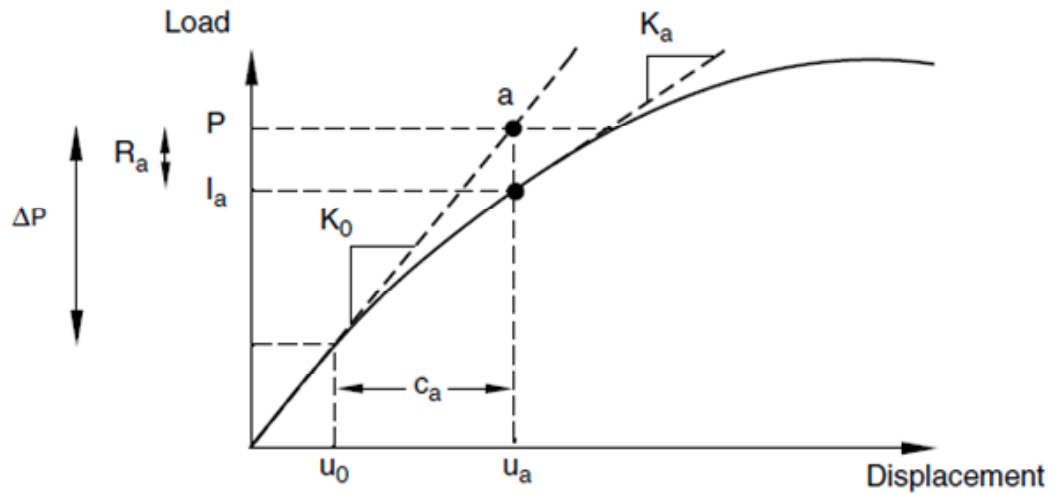


Figure 19. Newton-Raphson Method [36]

In the buckling problems that have been analyzed in this study, the model becomes unstable when secondary equilibrium path occurs since applied load reaches to the critical buckling load level. The viscous forces and viscous dissipated energy levels are very small while the model is stable and artificial damping has no effect. On the other hand, when the problem is unstable at the critical buckling load level, large deformations occur on the model and strain energy increases. To prevent divergence of the computation, to mitigate instabilities and to eliminate rigid body modes of the problem adaptive automatic stabilization scheme has been employed for the buckling analysis. An automatic stabilization scheme can be constituted by using several ways and these are entering a dissipated energy fraction, directly specifying a damping factor or specifying an initial damping factor with an adaptive automatic damping algorithm. The default values of damping factor and accuracy tolerance are

2×10^{-4} , 0.05 but these values should be adjusted with respect to convergence rate of the studied problem [36].

The optimal damping factor is determined manually by using trial and error procedure; damping factor may be increased if convergence problems occurs or may be decreased if the solution is impaired. Therefore, problem requires to be analyzed repeatedly with larger or lower damping factors, energy dissipated by viscous damping and total strain energy should be compared with each other to evaluate the convergence of solution [36].

4.3 Progressive Failure Analysis

The damage analysis used in this study is based on material stiffness degradation of model. The analysis procedure is developed for linear elastic and brittle materials. The stress levels, which damage initiations are expected with respect to specified allowable values of materials in fiber, matrix and shear directions, are determined by using Hashin's Failure Criterion [37] (Figure 20).

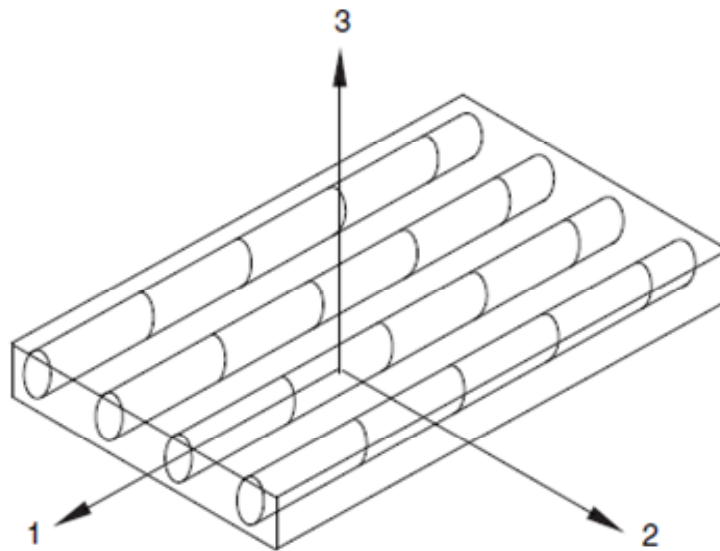


Figure 20. Uni-directions of Lamina [36]

Stress, strain relation used in damage analysis is [38];

$$\boldsymbol{\sigma} = \mathbf{C}_d \boldsymbol{\varepsilon} \quad (4.6)$$

\mathbf{C}_d is the elasticity matrix that can degrade the material stiffness in accordance with damage algorithm of progressive failure analysis [38].

$$\mathbf{C}_d = \frac{1}{D} \begin{bmatrix} (1-d_f)E_1 & (1-d_f)(1-d_m)\nu_{21}E_1 & 0 \\ (1-d_f)(1-d_m)\nu_{12}E_2 & (1-d_m)E_2 & 0 \\ 0 & 0 & (1-d_s)GD \end{bmatrix} \quad (4.7)$$

where;

$$D = 1 - (1-d_f)(1-d_m)\nu_{12}\nu_{21} \quad (4.8)$$

d_f indicates the current level of fiber damage, d_m indicates the current level of matrix damage, d_s indicates the current level of shear damage.

4.3.1 Hashin's Failure Criteria

Hashin's Criterion, which has been developed by Hashin and Rotem, is a stress-based failure criterion and it provides different modes of failure. The formulas correspond to failure modes of Hashin's Criterion can be written as follows [37];

Tensile Fiber Mode, $\sigma_{11} > 0$

$$\left(\frac{\sigma_{11}}{X_T}\right)^2 + \left(\frac{\tau_{12}}{S}\right)^2 \geq 1 \quad (4.9)$$

Compressive Fiber Mode, $\sigma_{11} < 0$

$$\left(\frac{\sigma_{11}}{X_C}\right)^2 \geq 1 \quad (4.10)$$

Tensile Matrix Mode, $\sigma_{22} > 0$

$$\left(\frac{\sigma_{22}}{Y_T}\right)^2 + \left(\frac{\tau_{12}}{S}\right)^2 \geq 1 \quad (4.11)$$

Compressive Matrix Mode, $\sigma_{22} > 0$

$$\left(\frac{\sigma_{22}}{Y_C}\right) \left[\left(\frac{Y_C}{2S}\right)^2 - 1 \right] + \left(\frac{\sigma_{22}}{2S}\right)^2 + \left(\frac{\tau_{12}}{S}\right)^2 \geq 1 \quad (4.12)$$

σ_{11} , σ_{22} , τ_{12} are the stress components and have been used to estimate damage initiation on the model [38].

4.3.2 Damage Evolution Procedure

Damage initiation is a procedure that specifies the stress level, which corresponds beginning of the material stiffness degradations. These damage initiation points are determined by using Hashin's Failure Criteria. In Abaqus, the damage initiation criteria for composites are based on Hashin's criteria which were introduced in the previous section. For every step and sub-step of the nonlinear FE solution, the components $\hat{\sigma}_{11}$, $\hat{\sigma}_{22}$, $\hat{\tau}_{12}$ of the effective stress tensor $\hat{\sigma}$ at every material point are calculated and used to re-evaluate the initiation criteria. The effective stress tensor is assumed to be stress acting over the area of a section that still remains undamaged and it is computed from the relation [36];

$$\hat{\sigma} = M\sigma \quad (4.13)$$

σ corresponds the true stress and \mathbf{M} is the damage operator;

$$\mathbf{M} = \begin{bmatrix} \frac{1}{(1-d_f)} & 0 & 0 \\ 0 & \frac{1}{(1-d_m)} & 0 \\ 0 & 0 & \frac{1}{(1-d_s)} \end{bmatrix} \quad (4.14)$$

The damage variables for each integration points for all plies are determined with respect to following expressions [36].

$$d_f = \begin{cases} d_f^t & \text{if } \hat{\sigma}_{11} \geq 0 \\ d_f^c & \text{if } \hat{\sigma}_{11} < 0 \end{cases}$$

$$d_m = \begin{cases} d_m^t & \text{if } \hat{\sigma}_{22} \geq 0 \\ d_m^c & \text{if } \hat{\sigma}_{22} < 0 \end{cases} \quad (4.15)$$

$$d_s = 1 - (1 - d_f^t)(1 - d_f^c)(1 - d_m^t)(1 - d_m^c)$$

The damage operator, \mathbf{M} , is an identity matrix before damage initiation starts. If damage initiation and evolution occurs for any failure mode, components of damage operator changes with respect to failure mode. If damage initiation procedure is employed without damage evolution procedure, it will only affect the outputs and material stiffness degradation cannot be carried out.

The damage variable for a definite failure mode is determined by using following expression [36];

$$d = \frac{\delta_{eq}^f (\delta_{eq} - \delta_{eq}^0)}{\delta_{eq} (\delta_{eq}^f - \delta_{eq}^0)}, \delta_{eq} \geq \delta_{eq}^0 \quad (4.16)$$

δ_{eq}^0 is the initial equivalent displacement level which corresponds to damage initiation point with respect to Hashin's Failure Criterion and δ_{eq}^f is the displacement

level which corresponds to completely damaged material. Damage variable versus equivalent displacement curve is given in Figure 21;

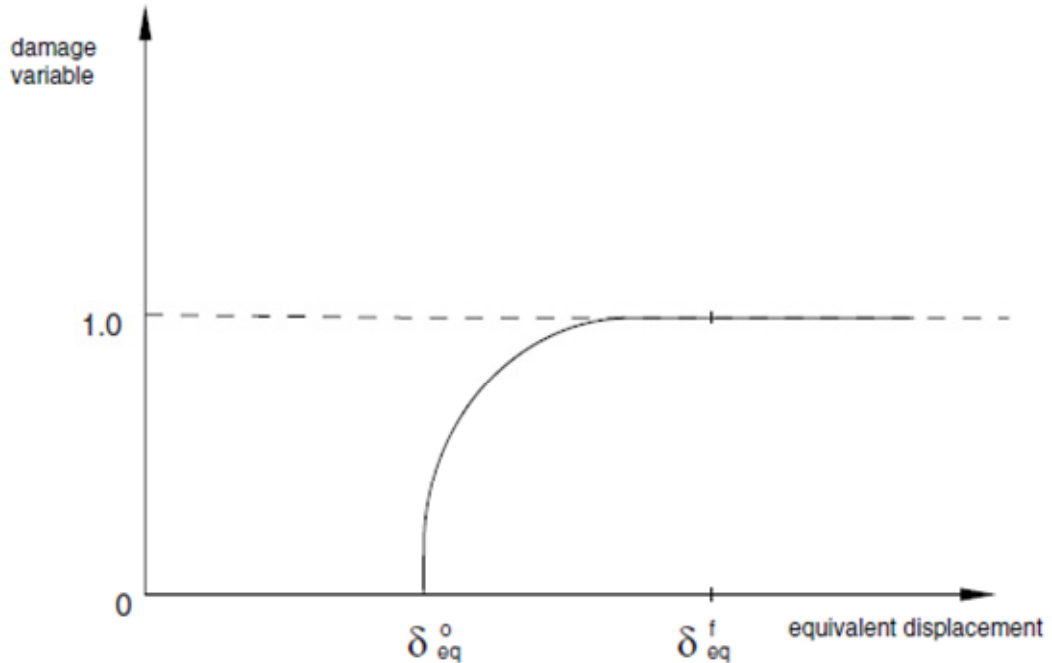


Figure 21. Damage Variable versus Equivalent Displacement [36]

The magnitude of initial equivalent displacement, δ_{eq}^0 , is depend on elastic stiffness properties and material strength allowables for all failure modes. The constitutive law of damage evolution procedure is defined with respect to stress-displacement relation, which is shown in Figure 22, for preventing the effects of mesh size on the solution. Constitutive law of damage evolution includes element characteristic length parameter and the damage variables are calculated iteratively in each increment for four failure modes. The slope of the stress-displacement curve is positive up to δ_{eq}^0 and the material properties are in the linear elastic region as shown in Figure 22. The negative slope of stress-displacement curve occurs after the damage initiation is achieved for particular failure mode and damage variables are started to evaluate [36];

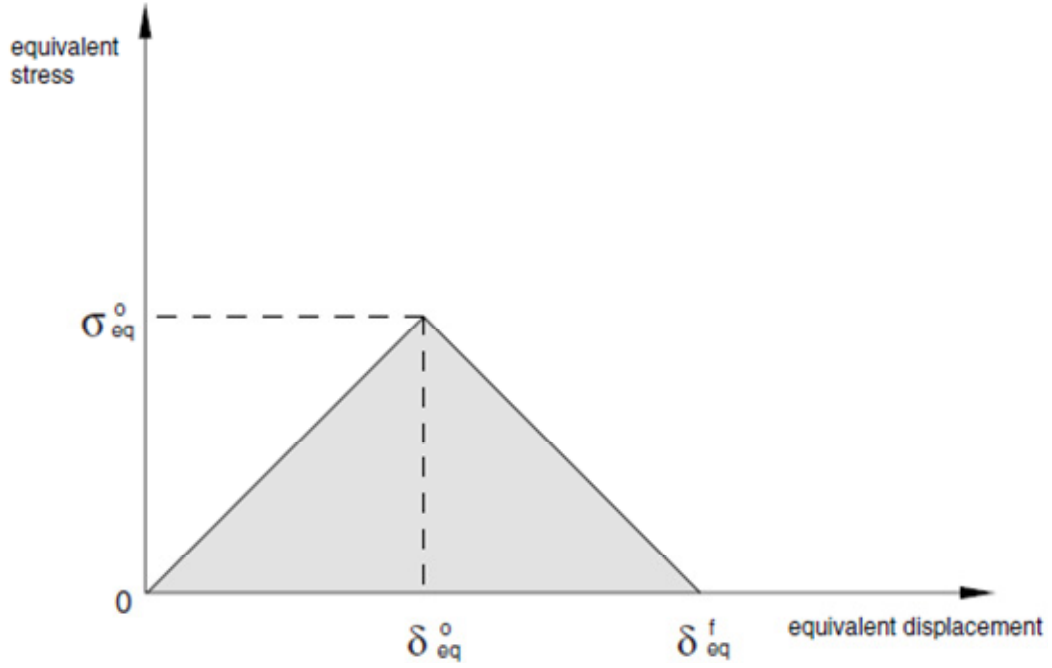


Figure 22. Equivalent Stress-Equivalent Displacement Curve [36]

Equivalent stress and displacement values are calculated by using formulas given below [36];

Fiber tension ($\hat{\sigma}_{11} \geq 0$):

$$\delta_{eq}^{ft} = L^c \sqrt{\langle \varepsilon_{11} \rangle^2 + \varepsilon_{12}^2} \quad (4.17)$$

$$\sigma_{eq}^{ft} = \frac{\langle \sigma_{11} \rangle \langle \varepsilon_{11} \rangle + \tau_{12} \varepsilon_{12}}{\delta_{eq}^{ft} / L^c} \quad (4.18)$$

Fiber compression ($\hat{\sigma}_{11} < 0$):

$$\delta_{eq}^{fc} = L^c \langle -\varepsilon_{11} \rangle \quad (4.19)$$

$$\sigma_{eq}^{fc} = \frac{\langle -\sigma_{11} \rangle \langle -\varepsilon_{11} \rangle}{\delta_{eq}^{fc} / L^c} \quad (4.20)$$

Matrix tension ($\hat{\sigma}_{22} \geq 0$):

$$\delta_{eq}^{mt} = L^c \sqrt{\langle \varepsilon_{22} \rangle^2 + \varepsilon_{12}^2} \quad (4.21)$$

$$\sigma_{eq}^{mt} = \frac{\langle \sigma_{22} \rangle \langle \varepsilon_{22} \rangle + \tau_{12} \varepsilon_{12}}{\delta_{eq}^{mt} / L^c} \quad (4.22)$$

Matrix compression ($\hat{\sigma}_{22} < 0$):

$$\delta_{eq}^{mc} = L^c \sqrt{\langle -\varepsilon_{22} \rangle^2 + \varepsilon_{12}^2} \quad (4.23)$$

$$\sigma_{eq}^{mc} = \frac{\langle -\sigma_{22} \rangle \langle -\varepsilon_{22} \rangle + \tau_{12} \varepsilon_{12}}{\delta_{eq}^{mc} / L^c} \quad (4.24)$$

L^c represents the characteristic length of the element and L^c is determined in accordance with the element geometry and formulation. For instance, it is the square root of element area for first order shell or membrane elements. Commercial FE software provides the L^c of the model in the output files [36].

The energy dissipated due to failure, G^c which corresponds to area of equivalent stress and equivalent displacement curve given in Figure 22, must be specified for all failure modes to employ the damage evolution procedure. The value of G^c affects the equivalent displacement, δ_{eq}^f , which corresponds to level that the material is completely damaged. As G^c increases, final equivalent displacement, δ_{eq}^f , also increases. In this thesis study, the value of energy dissipated due to failure is assumed with respect to a simple FE analysis [36].

4.3.3 Viscous Regularization Scheme

Some convergence difficulties may occur for the models, which damage evolution procedure is employed, while material stiffness degrades in nonlinear static analysis solutions. Commercial FE software provides a scheme to prevent divergence of

analysis called as Viscous Regularization, which regulate the tangent stiffness matrix to be positive for small time increments [36].

A viscous damage variable, \dot{d}_v , is determined by using the equation given below;

$$\dot{d}_v = \frac{1}{\eta}(d - d_v) \quad (4.25)$$

η is the viscosity coefficient of the model and d is the damage variable of the model without viscous regularization. Damage evolution of the viscous model is found using same equations [36];

$$\sigma = C_d \varepsilon \quad (4.6)$$

The damaged elasticity matrix, C_d , of the model is calculated by using viscous damage variables which are obtained from the equation given above. Viscosity coefficients of failure modes should be small values compared to time increment of the solution for providing convergence of the solution.

4.3.4 Determination of the Energies Dissipated due to Failures

The energies dissipated due to failures have been calculated by using FEA method in this thesis. G^c values have been determined individually for four failure modes of woven fabric and uni-directional tape composite materials. A finite strip, which has dimension 40 mm x 100 mm and one plied stacking sequence, has been modeled to find the equivalent stress versus equivalent displacement curves for fiber and matrix directions. Strip has been analyzed individually for all failure modes with 0 and 90 degree sequenced material directions. Finite element model of strip shown in Figure 23;

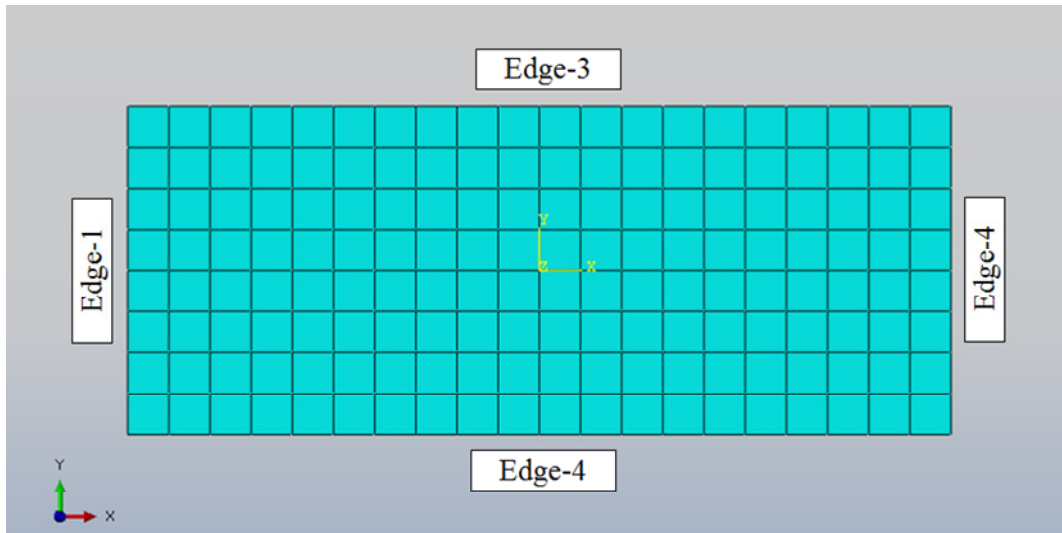


Figure 23. Finite Element Model of Finite Strip

Boundary conditions of the finite element model are given in Table 1;

Table 1. Boundary conditions for Finite Strip

Edge	Boundary Conditions
1	v, w
2	u, v, w
3	No Constraint
4	No Constraint

A non-linear static analysis has been carried out for plotting the stress-displacement curves of failure modes and the damage initiation procedure of commercial finite element software has been employed. When the damage initiation is observed for an element, the analysis has been stopped and the equivalent stress versus equivalent displacement curves have been plotted for the element by using expressions given in the damage initiation procedure. This approach is recurred for all failure modes of

materials and equivalent stresses versus equivalent displacement curves have been plotted. The loading and fiber directions are shown in Figure 24 for different failure modes.

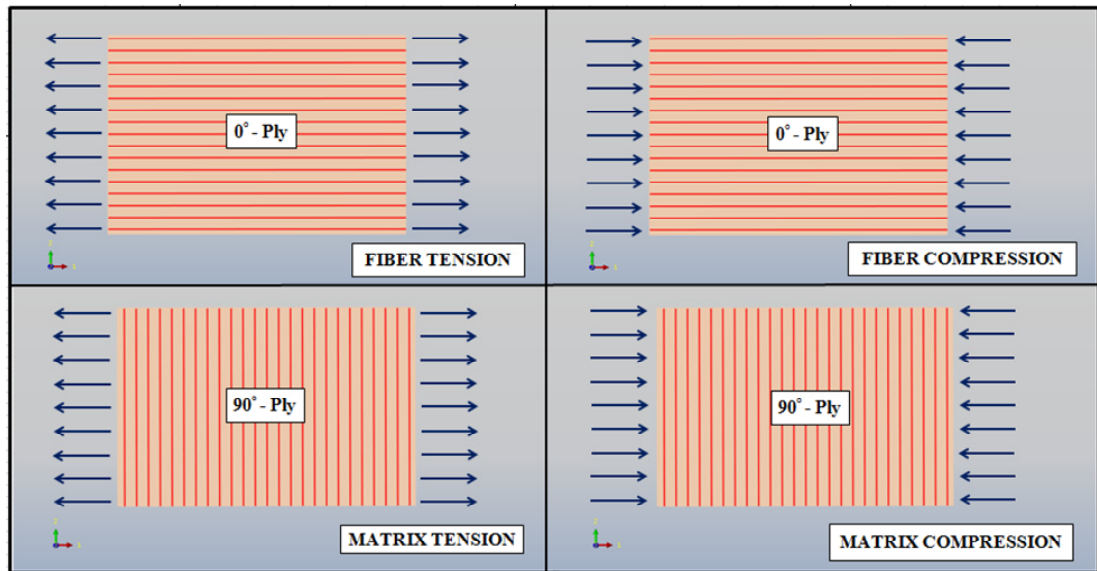


Figure 24. Loading and Ply directions for all Failure Modes

In literature, a number of property degradation models were developed for the progressive failure analyses. Most of these degradation models are based on two approaches; instantaneous unloading and gradual unloading. In instantaneous unloading case, when damage initiation is predicted by a failure mode, the material property associated with that failure mode is degraded instantly zero. In gradual unloading case, the material property associated with that failure mode is degraded gradually until the particular material property reaches to zero [39]. Both of these approaches are shown in Figure 25.

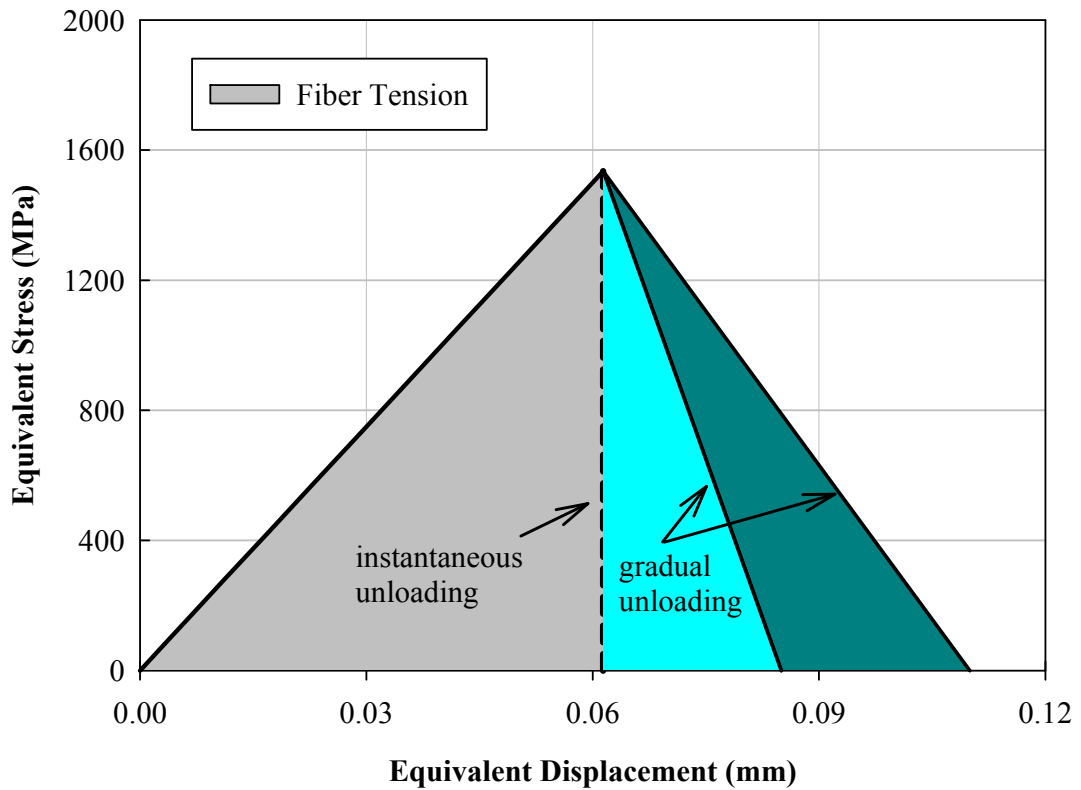


Figure 25. Assumption of Dissipated Energy due to Failure

In the analyses, the ply-discount theory is applied which is a common instantaneous unloading methodology used for degradation of material properties. In this method, one or more of the elastic material properties or constitutive components of a lamina are set to equal zero or a small fraction of the original value once failure is detected. However, some convergence difficulties have been occurred in the analysis due to instantaneous unloading of element stiffnesses. To prevent convergence difficulties, the G^c values have been determined by allowing a deformation which is a small fraction (5%) of the initial equivalent displacement due to lack of experimental material data. By using this assumption, the energies dissipated due to failures have determined for unidirectional and fabric laminae as shown in Figure 26-Figure 31 drawn for equivalent Stress versus equivalent displacement curves of relevant laminae. Table 2 lists the energies dissipated due to failures of UD and fabric laminae.

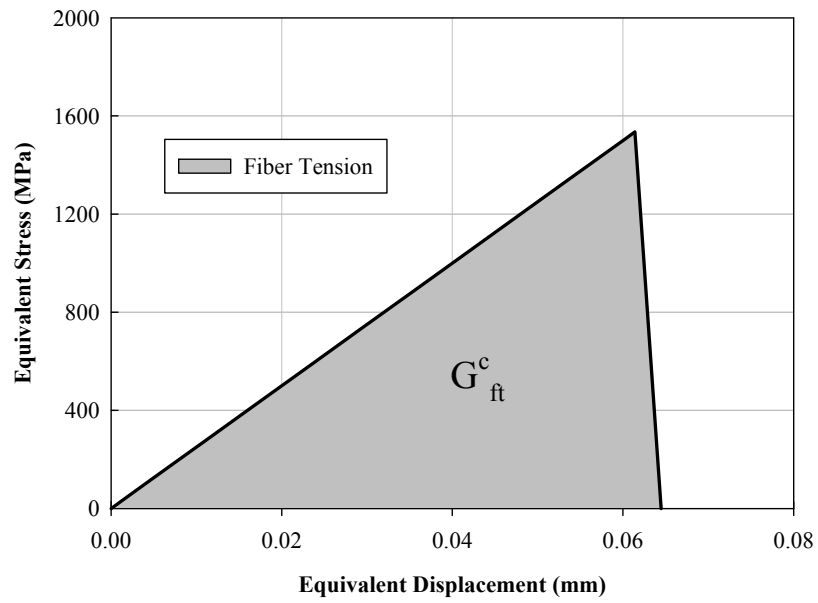


Figure 26. Equivalent Stress versus Equivalent Displacement for Fiber Tension of UD Lamina

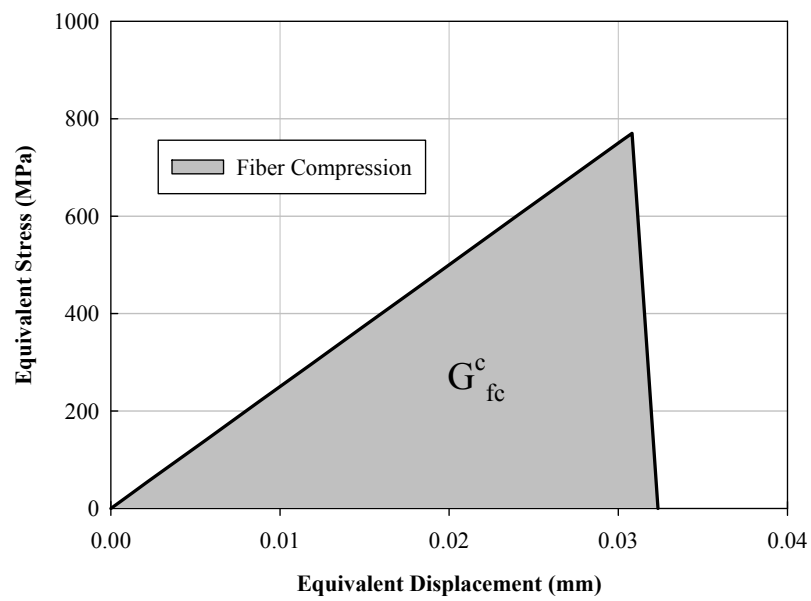


Figure 27. Equivalent Stress versus Equivalent Displacement for Fiber Compression of UD Lamina

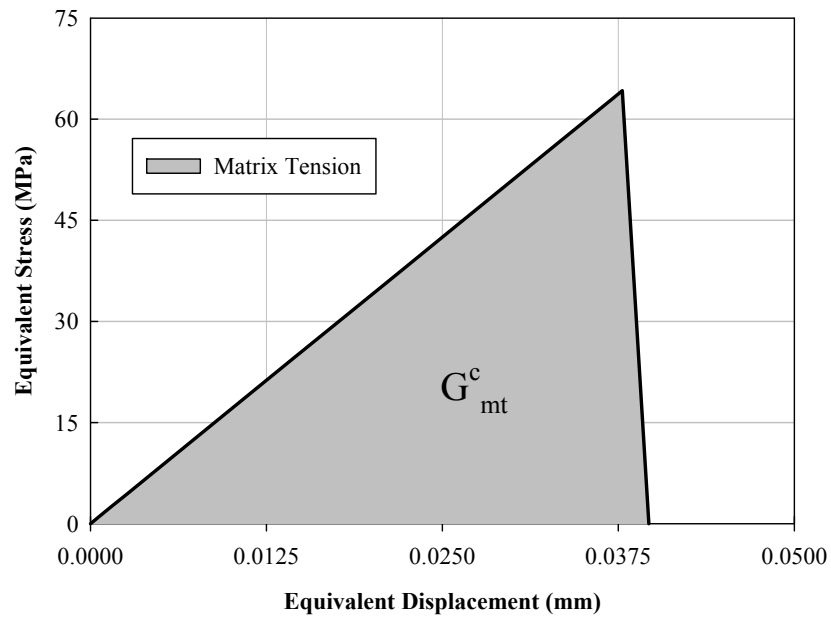


Figure 28. Equivalent Stress versus Equivalent Displacement for Matrix Tension of UD Lamina

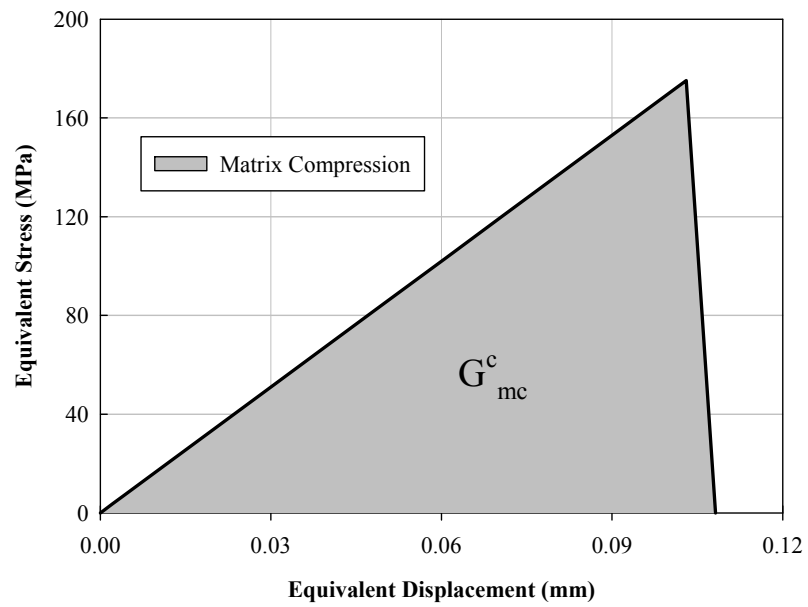


Figure 29. Equivalent Stress versus Equivalent Displacement for Matrix Compression of UD Lamina

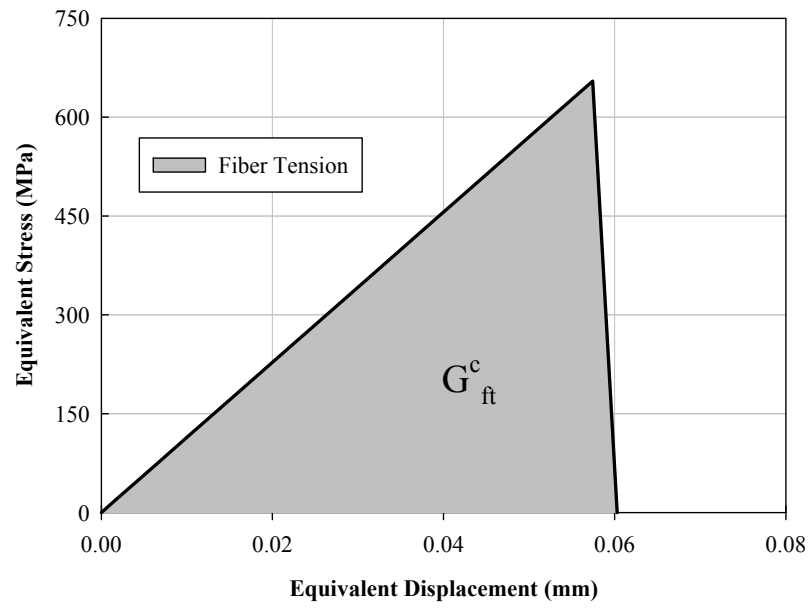


Figure 30. Equivalent Stress versus Equivalent Displacement for Fiber Tension of Fabric Lamina

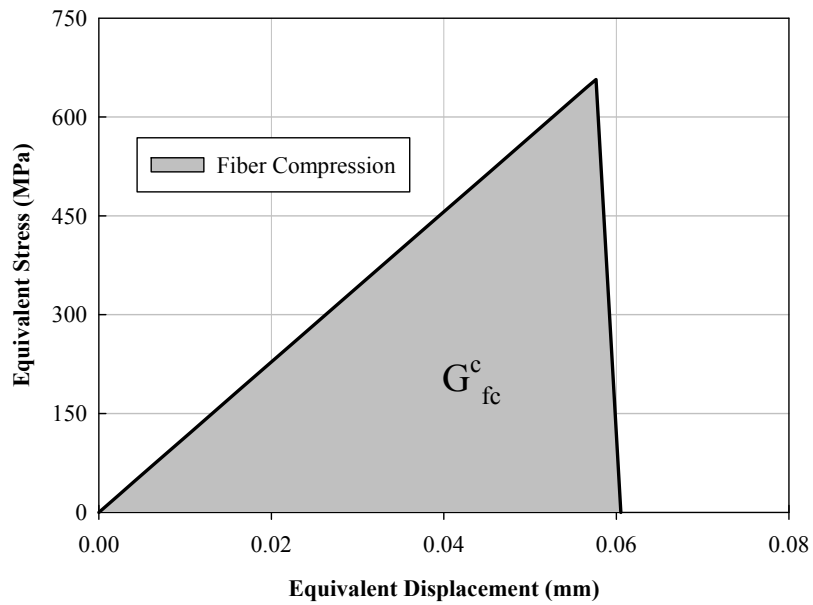


Figure 31. Equivalent Stress versus Equivalent Displacement for Fiber Compression of Fabric Lamina

Table 2. Energies Dissipated due to Failure Modes for UD and Fabric laminae

Energy Dissipated due to Failure [N/mm²]	G^c_{ft}	G^c_{fc}	G^c_{mt}	G^c_{mc}
Failure Mode	Fiber Tension	Fiber Compression	Matrix Tension	Matrix Compression
AS4 / 8552 Carbon Fibre Reinforced Epoxy Prepreg UD Tape	49.5	12.5	1.3	9.5
AS4 / 8552 Carbon Fibre Reinforced Epoxy Prepreg /5HS Fabric/280 g/m²	19.7	19.9	19.7	19.9

CHAPTER 5

EXPERIMENTS & MATERIALS

In this thesis, a number of experiments have been conducted to compare and verify the numerical results. For this purpose, two sets of tests were carried out for unidirectional tapes and woven fabrics. There are a lot of factors that affect the results adversely in the experiments. These factors are the imperfections and defects in the test specimens, geometrical eccentricities in the test fixtures, non-ideality of the boundary conditions, load introduction problems and wrong data measurements.

5.1 Test Fixture

The design and construction of the test fixture affects the accuracy of results in the plate buckling tests. If the composite plate is loaded eccentrically, the moments occur on the plate due to misalignment of the plate between the load actuator. As a result of that buckling occurs earlier than the expected load level. The design of boundary conditions is also important for loaded and unloaded edges of plate. If the actual boundary conditions do not provide intended condition, the data which are obtained from the tests would not reflect the actual conditions.

The test fixture is designed and manufactured to investigate the large displacement post-buckling behavior of composite laminated plates under compressive in-plane loading. All edges of plates have been supported to realize the plate buckling of composite plates at the test stage. The clamped boundary conditions have been applied for top and bottom edges of plates and simple supported boundary conditions have been applied for side edges of plates as shown in Figure 32 and Figure 33.



Figure 32. Test Fixture of Thesis Study

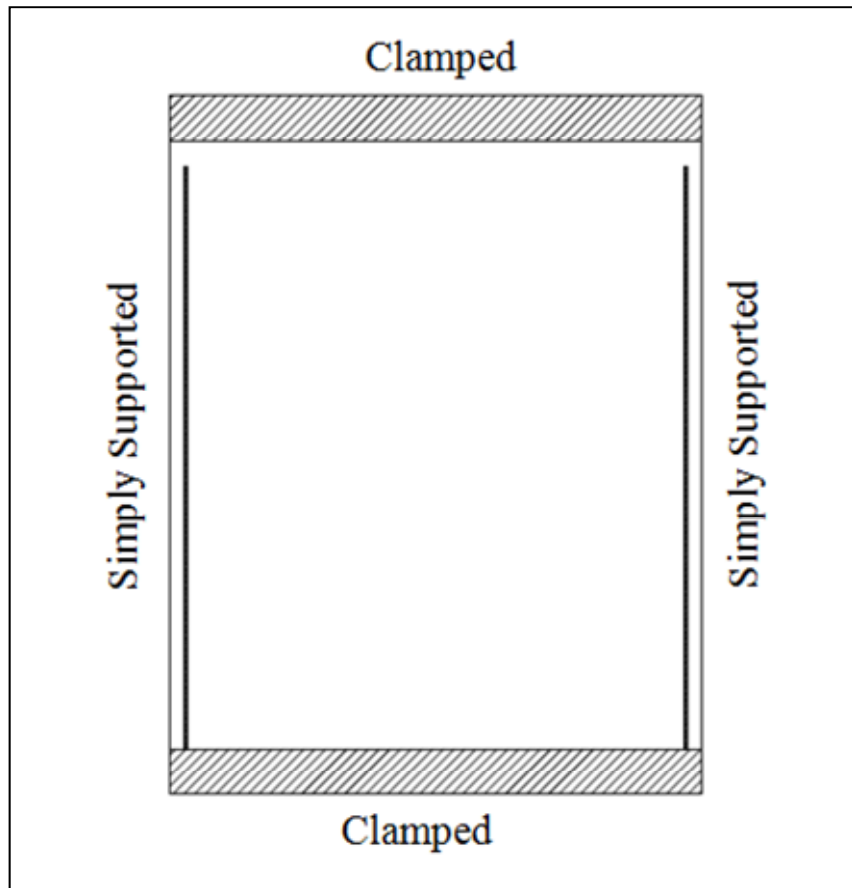


Figure 33. Boundary Conditions of Plate Edges

There are various applications to provide a clamped boundary condition. For instance, plates can be fixed using a potting material like epoxy resin or plates can be compressed between two metallic blocks. Potting method has been considered to create clamped boundary condition for loaded edges (top and bottom) but it is found difficult to obtain co-linearity between plate and load actuator during the curing of potting material. A mechanism has been developed which can easily align the upper and lower ends of the plate. The fixture of loaded edges consists of three parts per one edge. These are an interface element between load actuator and two L-section metallic blocks. The L-section metallic blocks compress the composite laminated plates to provide clamped boundary conditions. If an eccentricity is observed between plate and load actuator, the co-linearity was provided by using the relative

motion between interface element and L-section metallic blocks along the out-of-plane direction of composite plate as shown in Figure 34.

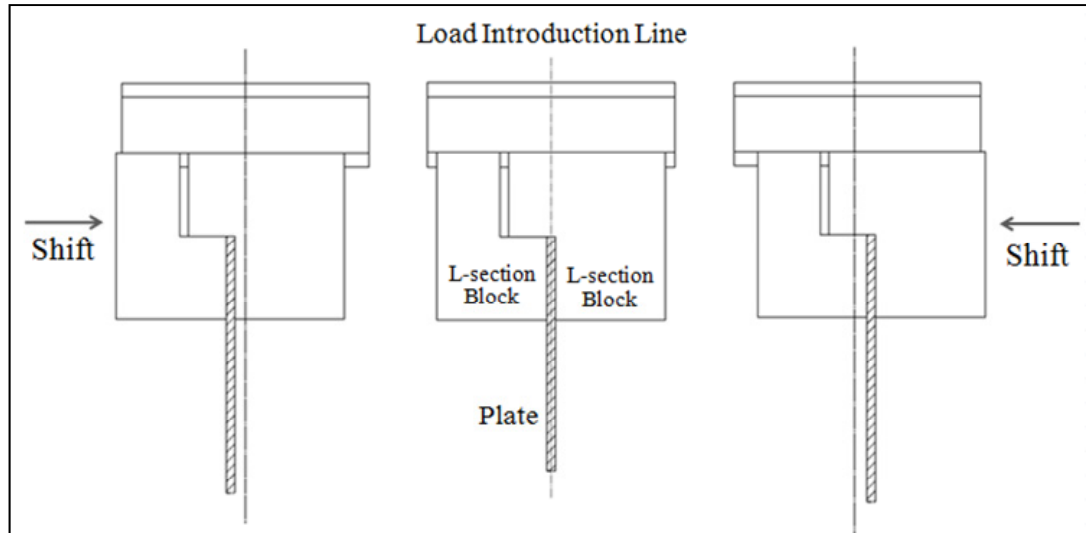


Figure 34. Providing co-linearity between Load Actuator and Plate with the help of Test Fixture

The translational movements of the side edges of plates should be restricted without developing any moments to satisfy the simple supported boundary conditions. For this purpose, the metallic knife edges which prevent the out of plane displacement of plate edges and allow the rotation about longitudinal axis of the knife edge have been used. However, the sharp of knife edges can create high stress concentrations and cause damage. Steel strips and rubber tape have been placed between knife edges and plates in order to prevent local damage or the unloaded edges have been supported by using metal roller bearings which allow in-plane motion in some previous studies. However, restrictions have been observed in the rotation of side edges for large deflections. One other method is to use rounded knife edges for preventing large stress concentrations. In this study, the rounded knife edges have been used to provide simple supported boundary condition on the side edges of plate as in Figure 35.

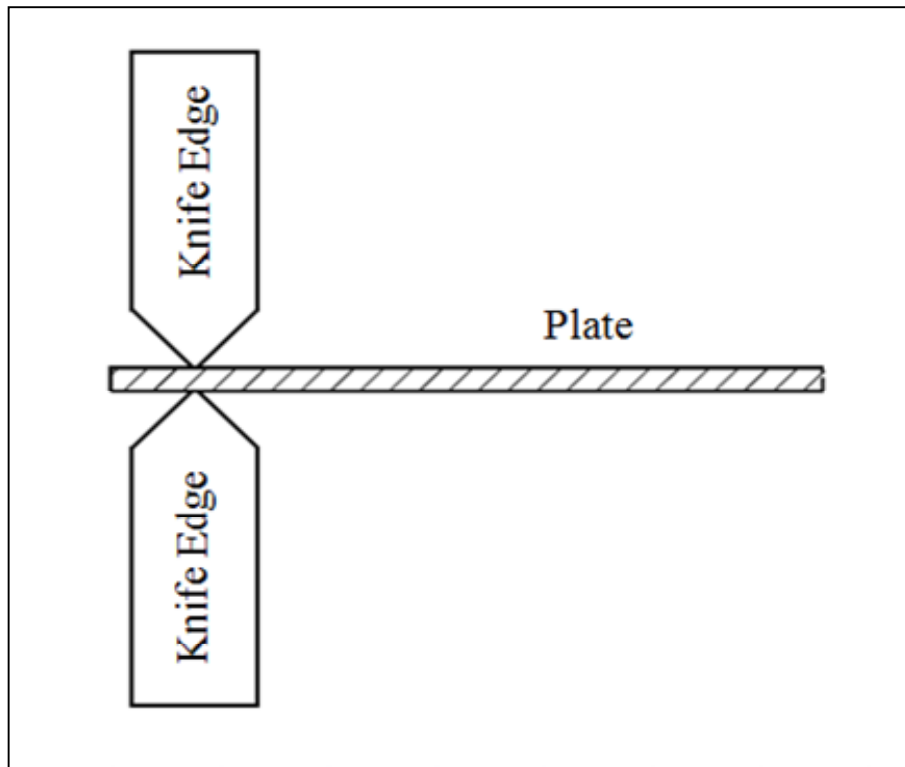


Figure 35. Knife Edges of Test Fixture

When compressive load is applied to the top side of the fixture, the plate starts to shorten in load direction. Therefore, a gap, which is shown in Figure 37, is provided between L-section blocks and knife edges in order to allow buckling of the plate. The gap, which is required to allow movement of loaded side of fixture due to shortening of plate under the compression have also been considered in the finite element analysis.

The overall in-plane dimensions of specimens are taken as 460 mm x 350 mm. 30 mm length of the specimens at both end are stuck in the metallic blocks of top and bottom fixtures to provide an ideal clamped boundary condition. Furthermore, knife edge supports are located 10 mm inward from the side edges of the specimens. Hence, the in-plane plate dimensions under the effect of buckling are 400 mm x 330 mm as shown in Figure 36 .



Figure 36. Panel Geometry and Boundary Conditions

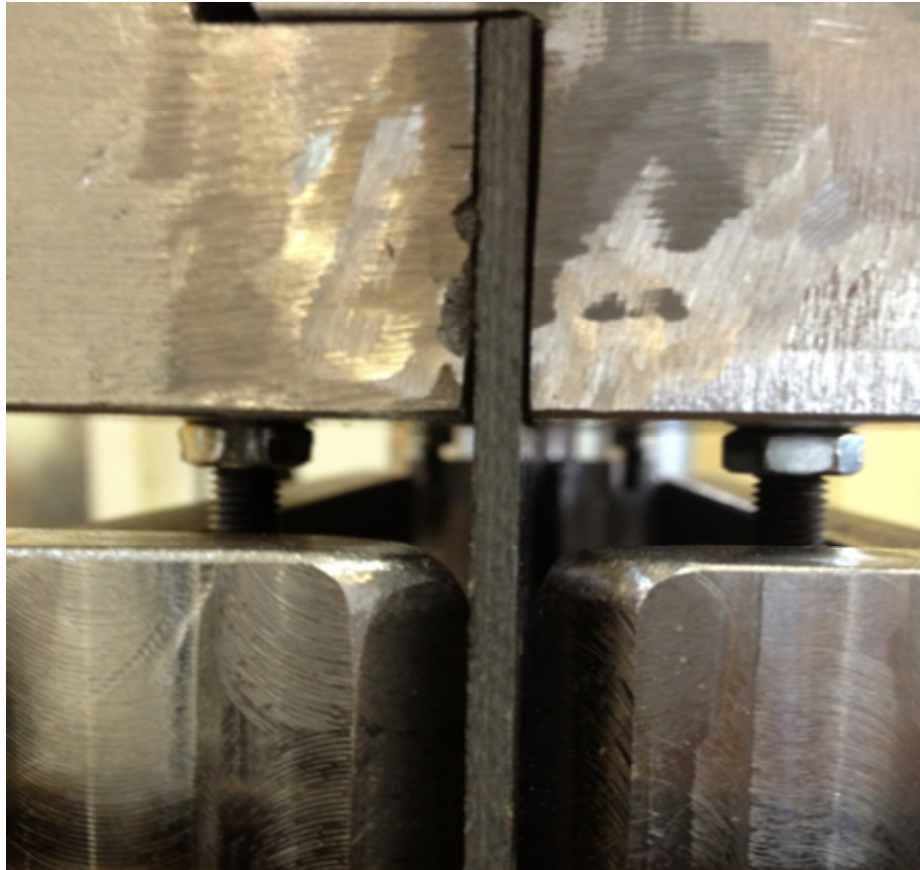


Figure 37. The 10 mm gap between L-section blocks and knife edges

All parts of fixture were manufactured using CNC milling machine due to requirement of tight tolerances, which is necessary to provide co-linearity and ideal boundary conditions. The material of test fixture is AISI 1040 hot-rolled steel alloy and machined parts of fixture have been assembled to each other by using high quality steel alloy bolts due to high load-carrying capacity of composite plates. Hot-rolled materials are selected to prevent the deformations due to residual stresses which occur on the machined parts as a result of the machining operation. Furthermore, lower ends of side fixtures were welded to L-section blocks at the bottom side of test fixture (Figure 38).

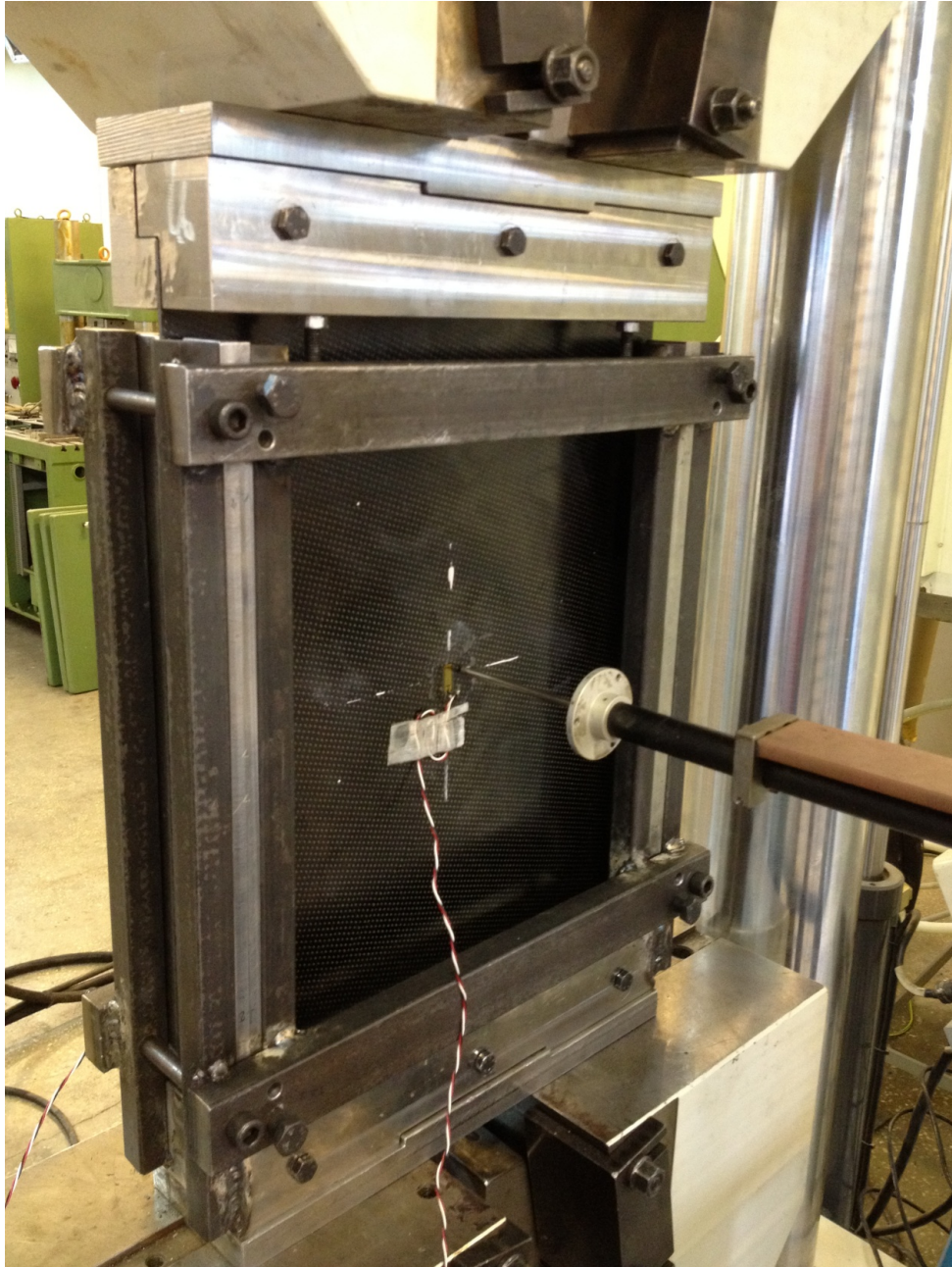


Figure 38. Front view of Test Fixture with Fabric Specimen

5.2 Test Specimens

Stacking sequences and mechanical properties of specimens are specified in sections 5.4 and 5.5. Two fabrics and two UD laminated specimen were experimented in this

study. Properties of specimens, which have been used in the experiments, are summarized in Table 3.

Table 3. Summary of Specimen Properties

Specimen Name	Stacking Sequence	Thickness [mm]	Height [mm]	Width [mm]
UD-1	[45/-45/0/45/90/90/-45/0] _s	2.944	460	350
UD-2	[45/-45/0/45/90/90/-45/0] _s	2.944	460	350
FABRIC-1	[45/0/45/0/45] _s	2.8	460	350
FABRIC-2	[45/0/45/0/45] _s	2.8	460	350

5.3 Test Equipment and Procedure

The buckling and post-buckling tests are performed on the composite flat laminated plates by a displacement controlled testing device which has 600 kN compressional loading capacity. At first, the test fixture and specimen are assembled to the testing device. Then, the LVDT transducer and testing device are calibrated with respect to commercial data storage software. The out of plane deflection of the midpoint of specimens is measured by using LVDT transducer and end-shortening data of specimens is obtained by recording displacement of the hydraulic piston of testing device. The hydraulic piston has been actuated by a velocity of 0.01 mm/sec. Axial loads are also delivered by the hydraulic press.

5.4 Mechanical Properties of Materials

The test specimens have been manufactured by using two different prepreg laminae. These are AS4 / 8552 Carbon Fiber Reinforced Epoxy Prepreg UD Tape and AS4 / 8552 Carbon Fiber Reinforced Epoxy Prepreg 5HS Fabric. Both of prepreg laminae consist of same fiber and matrix materials. AS4 / 8552 UD Tape is a uni-directional

fiber reinforced composite which all fibers are aligned in a single direction. AS4 / 8552 5HS is a fabric lamina, which the textile structure is formed by interlaced fibers that are 90° angle with each other [40]. The mechanical properties of AS4/8552 UD Tape and Fabric laminae used in the numerical analyses are given in Table 4 and Table 5.

Table 4. Mechanical Properties of Prepreg Laminae

Material	AS4 / 8552 Carbon Fibre Reinforced Epoxy Prepreg UD Tape	AS4 / 8552 Carbon Fibre Reinforced Epoxy Prepreg 5HS Fabric
Ply Thickness [mm]	0.184	0.28
E₁₁ [MPa]	130000	61000
E₂₂ [MPa]	8500	61000
G₁₂ [MPa]	4200	4200
v₁₂	0.35	0.05

Table 5. Strength Values of Laminae

Material	AS4 / 8552 Carbon Fibre Reinforced Epoxy Prepreg UD Tape		AS4 / 8552 Carbon Fibre Reinforced Epoxy Prepreg 5HS Fabric	
	A-Basis	B-Basis	A-Basis	B-Basis
X_T [MPa]	1800	1530	780	647
X_C [MPa]	1100	770	900	657
Y_T [MPa]	75	64	780	647
Y_C [MPa]	250	175	900	657
S [MPa]	95	95	109	109

The strength values of the materials are given in Table 5 and these values used in the thesis are taken from B-Basis value of material properties to be on the safe side. A-Basis and B-Basis values are determined statistically. In [41] the corresponding definitions given as;

“A-basis Value: A statistically-based material property; a 95% lower confidence bound on the first percentile of a specified population of measurements. Also a 95% lower tolerance bound for the upper 99% of a specified population.”

“B-basis Value: A statistically-based material property; a 95% lower confidence bound on the tenth percentile of a specified population of measurements. Also a 95% lower tolerance bound for the upper 90% of a specified population.”

5.5 Stackings of Laminates

The two different stackings have been considered for producing the laminated plates; one of them consists of completely fabric laminae and the other consists of completely uni-directional laminae. The ply stackings have been selected such that

either the plates are balanced or symmetric to prevent occurrence of B matrices in the stiffness matrix and secondary instabilities under compressive load.

The stacking sequences for UD laminate is $[45/-45/0/45/90/90/-45/0]_S$ and for fabric laminate is $[45/0/45/0/45]_S$. The stiffness matrix of UD is given in Table 6;

Table 6. Stiffness matrix of UD laminate

$$\begin{bmatrix} 157010 & 49982 & 0 & 0 & 0 & 0 \\ 49982 & 157010 & 0 & 0 & 0 & 0 \\ 0 & 0 & 53515 & 0 & 0 & 0 \\ \hline 0 & 0 & 0 & 109650 & 48639 & 11709 \\ 0 & 0 & 0 & 48639 & 92083 & 11709 \\ 0 & 0 & 0 & 11709 & 11709 & 51191 \end{bmatrix}$$

The stiffness matrix for woven fabric laminate is given in Table 7;

Table 7. Stiffness matrix of Fabric laminate

$$\begin{bmatrix} 121460 & 46544 & 0 & 0 & 0 & 0 \\ 46544 & 121460 & 0 & 0 & 0 & 0 \\ 0 & 0 & 50304 & 0 & 0 & 0 \\ \hline 0 & 0 & 0 & 77337 & 32423 & 0 \\ 0 & 0 & 0 & 32423 & 77337 & 0 \\ 0 & 0 & 0 & 0 & 0 & 34880 \end{bmatrix}$$

As seen in the stiffness matrices of laminates, all components of B matrices are zero. The D_{16} and D_{26} components of D matrices exist in the stiffness matrix of the UD plate due to angle ply stacking of laminate however these components do not exist in the fabric laminate since elastic moduli of 1- and 2- material directions of fabric lamina are equal to each other due to quasi-isotropic behavior of fabric lamina.

5.6 Curing of Composite Laminates

Curing Process is performed to change the properties of a thermosetting resin irreversibly by a chemical reaction. This process has been carried out by using pressure and heat. Furthermore, the thermosetting material is subjected to several specified conditions in a schedule of time periods in order to obtain expected property level [40].

The individual sections or layers of a composite structure are bonded with each other by curing process. That is to say, the matrix material of prepreg lamina becomes intact and capable to carry applied loads with carbon fibers [40].

There are many different curing processes such as pultrusion die cure and consolidation, RTM and autoclave curing. The composite laminates, which are tested in this study, have been cured at 175 ± 10 °C under pressure at 6.8 ± 0.5 bar in autoclave which is a pressure vessel capable of applying high internal pressure and high temperature levels. Total duration of the autoclave process is about 130-180 minutes. Furthermore, the vessel of autoclave is purged of oxygen using an inert gas to prevent thermal combustion or charring of the materials which are cured [40].

A flat tool was used during the curing process of the composite plates which were used in the experiments. The flatness of the tool is an important parameter to take identical results between experiments and numerical results. The imperfection of flatness may develop extra bending moments on the plates that may causes early failure of specimens. A bagging film was placed on the plates being cured and vacuum was applied between film and plates during the curing process, so, the plies

of plate were compressed through the thickness. When the temperature of the process is increased, the viscosity of resin changes and the gases within plies tries to escape. The evacuation of gases was provided by using a porous bleeder layer during the curing process and occurrence of porosities between layers is prevented by this method [40].

5.7 Cure Cycle of Specimens

Cure cycle of composite plates, which consist of AS4/8552 UD and Fabric laminae, are given in Figure 39 and Figure 40 for temperature and pressure respectively;

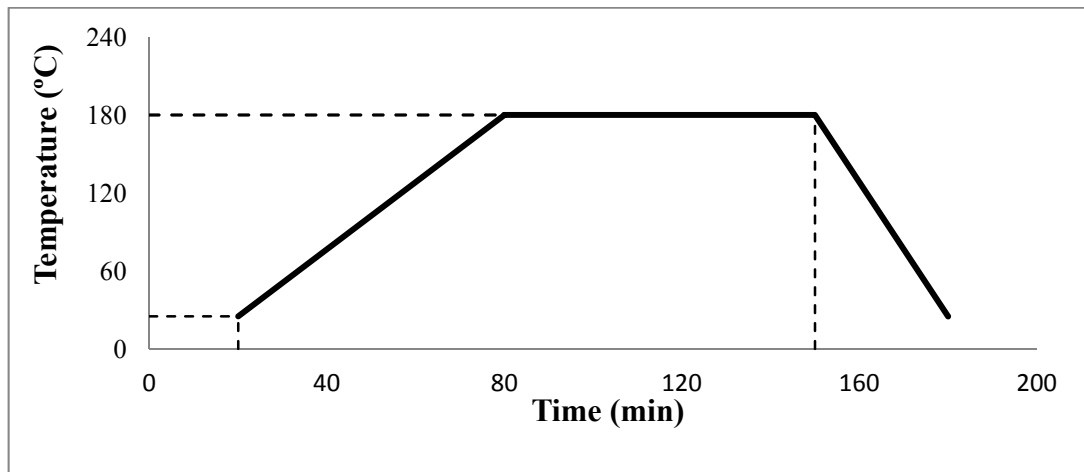


Figure 39. Temperature versus Time graph of Cure Cycle

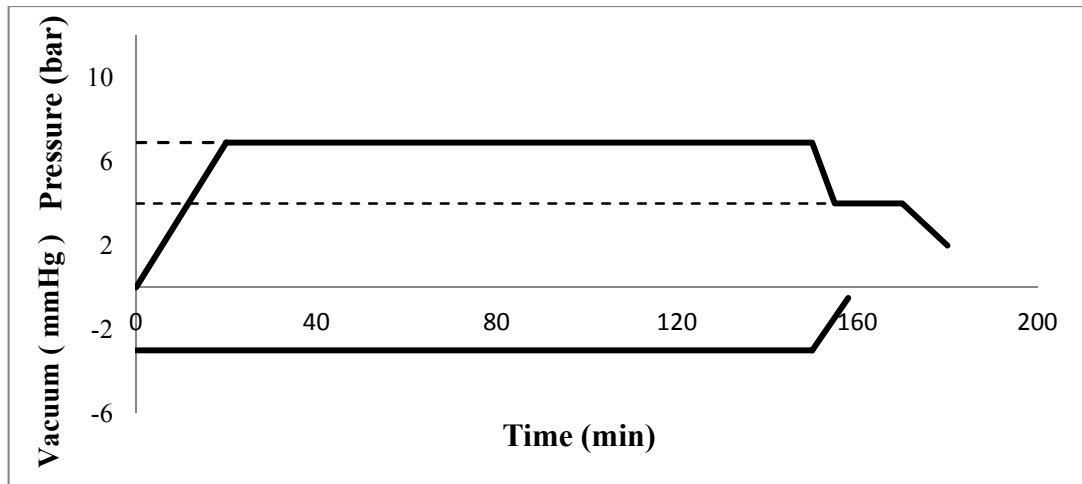


Figure 40. Pressure versus Time graph of Cure Cycle

5.8 Cutting of Specimens

Several manufacturing defects (thickness variation, geometric imperfections, initial delaminations, porosities) can occur in specimens during the curing process. Generally, defects are observed near the edges due to vacuum bagging and autoclave process. Furthermore, the opposite edges of specimens must be parallel to each other and the corners must be perpendicular for obtaining identical results by numerical methods and experiments. Satisfying these requirements is difficult, if the specimens are cured with the exact dimensions. Therefore, the specimens were manufactured 25 mm larger than the required specimen dimension.

After the curing process, the specimens have been cut to the required dimension with the help of a CNC milling machine. Cutting of the specimens is one of the important steps during the composites manufacturing since cutting tool or vibrations on the specimens may inflict damages on the edges of laminates. UD and fabric specimens were cut by using special cutting tool to prevent initial delaminations and fiber breakouts. Furthermore, to prevent mechanical vibrations which have been observed on the laminates during the cutting operations due to small thickness of specimens, soft chipboard is located under the specimens.

CHAPTER 6

COMPARISON OF NUMERICAL AND EXPERIMENTAL RESULTS

6.1 The Finite Element Model

The finite element mesh is given in Figure 41. The boundary conditions, which are used in the experiments, have been simulated in the FE model as shown in Table 8.

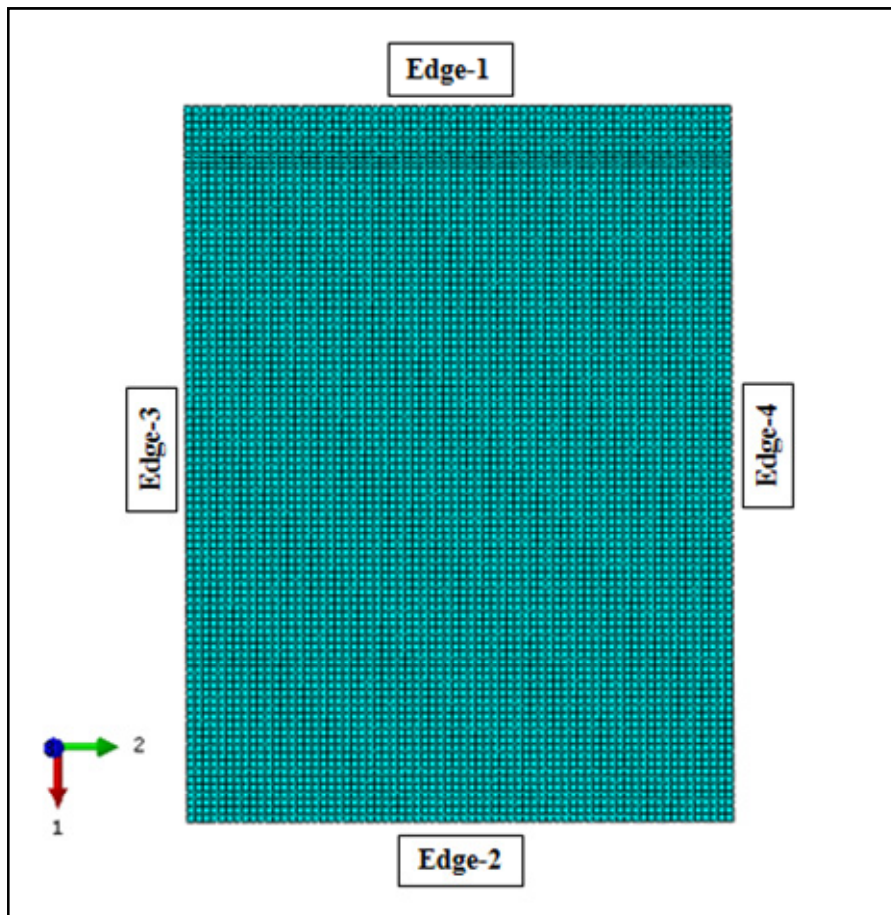


Figure 41. Finite Element Model of Laminates

Table 8. Boundary Conditions of Model [39]

Edge	Restricted Boundary Conditions
1	$v, w, \theta_x, \theta_y, \theta_z$
2	$u, v, w, \theta_x, \theta_y, \theta_z$
3	w, θ_y, θ_z
4	w, θ_y, θ_z

The built-in condition is applied by restraining all degrees of freedom on the lower edge of FE model. On the top edge, the only vertical displacement is allowed and an incremental vertical compressive load is applied. Both of side edges are only constrained in the out of plane deflection and horizontal rotations to simulate the effects of the knife edges.

Firstly, to compare with the experiments two different panels 460 mm x 350 mm were modeled. There are UD plate $[45/-45/0/45/90/90/-45/0]_s$ and in Fabric plate $[45/0/45/0/45]_s$. The nodes which are in the region clamped by the metallic blocks of fixture in the experiments have been constrained to satisfy the clamped conditions. For sides, the nodes which are in contact with the knife edges in the experiments have been constrained in the out-of-plane direction and horizontal rotation are also prevented (Figure 42).

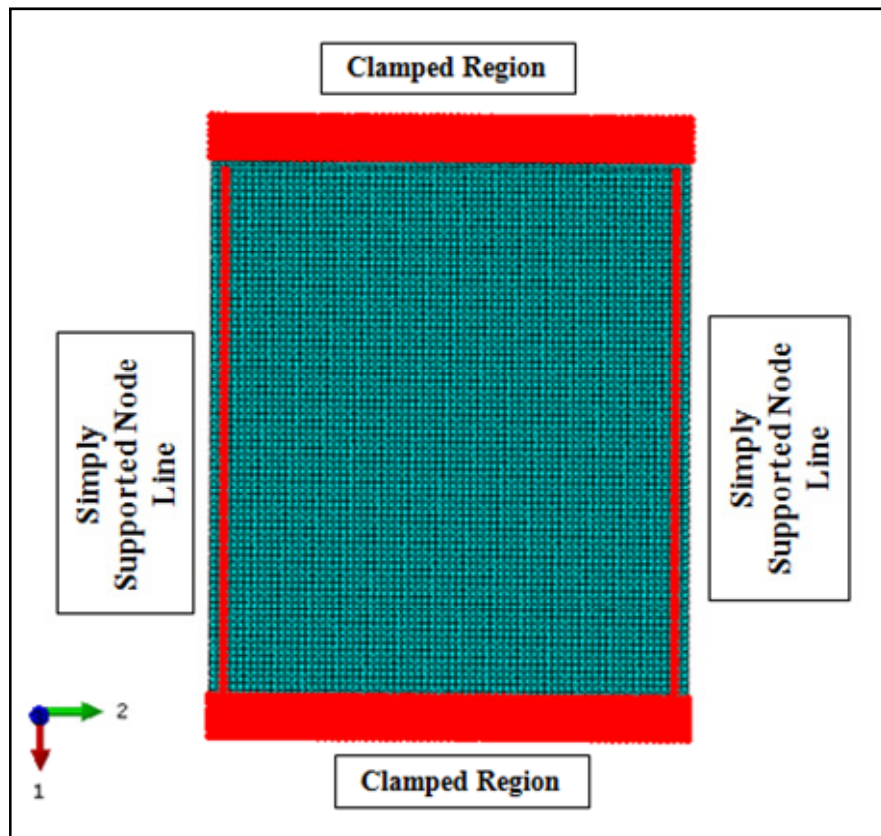


Figure 42. Constrained node region and lines on the FE model

The FE mesh consists of 6510 four-node shell elements, which are approximately 5 mm x 5 mm in size, and 6674 nodes. The gap between knife edges and metallic blocks has been modeled finer than other regions. The approximate element size is 3 mm x 5 mm for this particular unconstrained region. Two different four-noded shell elements have been used for the analyses. The unconstrained region of the FE model is shown in Figure 43;

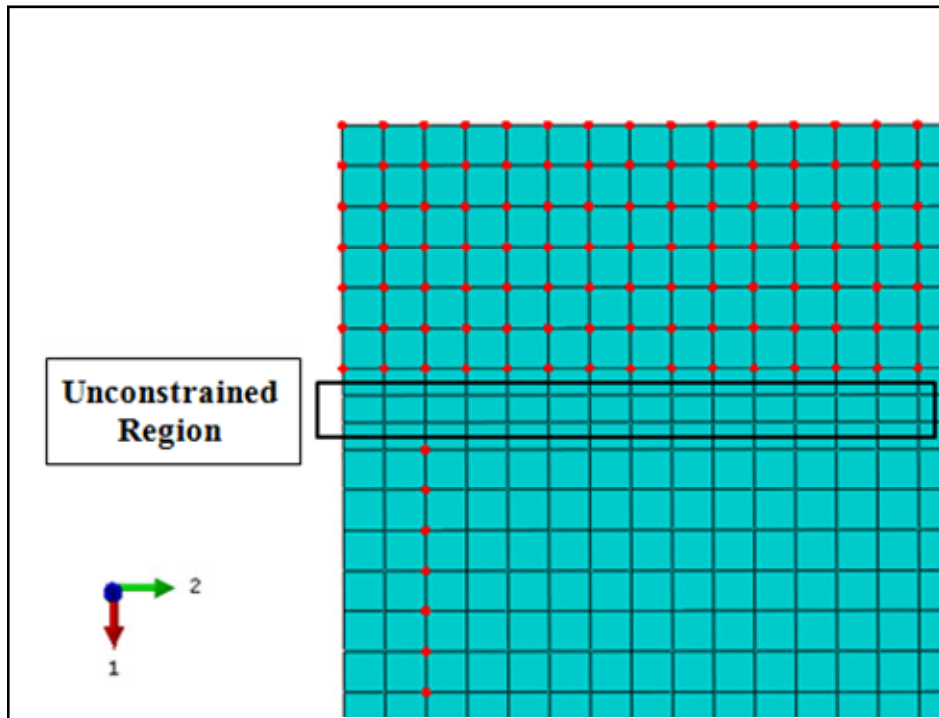


Figure 43. Unconstraint region in the FE model

The stacking sequences of the laminates are given in Figure 44 and Figure 45. The red colored lines represent the fiber directions of the plies.

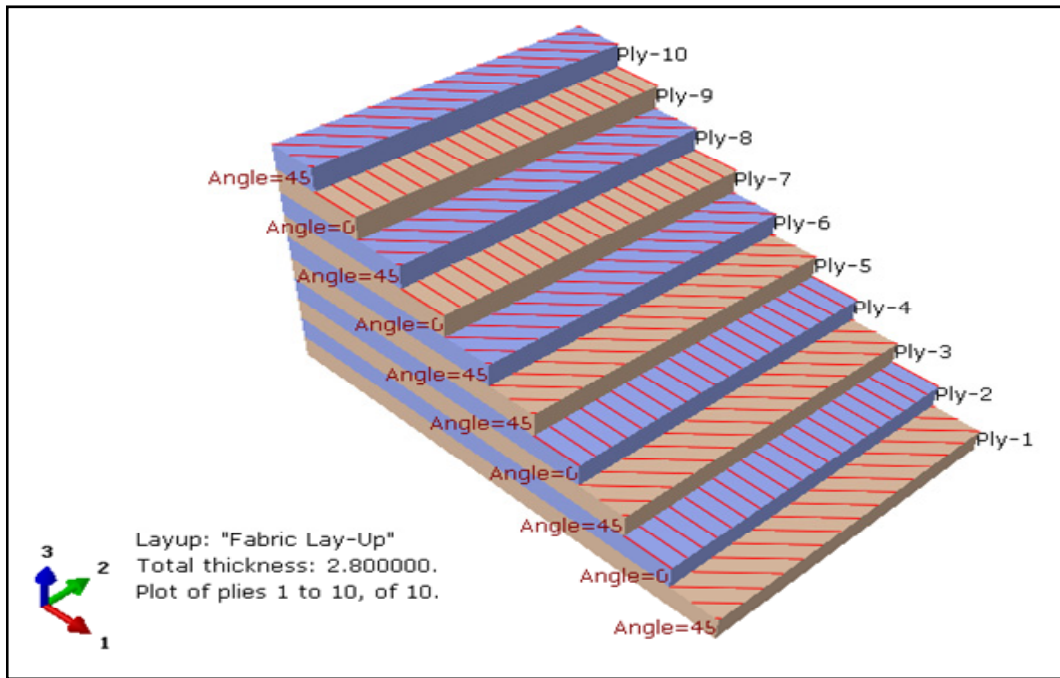


Figure 44. Ply stacking of Fabric laminate

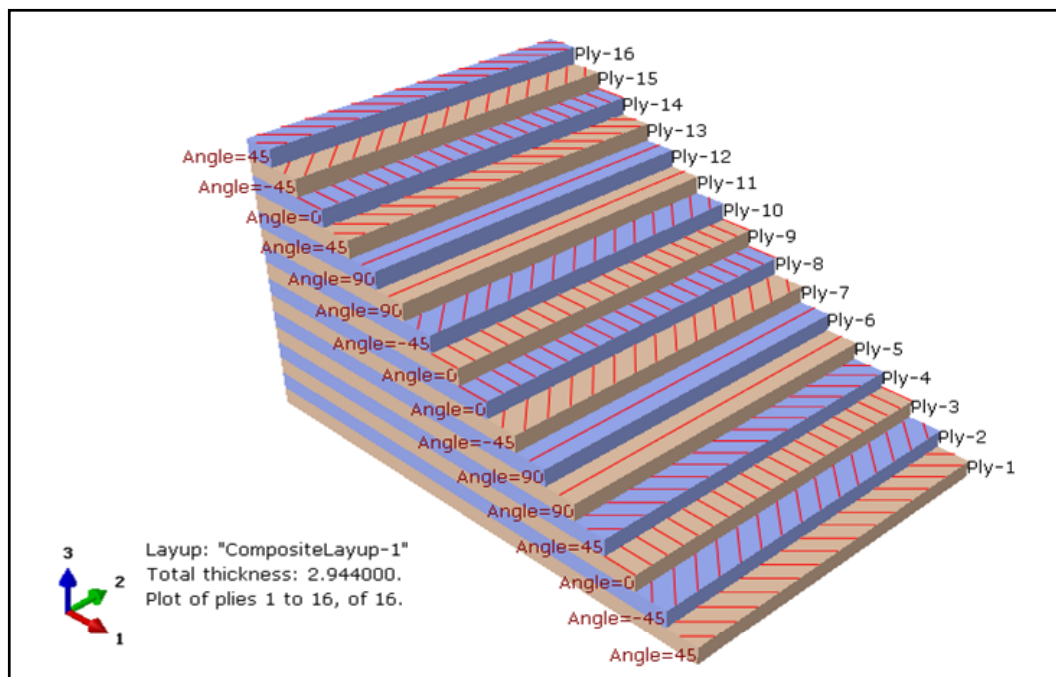


Figure 45. Ply stacking of UD laminate

6.2 Eigenvalue Buckling Results and Comparison of Elements

The critical buckling loads and mode shapes for the first buckling mode of laminates have been obtained by employing the Linear Eigenvalue Extraction method. Table 9 lists the results of the linearized buckling analyses of the laminates which are used in the experiments.

Table 9. Critical Buckling Load of Laminates

Element Type	First Eigenvalue Buckling Load (kN)	
	Full Integration	Reduced Integration
UD Laminate	22.243	22.245
FABRIC Laminate	16.300	16.298

As shown in Table 9, the critical buckling loads which are obtained from full integration and reduced integration shell elements are almost identical with each other. Out-of-plane deformation shapes of first modes are shown in Figure 46 and Figure 47.

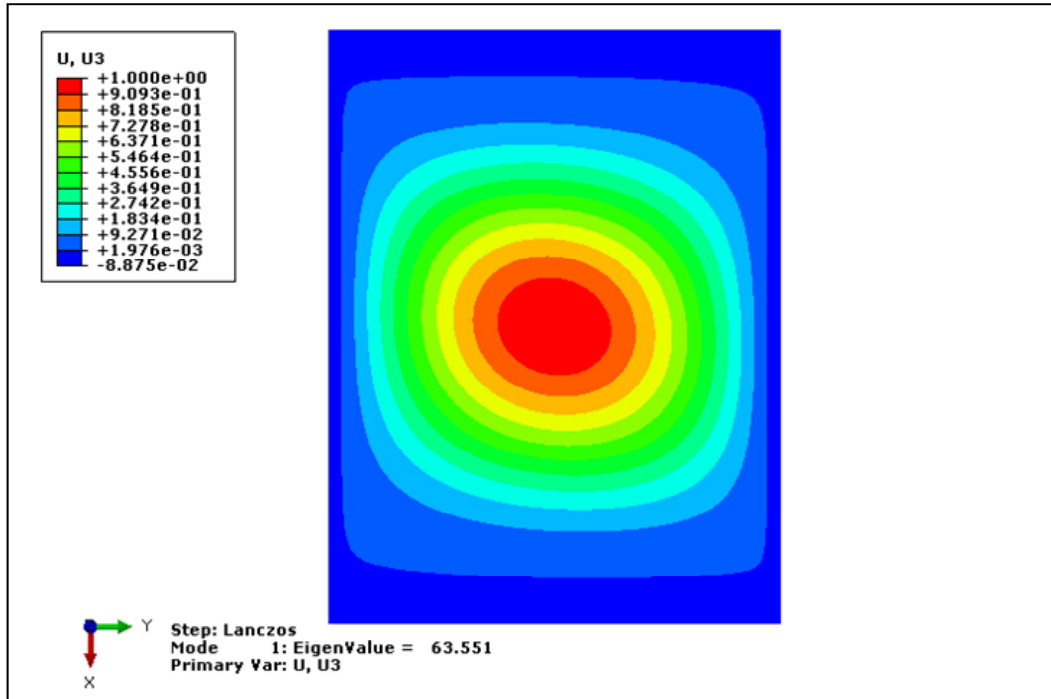


Figure 46. Out-of-plane displacement shape of UD laminate for the first mode

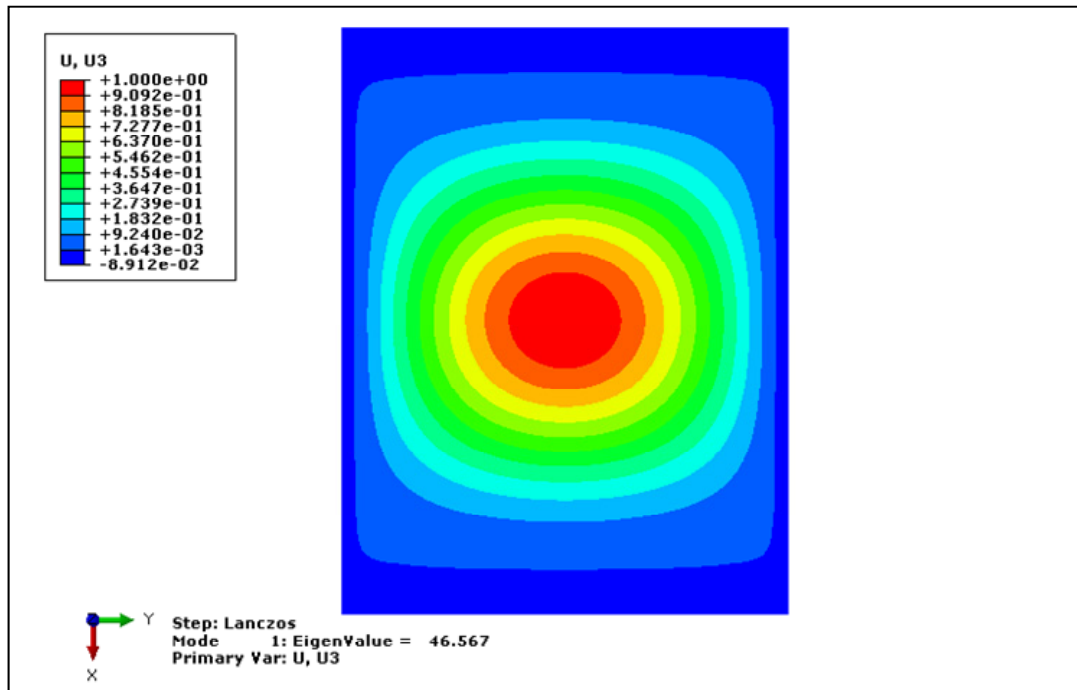


Figure 47. Out-of-plane displacement shape of FABRIC laminate for the first mode

In this section, post-buckling performances of fully integrated finite membrane strain and reduced integration finite membrane strain shell elements are compared by using load-deformation curves of UD and Fabric laminates which are obtained from FE analyses. Comparisons of elements are shown in Figure 48 and Figure 49.

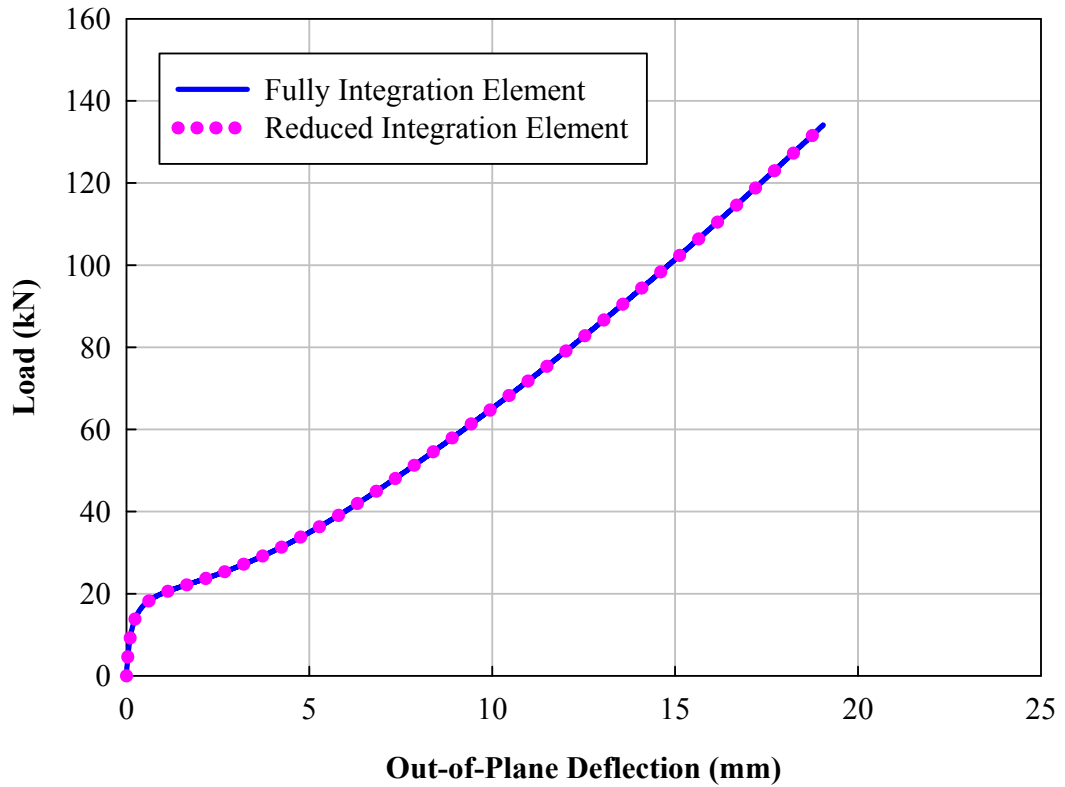


Figure 48. Load-deformation behavior of UD plates for fully and reduced integration shell elements

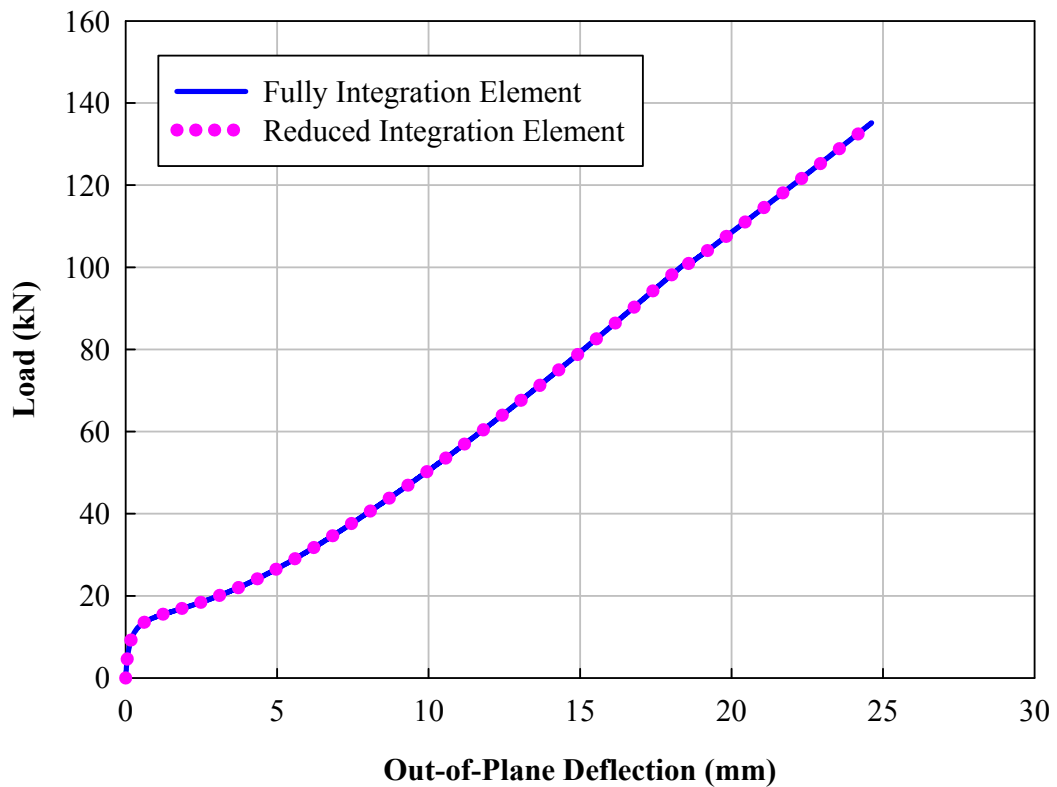


Figure 49. Load-deformation behavior of FABRIC plates for fully and reduced integration shell elements

As shown in Figure 48 and Figure 49, load-deformation curves which are obtained from FE models that consist of fully integrated and reduced integration shell elements are almost identical with each other. Computation time of fully integrated shell element is greater than the reduced integration shell element. Reduced integration elements require hourglass control and fine mesh for an accurate large displacement analysis.

6.3 Numerical Method Comparison

Newton-Raphson and Riks Method were employed for the non-linear static analyses by the used commercial finite element software. Progressive failure option was

implemented into non-linear analyses which are performed by using Newton-Raphson method because of long computation time and convergence difficulties of Riks Method with progressive failure. As shown in Figure 50 and Figure 51, the post-buckling analyses which are performed by using Riks and Newton-Raphson method with Progressive Failure Analysis are plotted and compared with each other. Comparisons showed that the numerical methods which were used in the non-linear analyses agreed well with each other.

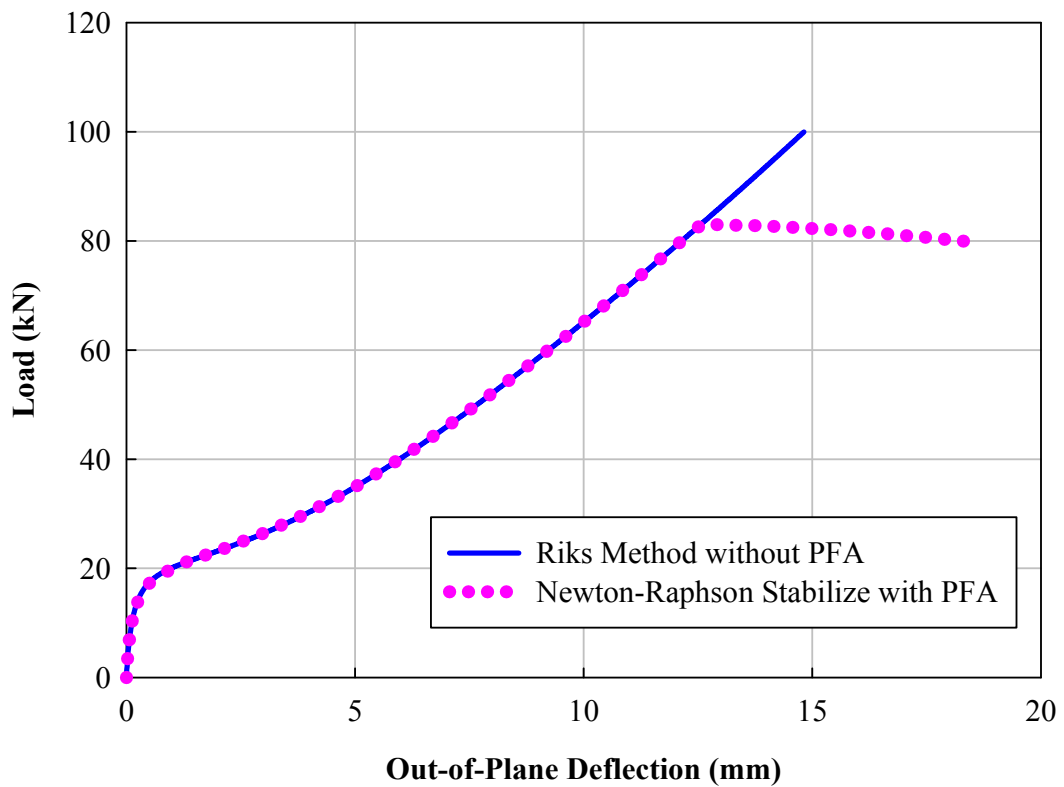


Figure 50. Load-deformation behavior of UD plates for Riks and Newton-Raphson Stabilize Methods

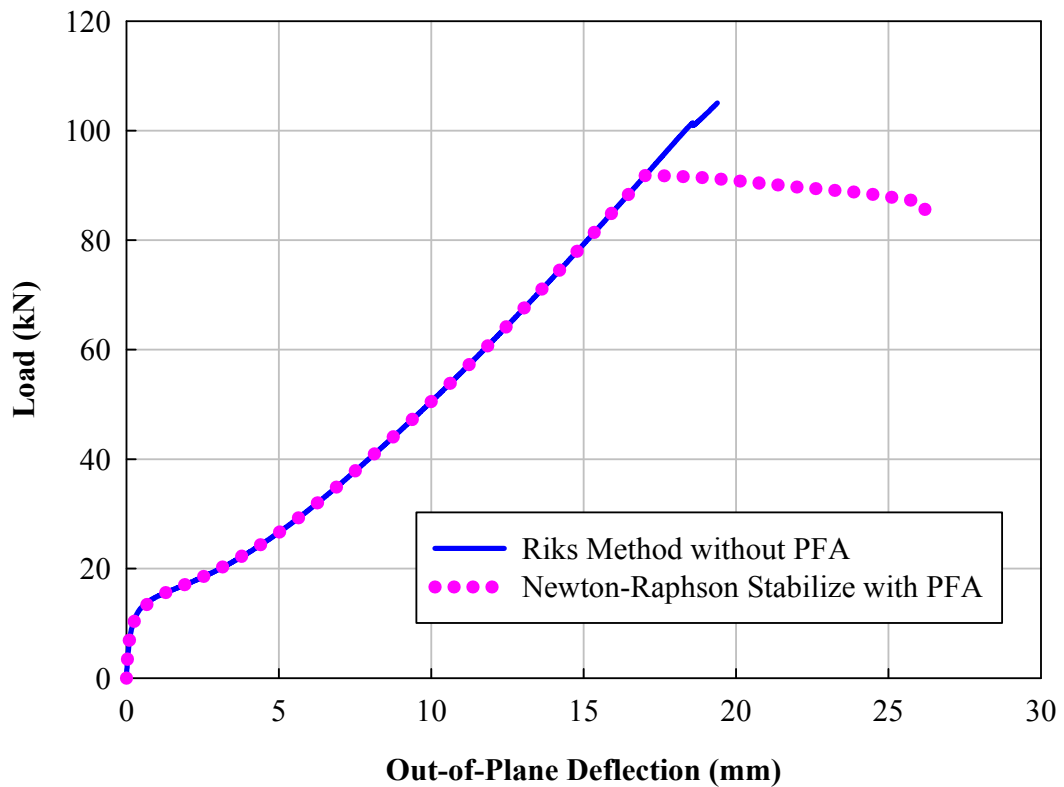


Figure 51. Load-deformation behavior of Fabric plates for Riks and Newton-Raphson Stabilize Methods

6.4 Effect of Initial Geometric Imperfection

Linear Eigen Value Analysis is often used in the design level of structures and results which are obtained from this method are valid for the perfect geometrical dimensions and material properties of structure. Nevertheless, it is difficult to attain a perfect geometry and material properties by using current manufacturing methods for the structure. Furthermore, it may not be possible to provide perfect loading and boundary condition by the test approach. Therefore, non linear static analyses were carried out by introducing initial geometric imperfections, which were determined using the mode shapes obtained from Linear Eigenvalue Analyses, into finite element models.

The same geometrical shapes of the first linear buckling modes of the plates were used in finite element analyses. The amplitudes of mode shapes were chosen to be 0.1-5% of the plates' thicknesses. Buckling and post-buckling behaviors of FE models which have different initial geometric imperfection amplitudes are shown in Figure 52 and Figure 53. The results in post-buckling range are not affected due to use of different initial imperfection amplitude. Bifurcation from primary equilibrium path to secondary equilibrium path is sharp for a perfect geometry and this sharpness becomes smoother with increasing initial geometric imperfections as shown in the figures. The buckling behaviors of plates which were tested in this thesis study are found similar with the FE results which have 5 % initial geometric imperfection.

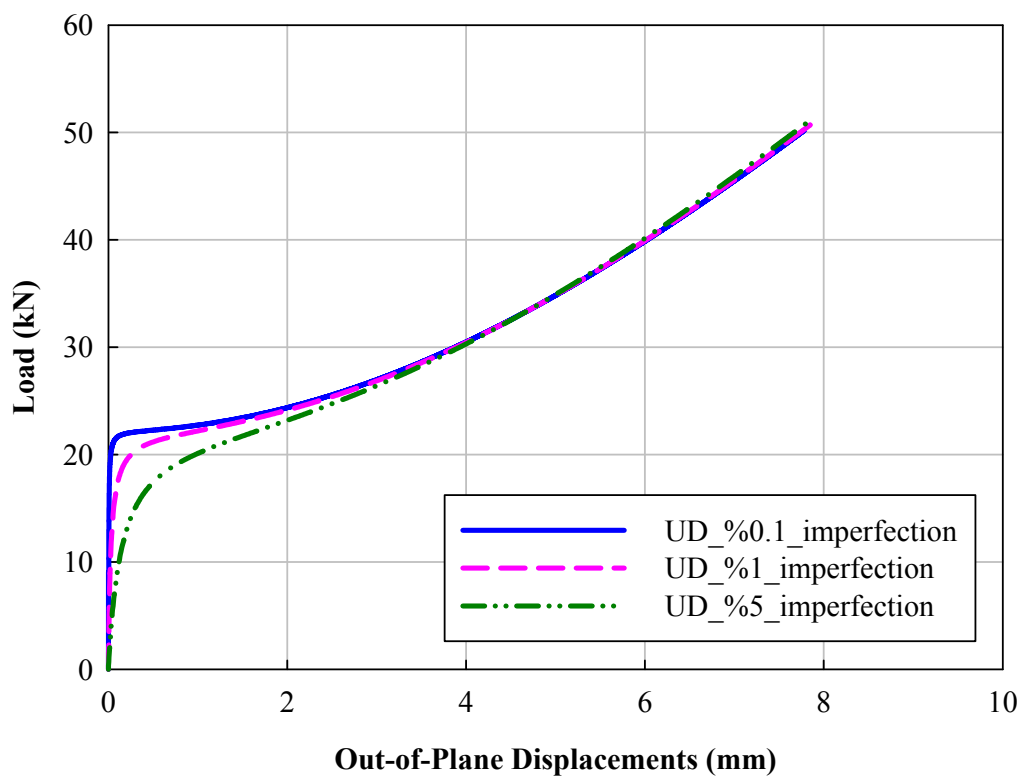


Figure 52. Buckling of UD plates with increasing initial shape imperfections

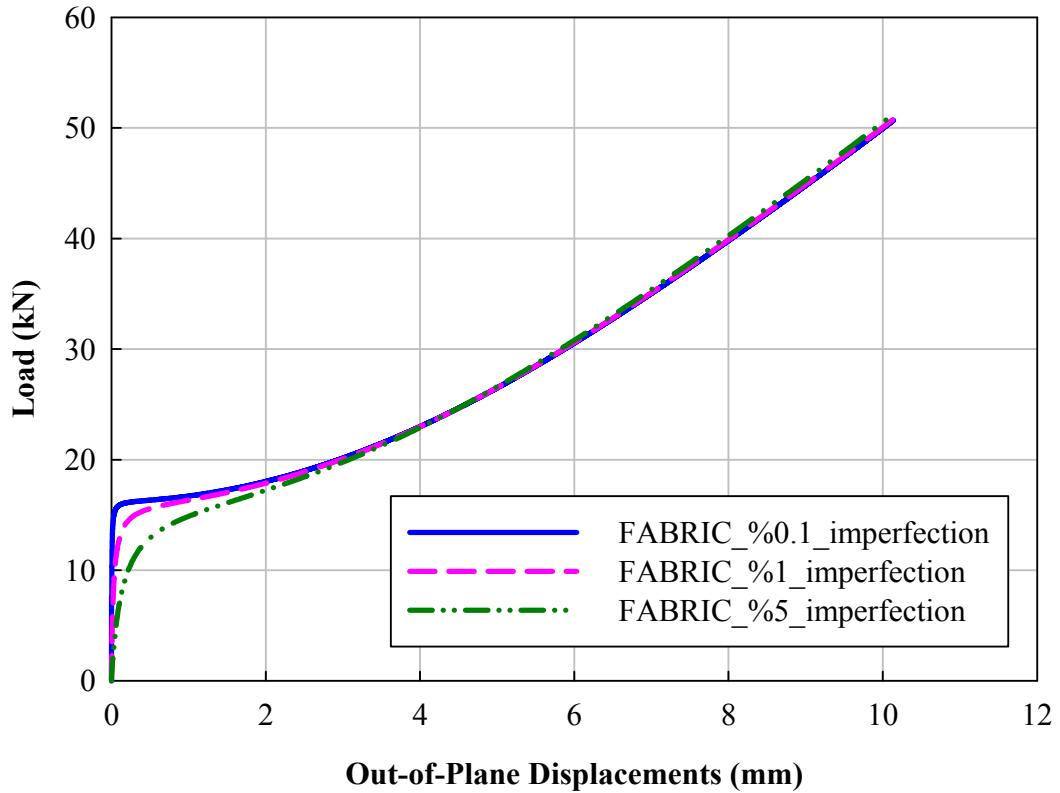


Figure 53. Buckling of FABRIC plates with increasing initial shape imperfections

6.5 Comparison of FE Results and Experiments

At first, linear eigen value analyses were conducted for the UD and FABRIC specimens and first mode shapes were scaled using an imperfection with an amplitude corresponding to 5% of plates' thicknesses. Then, two different numerical methods were carried out for the non linear analyses. These are Riks arc-length scheme and Newton-Raphson by viscous damping (adaptive automatic stabilization scheme) with the value of the energy dissipation fraction of 2×10^{-8} . Progressive failure option was introduced into non linear analyses.

In testing of specimens, the upper die was actuated with a speed of 0.01mm/sec and axial compressive reaction load which corresponded to the applied displacement was taken and plotted. Figure 54 and Figure 55 compares the experimental results with

the finite element solutions for out-of-plane displacement and end-shortening considering two unidirectional laminates UD-1 and UD-2. The first buckling mode of UD laminates has one longitudinal half-wave and maximum out-of-plane deflection is observed at center of plates. Finite element analyses have been carried out by using 5 % imperfection. The critical buckling load, which is obtained from linear Eigen value analysis, is about 22.2 kN for UD plate and agreed well with the experimental results of UD-1. Buckling of UD-2 was observed earlier in experiments than results of the linear eigen value and non linear analyses as seen in Table 9 and Figure 54. Post-buckling behavior of UD-1, obtained in the experiment, is similar with the finite element results. However, after a load level of 45 kN the out-of-plane deflection obtained by the experiment is found greater than the finite element result. On the other hand, post-buckling characteristics of UD-2 is similar with the analysis but load carrying capacity and critical buckling load are lower than the finite element result and experimental result obtained for UD-1.

As seen in Figure 54, finite element model, which includes progressive failure scheme, exhibits the structural failure of UD plate at load level of 82.981 kN. On the other hand, UD-1 failed catastrophically at a load of 84.4 kN and UD-2 failed at a load of 78 kN in the experiments. Damage initiation load of UD-1 in the experiments and finite element model is almost same with each other but failure location of UD-1 is closer to the gap between knife edges and metallic blocks. This result may be attributed to stress concentrations which occur on the corners of knife edges. Failure of UD-2 was observed earlier than expected load level.

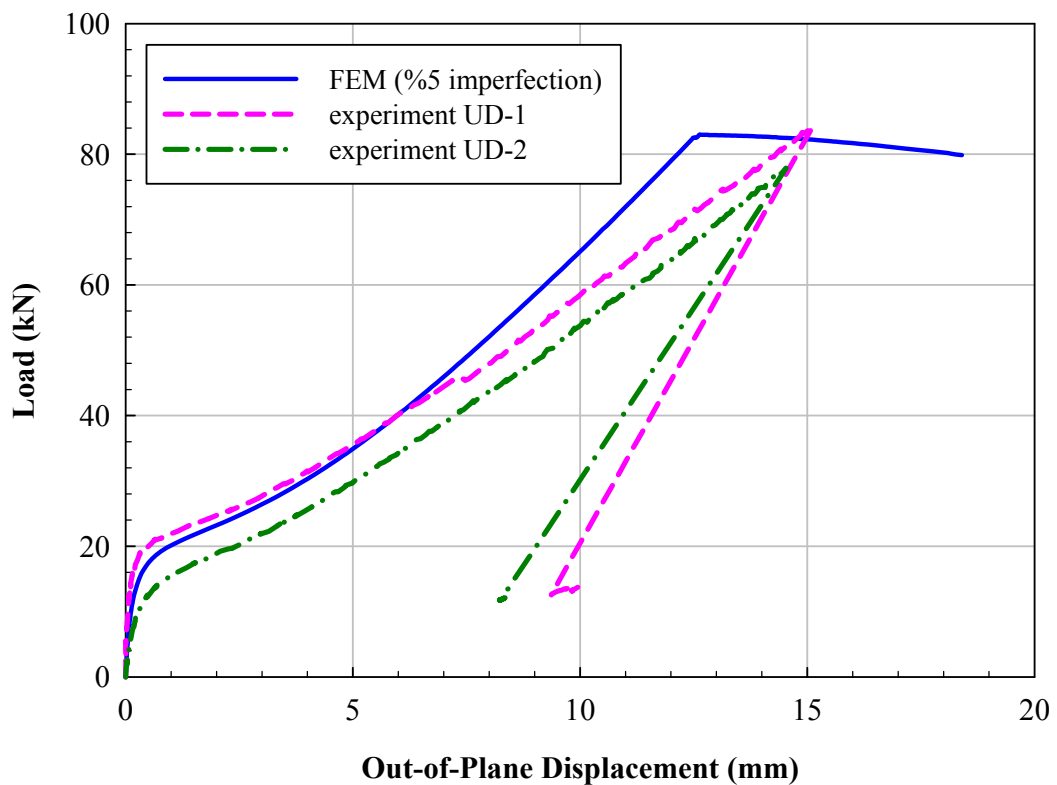


Figure 54. Load versus out-of-plane displacement curves of UD specimens and FEM Results

As seen in Figure 55, the load versus end-shortening curves of experiments shifted at the beginning of the loading. The unexpected condition in test fixture, geometry of plates or assembly tolerances can cause shifting of experimental data. Load versus end-shortening displacement curves of UD-1 and UD-2 are similar with the finite element results if shifting is neglected.

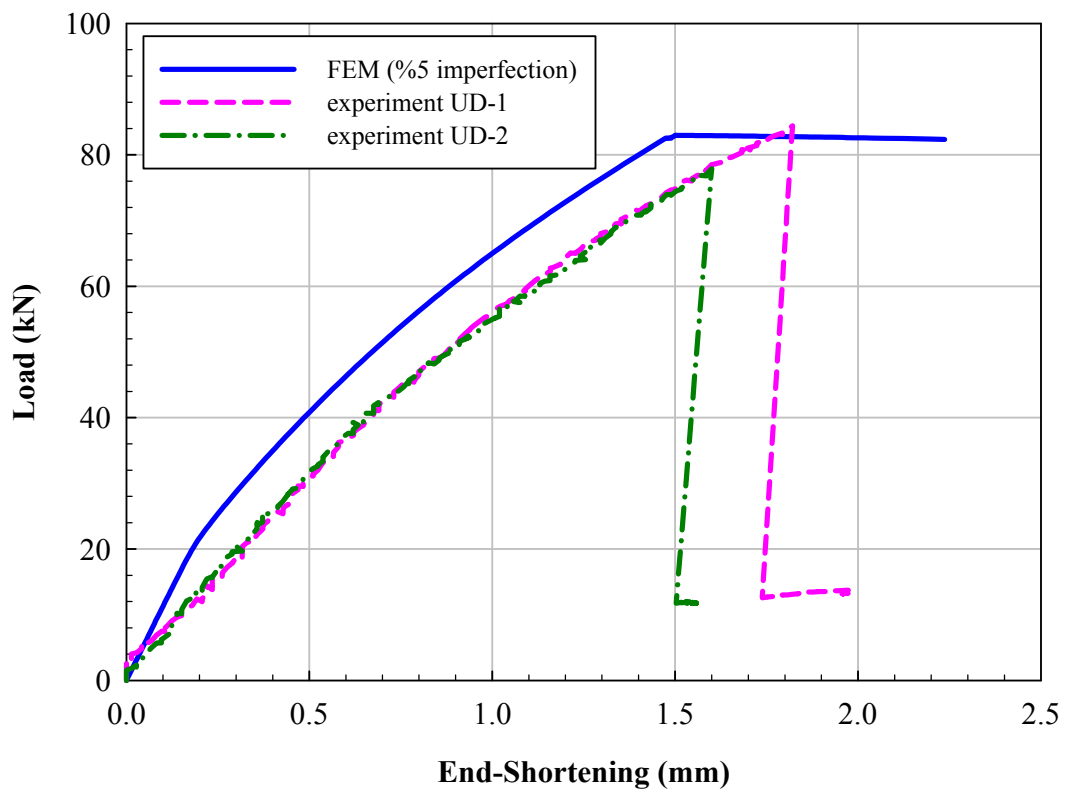


Figure 55. Load versus end-shortening displacement curves of UD specimens and FEM Results

Failure of UD-1 specimen was observed at upper end of knife edges. All of the layers in the UD-1 specimen were collapsed due to stress concentrations on the knife edges (Figure 56).



Figure 56. Failure of UD-1 Specimen

The damage initiation is first observed at the upper end of the knife edges and then propagated towards the center of specimens. The tests were stopped after observation of damage evolution (Figure 57).



Figure 57. Failure path of UD-1

In the numerical analyses, the first ply failure was observed for the layer-1 of UD laminate since compressive stress in the matrix exceeded the allowable limit as shown in Figure 58. Next matrix failure was observed at layer-16 due to tension in the same region. Figure 59 shows the compression failure indices for fibers at the load level of first matrix failure. Figure 60 shows the matrix failure progress when the first fiber failure is observed due to compression. The first fiber failure was predicted in layer-1 and layer-16 together because of compression after the matrix failures. Figure 62 shows damage evolutions of UD specimens for matrix and fiber compression.

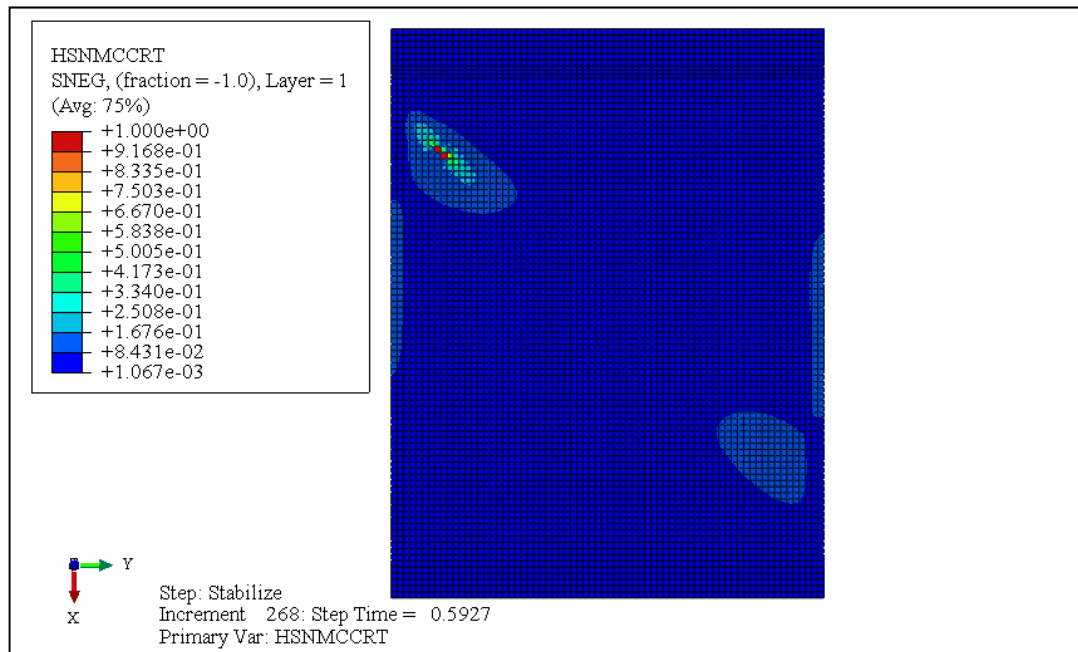


Figure 58. First ply failure of UD plate in matrix compression at load step $P=82.979$ kN (Layer 1)

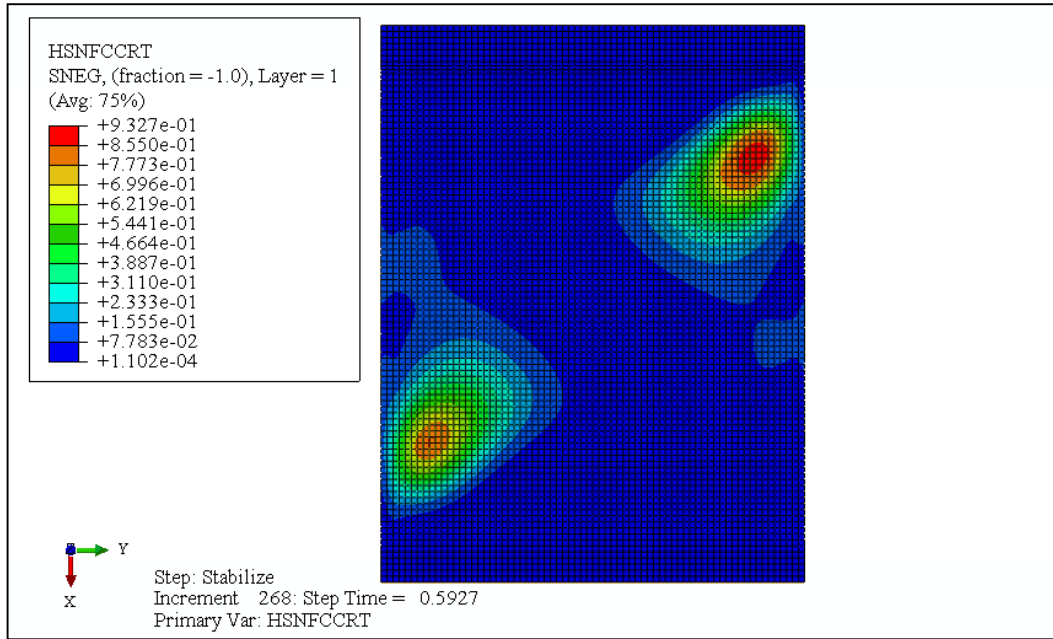


Figure 59. Fiber compression failure index with respect to Hashin's criterion at load step of first ply failure (Layer 1)

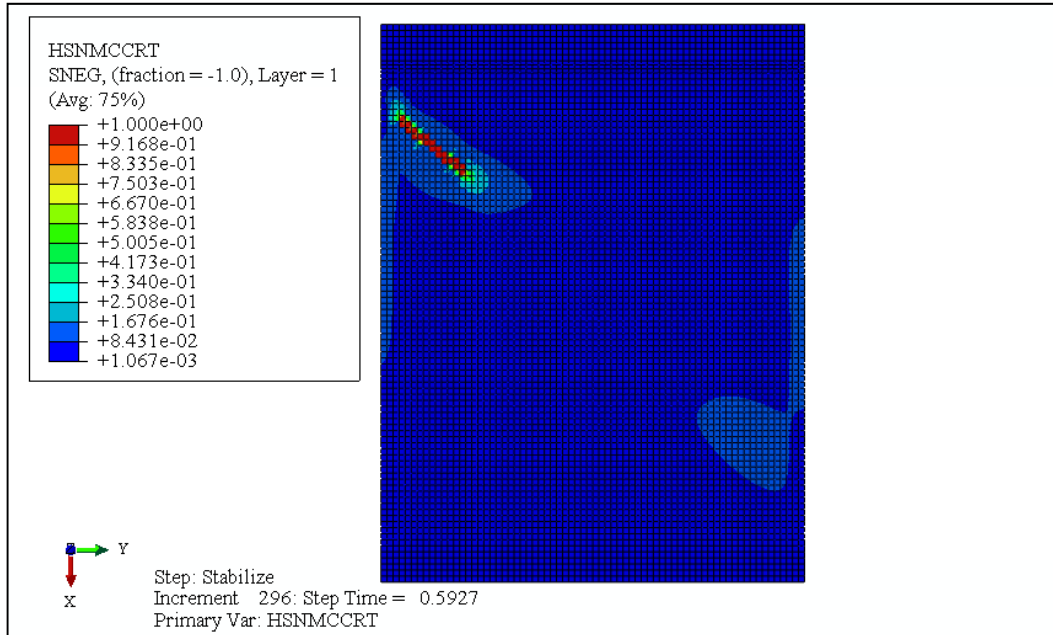


Figure 60. Matrix compression failure index of UD laminate at load step of first fiber compression failure (Layer 1)

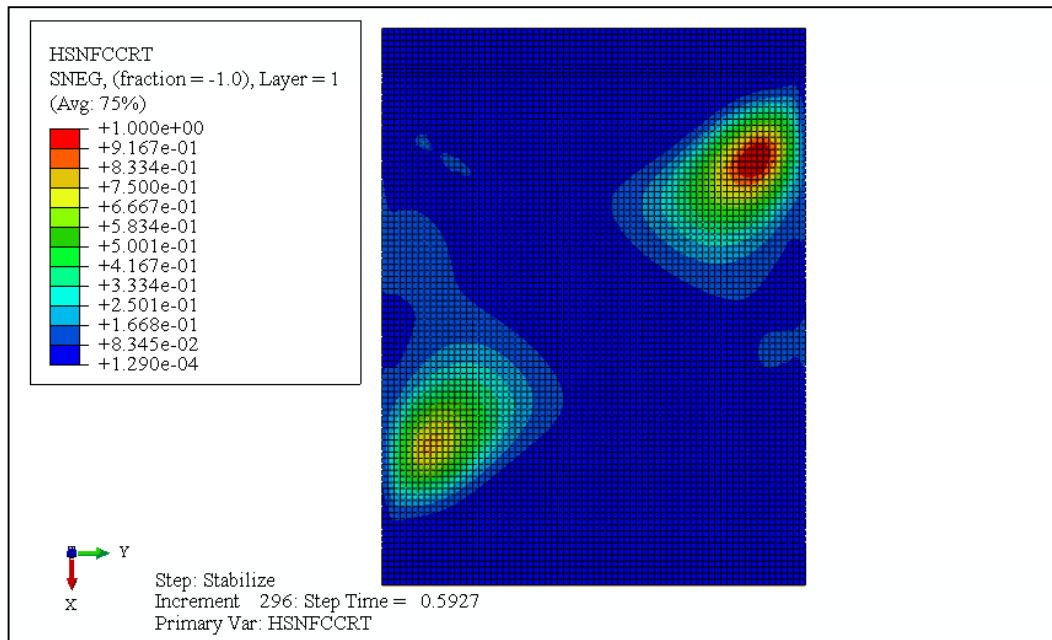


Figure 61. Fiber compression failure index of UD laminate at load step $P=82.932 \text{ kN}$
(Layer 1)

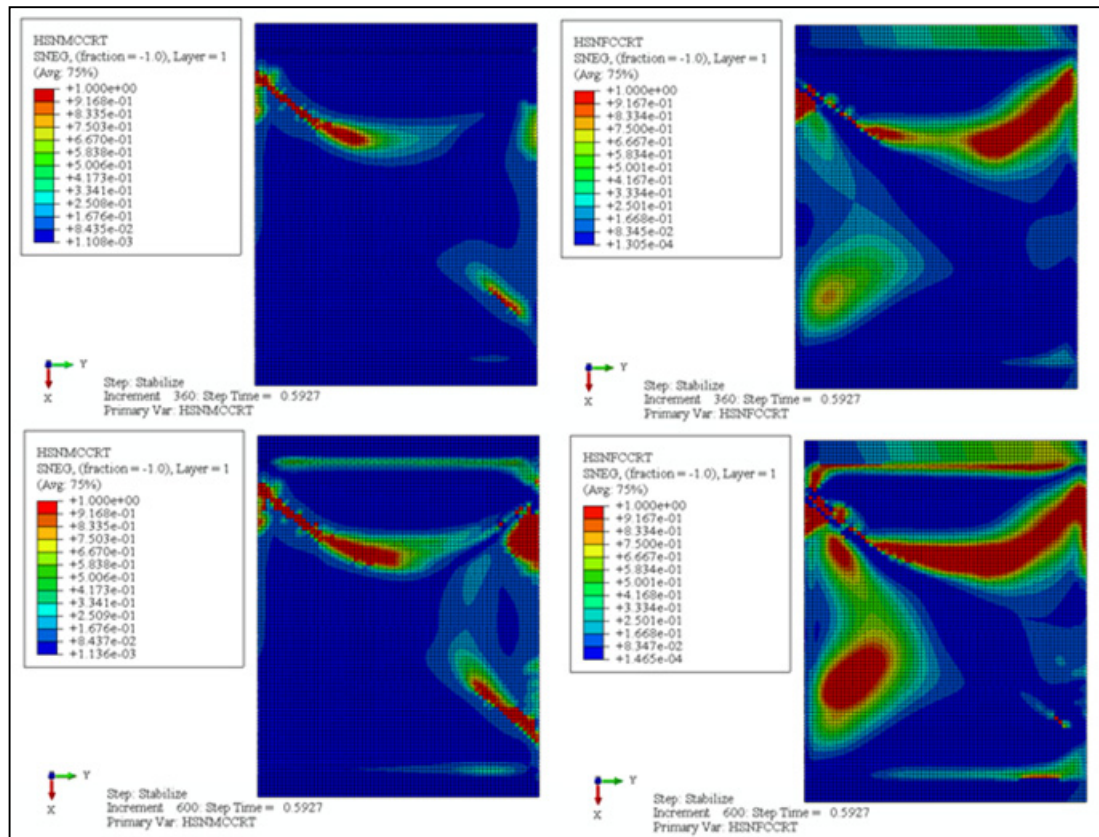


Figure 62. Damage evolution of UD laminate (Layer 1) after failure initiation (left side: matrix compression, right side: fiber compression)

The experimental and numerical load versus out-of-plane and end-shortening relations obtained for two fabric specimens FABRIC-1 and FABRIC-2 are given in Figure 63 and Figure 64 respectively. The first buckling mode of FABRIC laminates has one longitudinal half-wave and maximum out-of-plane deflection is observed at center of plates in experiments. The critical buckling load, which is obtained from linear eigen value analysis, is about 16.3 kN for FABRIC plate and agreed well with the experimental results of FABRIC-1 and FABRIC-2 specimens. However, critical buckling load of FABRIC-2 is observed earlier than results of the linear eigen value analysis, non linear analysis and FABRIC-1 as seen in Table 9 and Figure 63. Post-buckling behavior of FABRIC-1 which is obtained from experiments is similar with the finite element results. However, after a load level of 50 kN the out-of-plane deflection determined by experiments is found greater than the finite element result.

On the other hand, post-buckling characteristics of FABRIC-2 is similar with the analysis but load carrying capacity and critical buckling load are lower than the finite element analysis and experimental result of FABRIC-1.

As seen in Figure 63, finite element model, which includes progressive failure scheme, exhibits the structural failure of FABRIC plate at load level of 91.8 kN. On the other hand, FABRIC-1 failed catastrophically at a load of 77.8 kN and FABRIC-2 failed at a load of 71 kN in the experiments. In conclusion, the fabric specimens failed earlier than expected load level in the experiments.

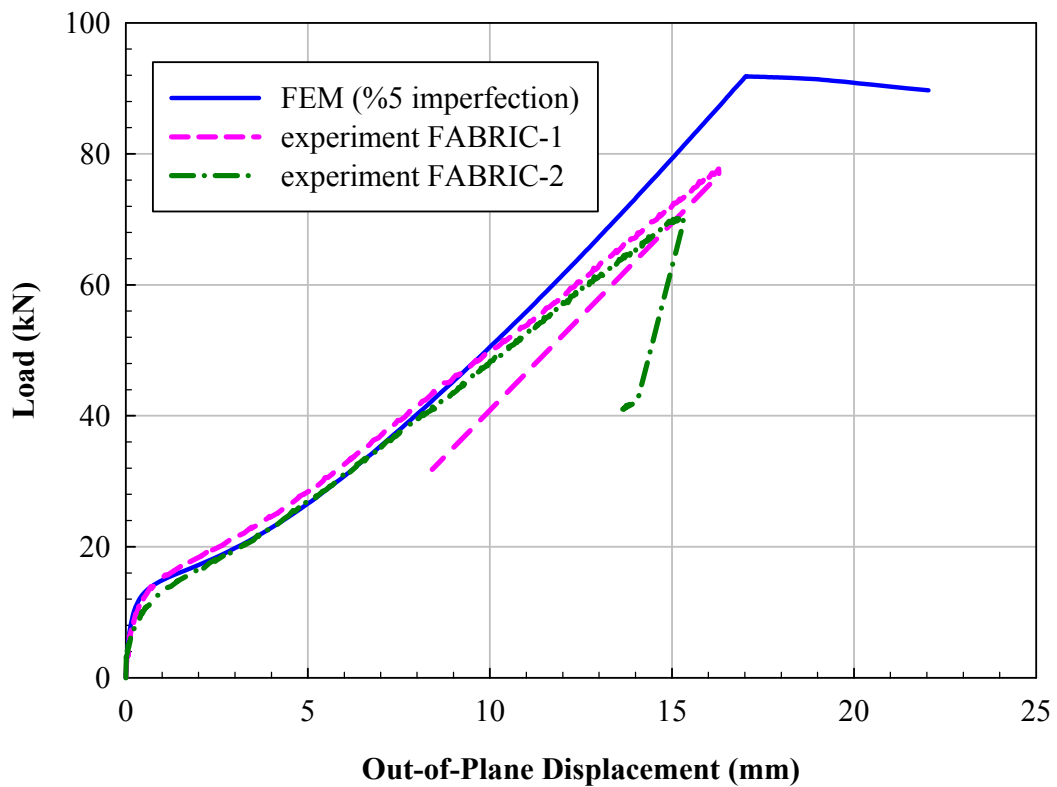


Figure 63. Load versus out-of-plane displacement curves of FABRIC specimens and FEM Results

As Figure 64 shows, load versus end-shortening displacement results of FABRIC-1 and FABRIC-2 agreed well with the experimental results. Shifting of test environment is at a negligible level. Table 10 lists the failure loads which are obtained from experiments and numerical analyses.

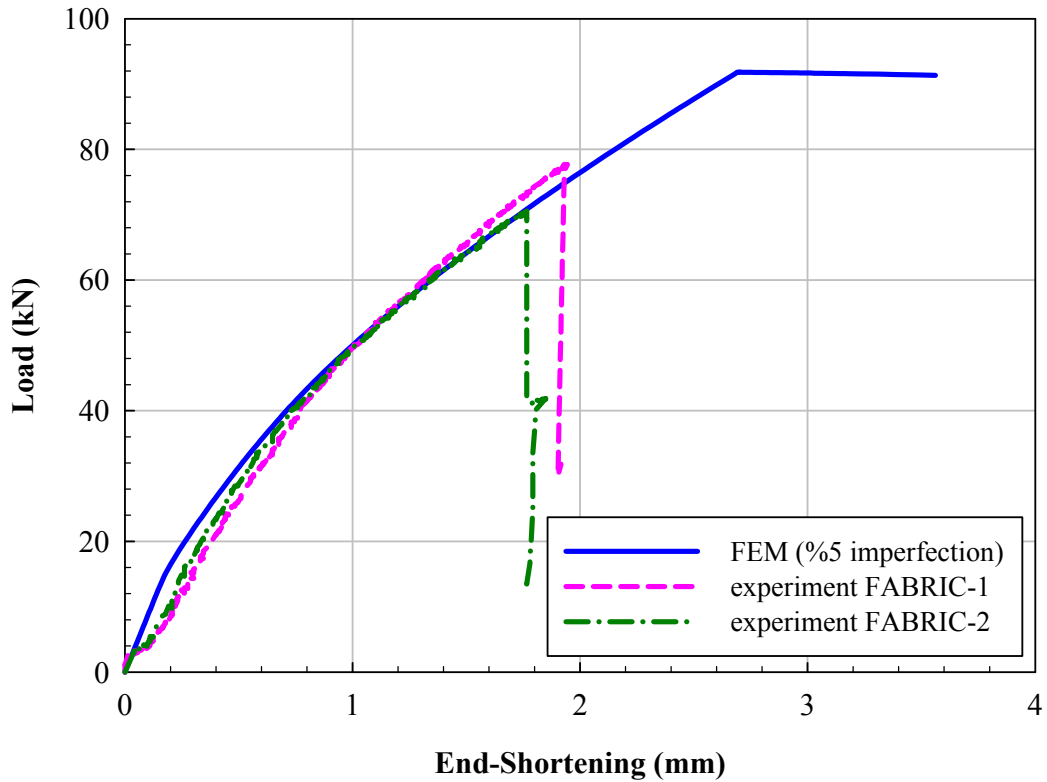


Figure 64. Load versus end-shortening displacement curves of FABRIC specimens and FEM Results

Table 10. Failure loads of specimens and differences between FE results

Specimen	Failure Load (Experiment) [kN]	Failure Load (Numerical) [kN]	Difference (%)
UD-1	84.4	82.9	1.8
UD-2	78	82.9	-5.9
FABRIC-1	77.8	91.8	-15.3
FABRIC-2	71	91.8	-22.7

In the numerical analyses, the first ply failure was observed for the layer-1 of fabric laminate since compressive stress in the matrix exceeded the allowable limit (Figure 65). Figure 66 shows the compression failure indices for fibers at the load level of first matrix failure. The first fiber failure was predicted in layer-1 because of compression after the matrix failure. Figure 67 shows the matrix failure progress when the first fiber failure is observed due to compression. The first fiber failure was predicted in layer-1 because of compression after the matrix failures. Figure 69 shows damage evolutions of Fabric specimens for matrix and fiber compression.

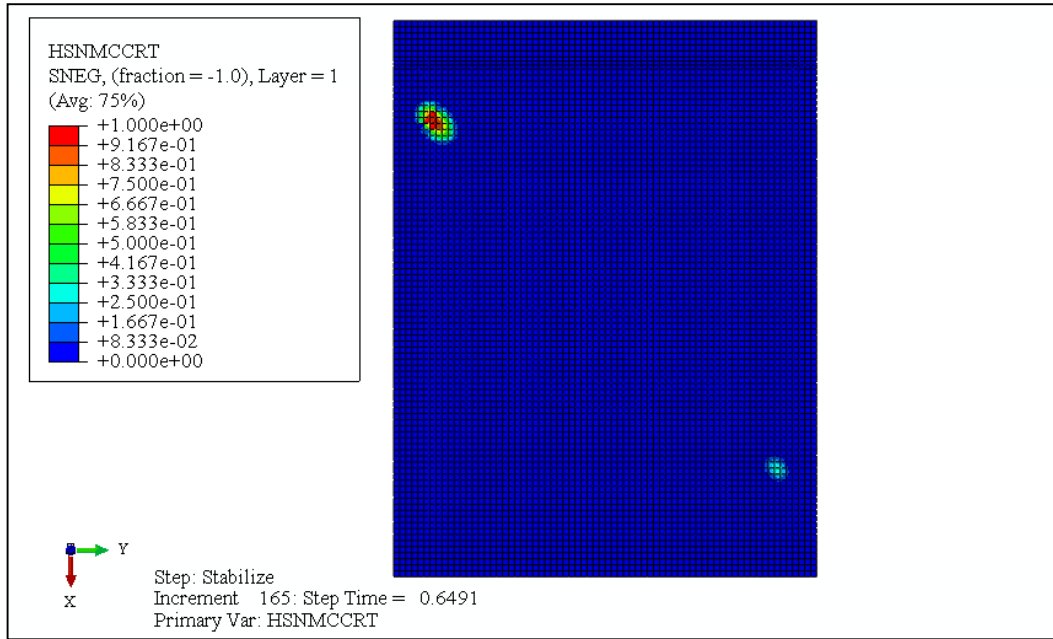


Figure 65. First ply failure of fabric laminate in matrix compression at load $P=90.877\text{ kN}$ (Layer 1)

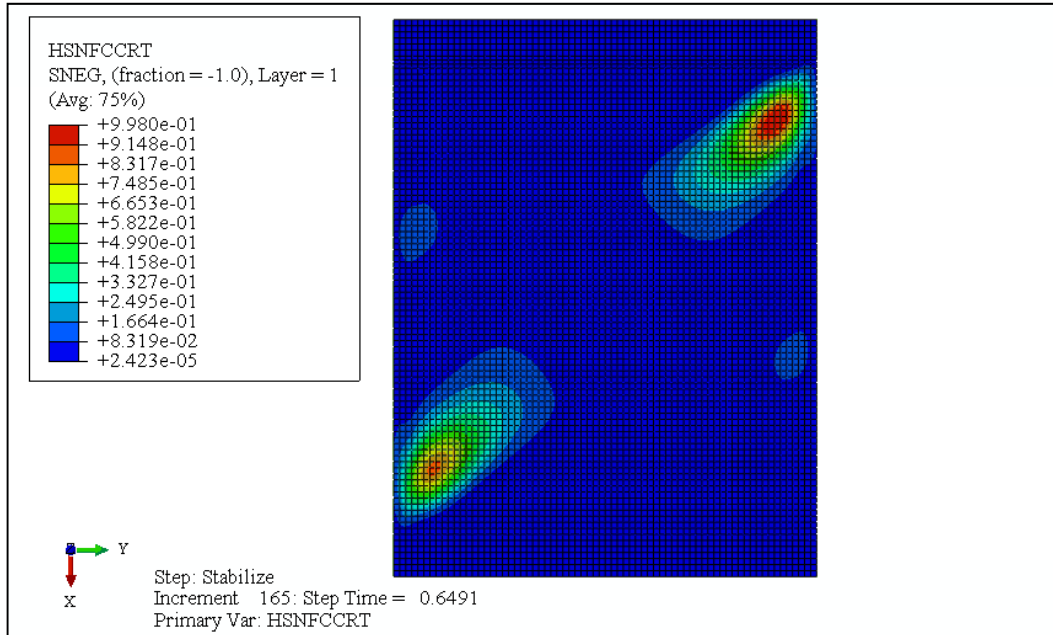


Figure 66. Fiber compression failure index of fabric laminate at load $P=90.877\text{ kN}$ (Layer 1)

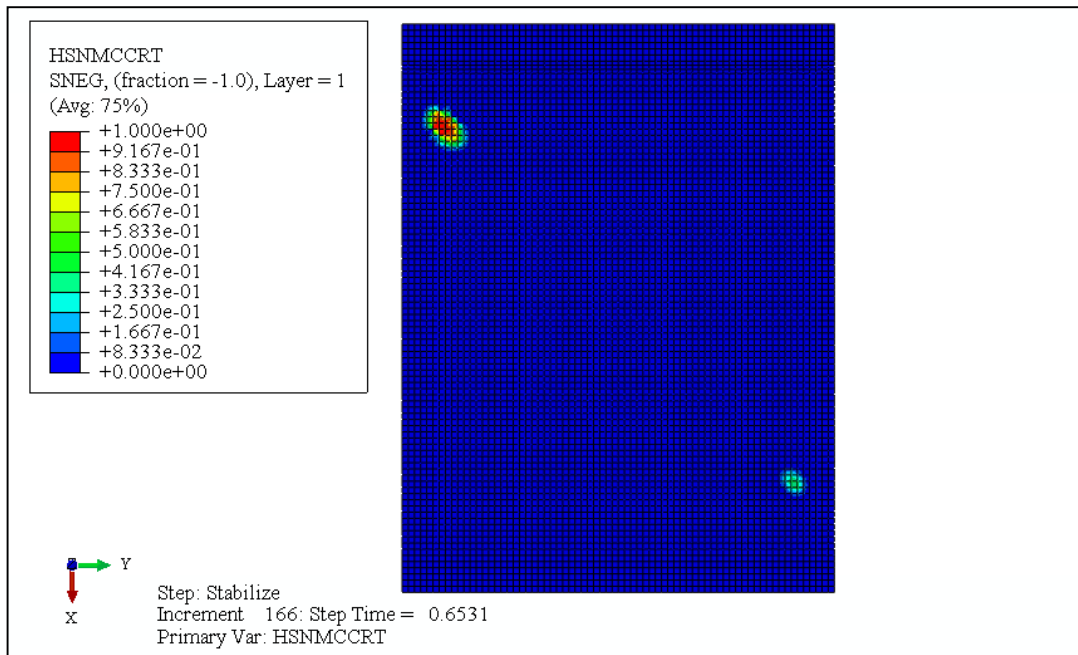


Figure 67. Matrix compression failure index at load $P=91.437\text{ kN}$ (Layer 1)

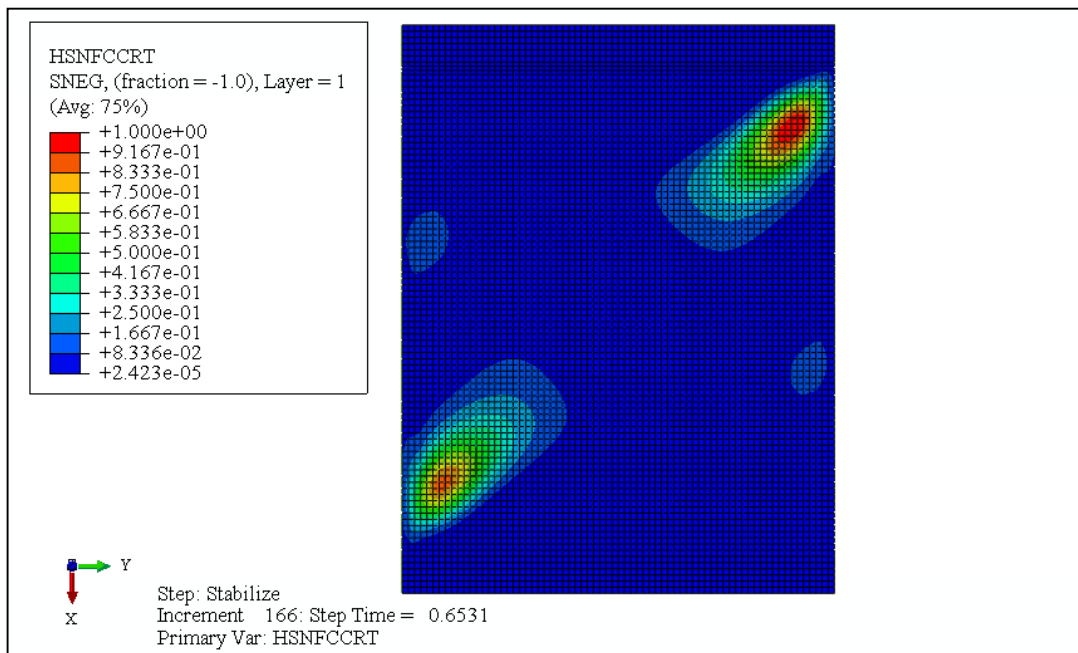


Figure 68. Fiber compression failure index of fabric laminate at load $P=91.437\text{ kN}$ (Layer 1)

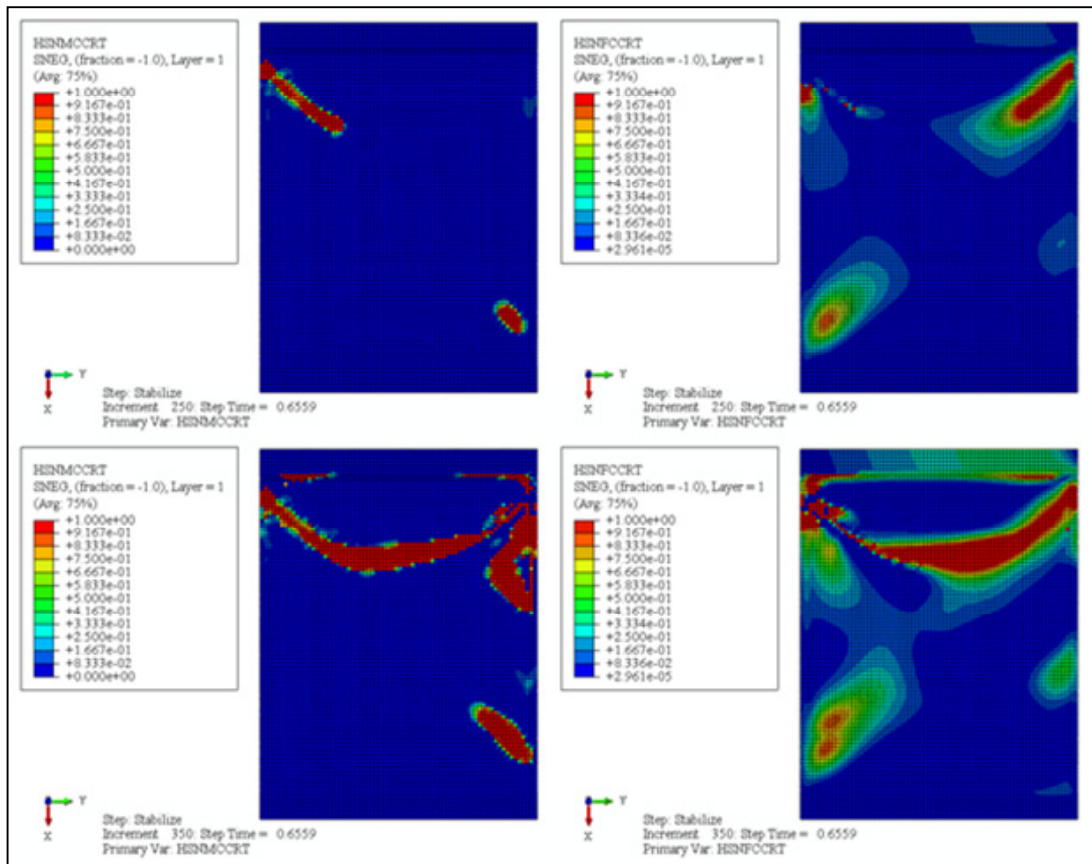


Figure 69. Damage evolution of fabric laminate in Layer 1 after failure initiation (left side: matrix compression, right side: fiber compression)

CHAPTER 7

EFFECTS OF PLY ANGLE AND THICKNESS ON BUCKLING AND POSTBUCKLING

After comparing the experimental results with the numerical ones and verifying the finite element results. A number of numerical analyses have been realized to evaluate the effect of ply angle orientations and thicknesses on the composite laminates. Results are presented to investigate critical buckling loads, post-buckling behaviors and failure characteristics of different laminates. The finite element models of UD and Fabric plates, which were used for validation of experiments, were modified for various ply angles and stacking sequences. Boundary conditions, loading type, material properties and element types were kept as is on the finite element models.

At first, linear eigen value analyses were performed and critical buckling loads, geometrical shape of the first buckling modes were obtained. Secondly, non-linear analyses with progressive failure scheme were carried out by using finite element models including initial geometric imperfections which were determined using the first mode shapes obtained from linear eigen value analyses. The amplitude of initial geometric imperfections were assumed 1% of the panel thicknesses for these numerical examples. At the end of the analyses, the changes on the critical buckling loads, mode shapes, post-buckling behaviors and failure characteristics of laminates by ply angle variation and thickness were investigated and plotted.

The material of first model is AS4/8552 Carbon Fiber Reinforced UD Tape and the stacking sequences are $[\theta/-\theta]_s$, $[\theta/-\theta]_{2s}$, $[\theta/-\theta]_{4s}$, with the 0.184 mm ply thickness. The material of second model is AS4/8552 Carbon Fiber Reinforced 5HS Fabric and the stacking sequences are $[\theta/-\theta]_s$, $[\theta/-\theta/\theta/-\theta/\theta]_s$, $[\theta/-\theta]_{4s}$ with the 0.28 mm ply thickness.

7.1 Variation of Critical Buckling Load with Ply Angle

The variations of critical buckling loads with ply angle have been determined for the laminates which have the same thicknesses that were used in the experiments.

As shown in Figure 70, angle variation does not affect excessively the critical buckling loads of Fabric laminates due to quasi-isotropic material properties of AS4/8552 5HS Fabric prepreg. However, the critical buckling loads of UD laminates decrease with increasing ply angle since longitudinal stiffness of AS4/8552 UD tape is greater than transverse stiffness.

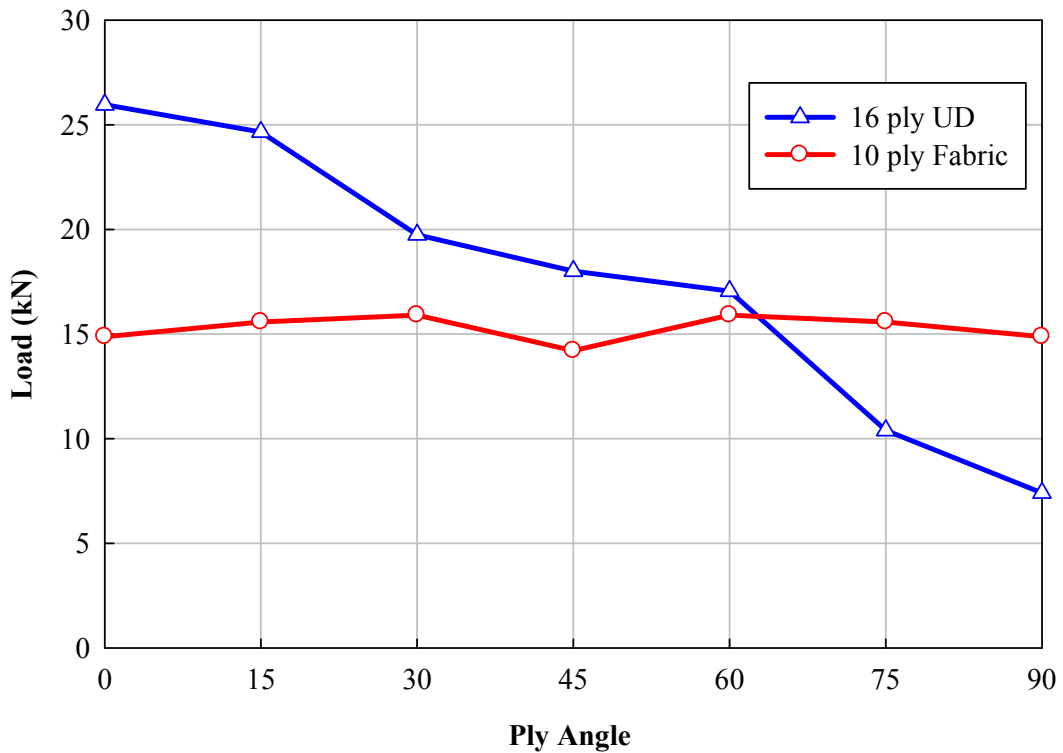


Figure 70. Variation of critical buckling loads of angle ply $[\theta/-\theta]_{4S}$ UD laminates and $[\theta/-\theta/\theta/-\theta/\theta]_S$ Fabric laminates

Furthermore, first buckling modes of UD and Fabric laminates have one longitudinal half wave patterns except $[60/-60]_{4s}$, $[75/-75]_{4s}$, $[90/-90]_{4s}$ UD laminates. These laminates have two longitudinal half wave pattern for first buckling mode.

7.2 Effects of Thickness and Ply Angle Variation on Buckling Load and Post-buckling Behavior for UD Laminates

The critical buckling load levels of UD laminates increase with increasing laminate thickness (Figure 71). First buckling modes of UD laminates for each laminate thickness have one longitudinal half wave patterns except 60, 75 and 90 degree oriented UD laminates. These laminates have two longitudinal half wave patterns in first buckling mode for each laminate thickness.

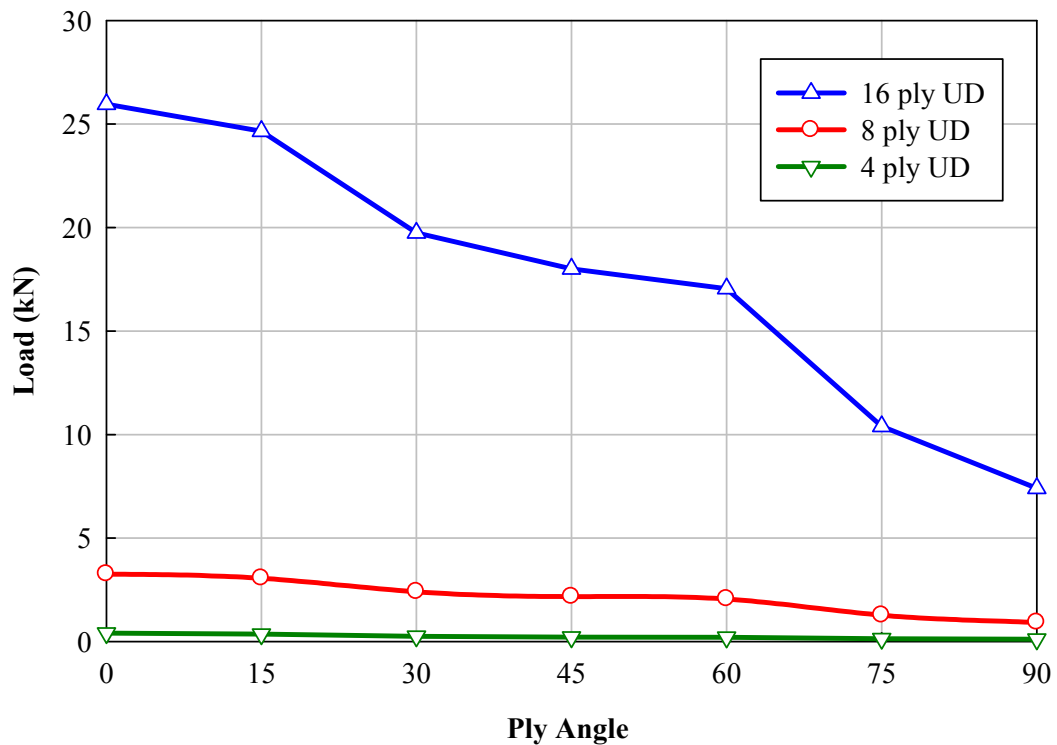


Figure 71. Variation of critical buckling loads of angle ply $[\theta/-\theta]_s$, $[\theta/-\theta]_{2s}$, $[\theta/-\theta]_{4s}$ UD laminates

As shown in Figure 72, $[0/-0]_S$ UD laminate have higher buckling load than $[15/-15]_S$ UD laminate but failure strength of $[15/-15]_S$ is greater than $[0/-0]_S$. The first buckling mode shapes of laminates which are $[60/-60]_S$, $[75/-75]_S$ and $[90/-90]_S$ have two longitudinal half waves and the other laminates have one. On the other hand, $[45/-45]_S$ laminate was observed to buckle in one half wave at the loading 0.22 kN and a mode-jump to two half-waves occurred at the loading 2.9 kN.

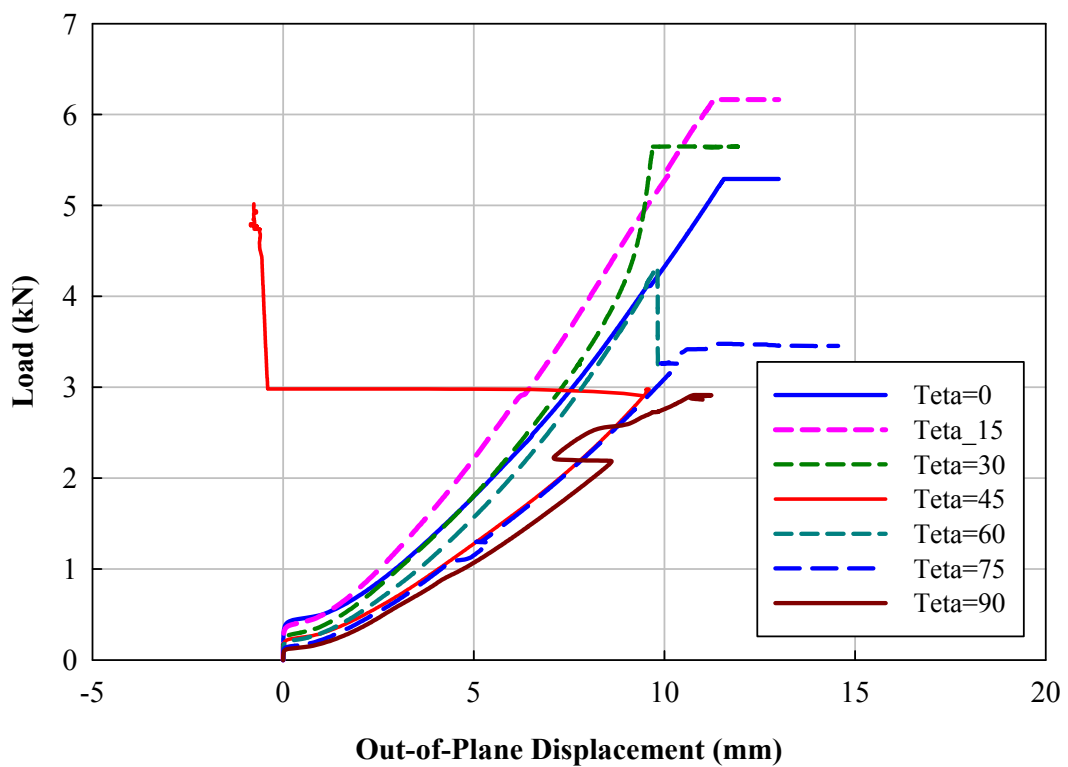


Figure 72. Load versus out-of-plane displacements of angle ply $[\theta/-\theta]_S$ UD laminates

Mechanical stiffness of $[0/-0]_s$, $[15/-15]_s$, $[30/-30]_s$ are similar with each other. Load-carrying capacities of the other laminates decrease gradually (Figure 73). The lowest load-carrying capacity is observed for $[90/-90]_s$ UD laminate in longitudinal direction. Table 11 lists the critical buckling loads and failure loads of $[\theta/-\theta]_s$ UD laminates.

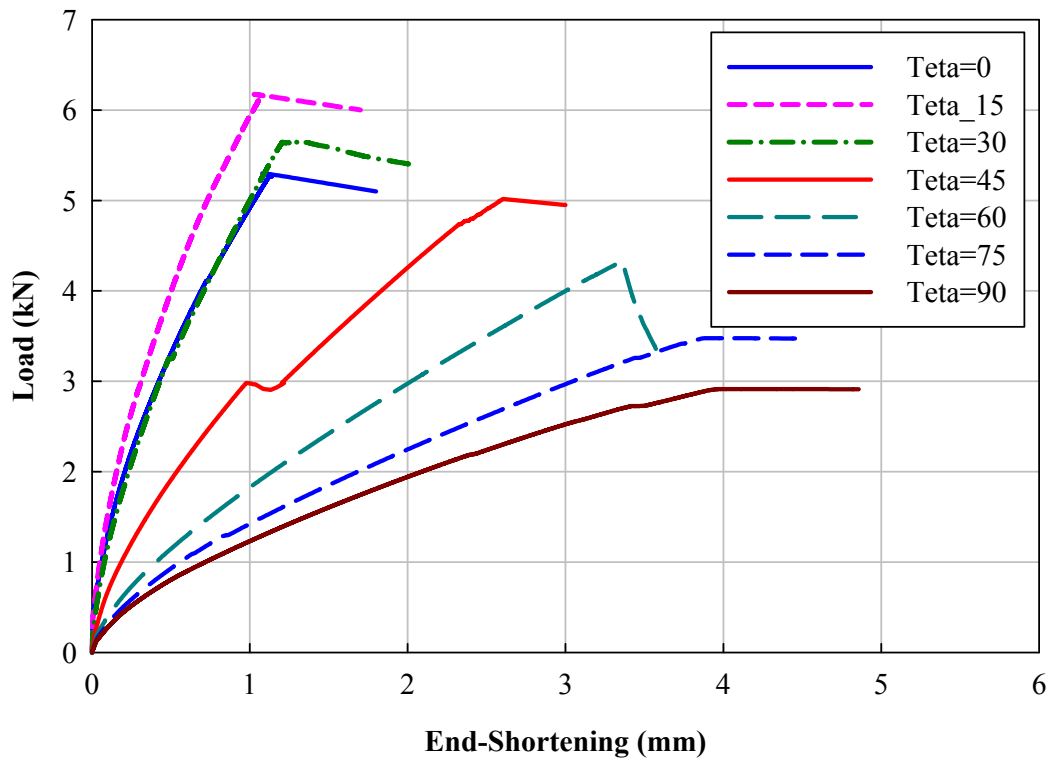


Figure 73. Load versus end-shortening displacements of angle ply $[\theta/-\theta]_s$ UD laminates

Table 11. Buckling and failure loads of angle ply $[\theta/-\theta]_s$ UD laminates

Laminate	Buckling Load [kN]	Failure Load [kN]
$[0/-0]_s$	0.41	5.3
$[15/-15]_s$	0.36	6.2
$[30/-30]_s$	0.26	5.6
$[45/-45]_s$	0.22	5.0
$[60/-60]_s$	0.21	4.3
$[75/-75]_s$	0.14	3.5
$[90/-90]_s$	0.12	2.9

As shown in Figure 74, $[0/-0]_{2S}$ UD laminate have higher buckling load than $[15/-15]_{2S}$ UD laminate but failure strength of $[15/-15]_{2S}$ is greater than $[0/-0]_{2S}$. The first buckling mode shapes of laminates which are $[60/-60]_{2S}$, $[75/-75]_{2S}$ and $[90/-90]_{2S}$ have two longitudinal half wave and the other laminates have one. On the other hand, $[75/-75]_{2S}$ laminate was observed to buckle in one half wave at the loading 1.3 kN and a mode-jump to two half-waves occurred at the loading 11 kN.

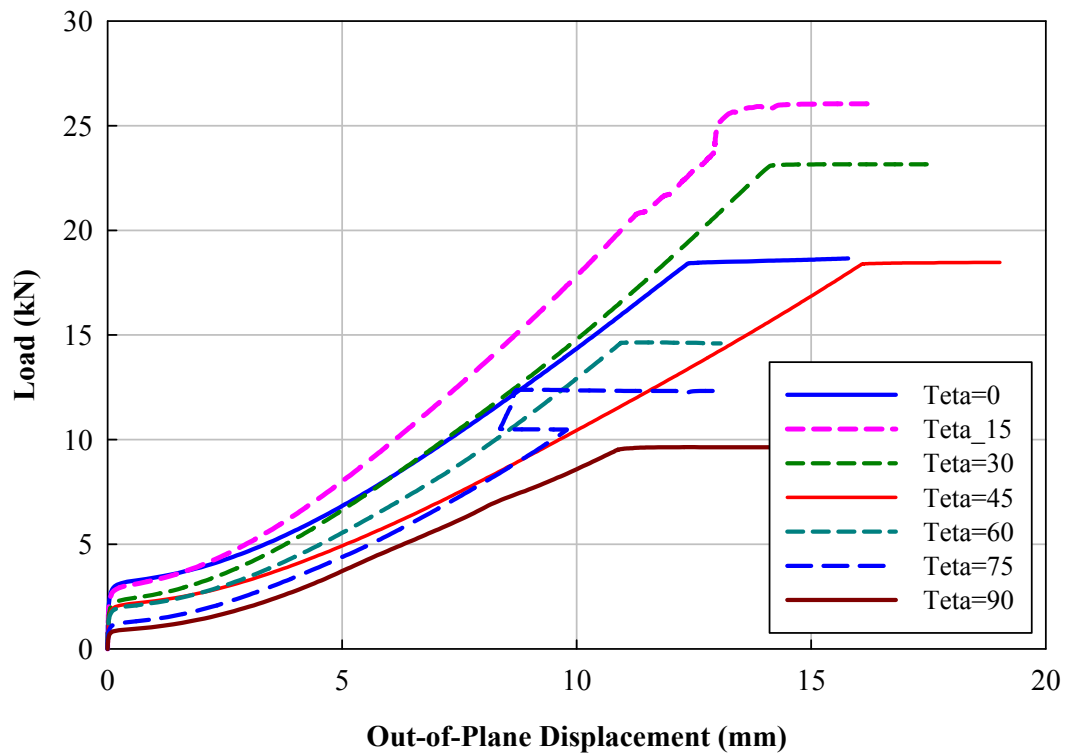


Figure 74. Load versus out-of-plane displacements of angle ply $[\theta/-\theta]_{2S}$ UD laminates

Mechanical stiffness of $[0/-0]_{2S}$, $[15/-15]_{2S}$, $[30/-30]_{2S}$ are similar with each other (Figure 75). Load-carrying capacities of the other laminates decrease gradually. The lowest load-carrying capacity is observed for $[90/-90]_{2S}$ UD laminate in longitudinal direction. Table 12 lists the critical buckling loads and failure loads of $[\theta/-\theta]_{2S}$ UD laminates.

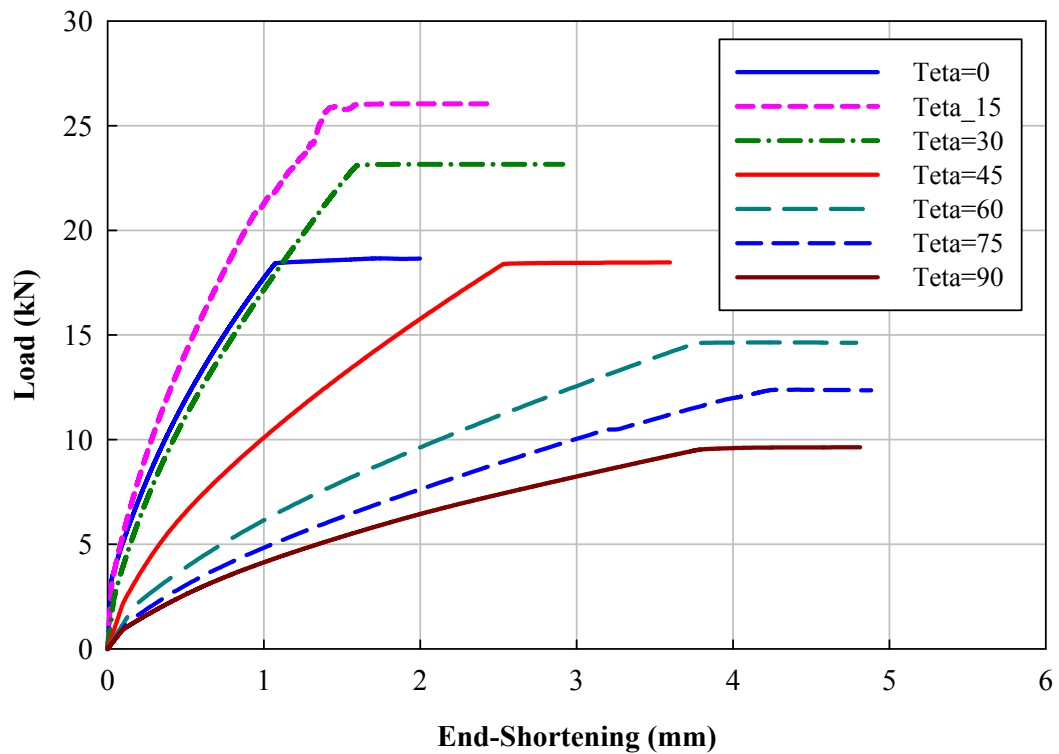


Figure 75. Load versus end-shortening displacements of angle ply $[\theta/-\theta]_{2S}$ UD laminates

Table 12. Buckling and failure loads of angle ply $[\theta/-\theta]_{2S}$ UD laminates

Laminate	Buckling Load [kN]	Failure Load [kN]
[0/-0]_{2S}	3.3	18.7
[15/-15]_{2S}	3.1	26.0
[30/-30]_{2S}	2.4	23.2
[45/-45]_{2S}	2.2	18.5
[60/-60]_{2S}	2.1	14.6
[75/-75]_{2S}	1.3	12.4
[90/-90]_{2S}	0.9	9.6

Figure 76 shows that critical buckling loads of UD laminates decrease with increasing ply angle but this situation is not valid for the post-buckling behaviors and failure characteristics. For instance, $[15/-15]_{4S}$ UD laminate have higher buckling load than $[30/-30]_{4S}$ UD laminate but failure strength of $[30/-30]_{4S}$ is greater than $[15/-15]_{4S}$. Furthermore, the first buckling mode shapes of laminates which are $[60/-60]_{4S}$, $[75/-75]_{4S}$ and $[90/-90]_{4S}$ have two longitudinal half wave the other laminates have one. The differences between mode shapes which have one longitudinal half wave and two longitudinal half waves are shown in Figure 77 and Figure 78.

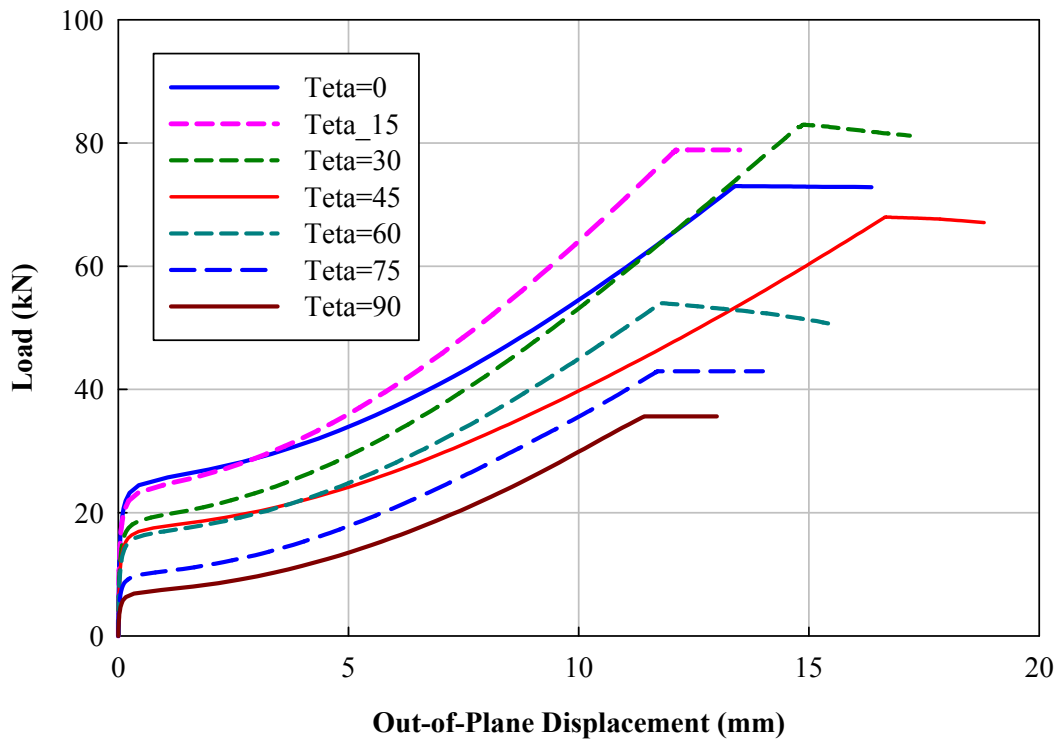


Figure 76. Load versus Out-of-Plane displacements of angle ply $[\theta/-\theta]_{4S}$ UD laminates

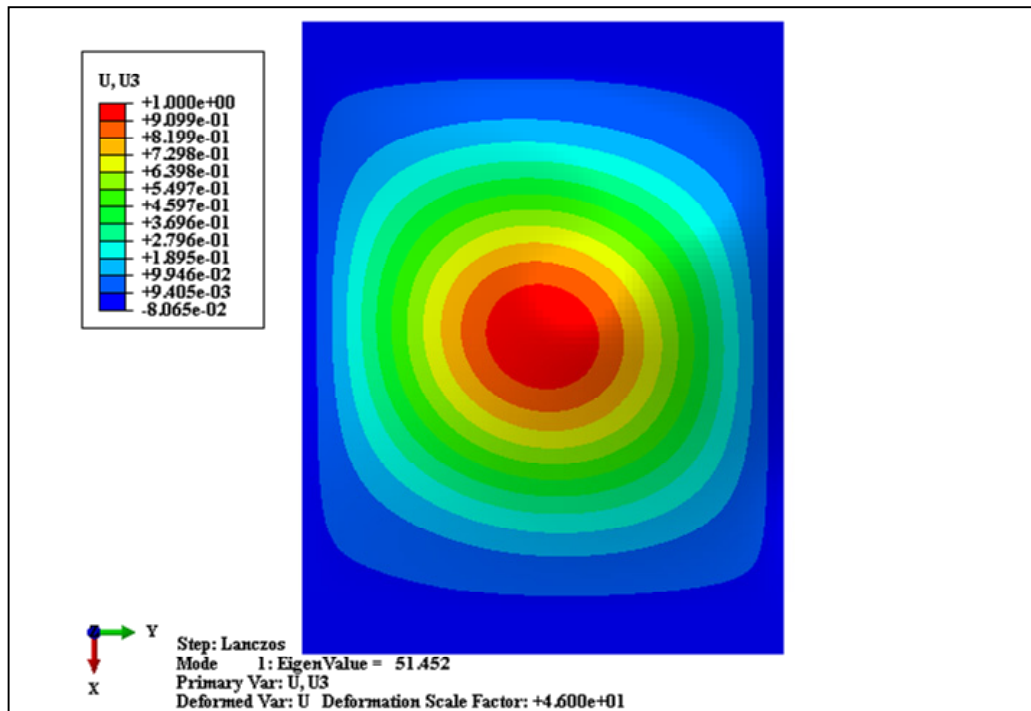


Figure 77. Out-of-plane displacement shape of $[45/-45]_{4s}$ UD laminate

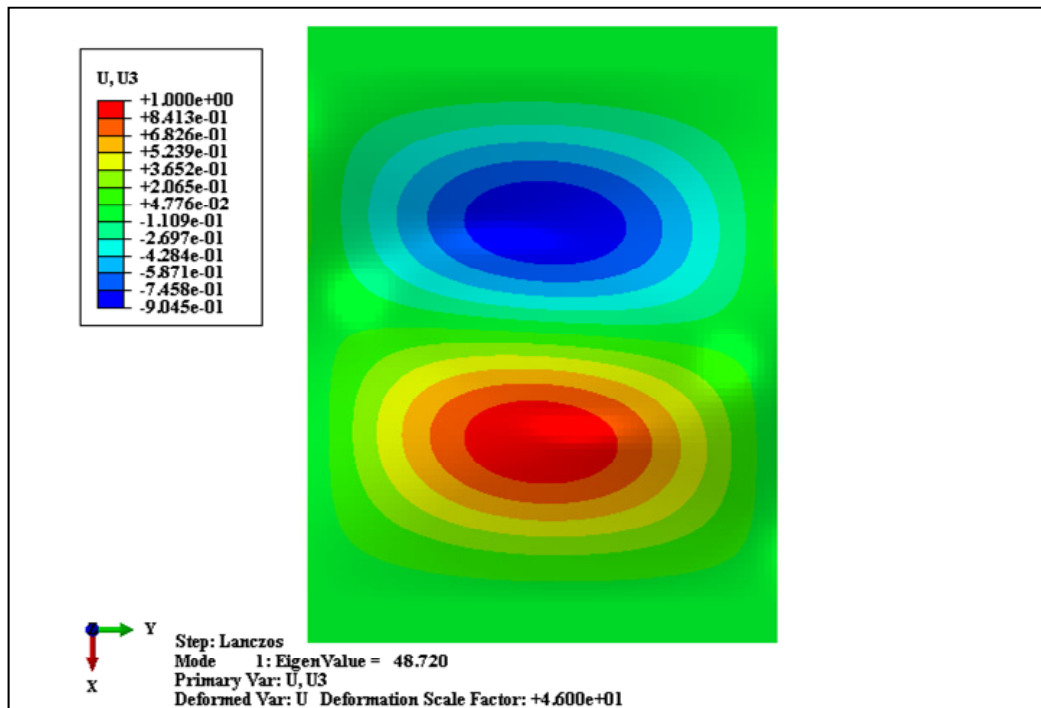


Figure 78. Out-of-plane displacement shape of $[60/-60]_{4s}$ UD Laminate

As shown in Figure 79, mechanical stiffness of $[0/-0]_{4S}$, $[15/-15]_{4S}$, $[30/-30]_{4S}$ are greater than the other laminates in longitudinal direction of plates. The lowest load-carrying capacity is observed for $[90/-90]_{4S}$ UD laminate in longitudinal direction. Table 13 lists the critical buckling loads and failure loads of $[\theta/-\theta]_{4S}$ UD laminates.

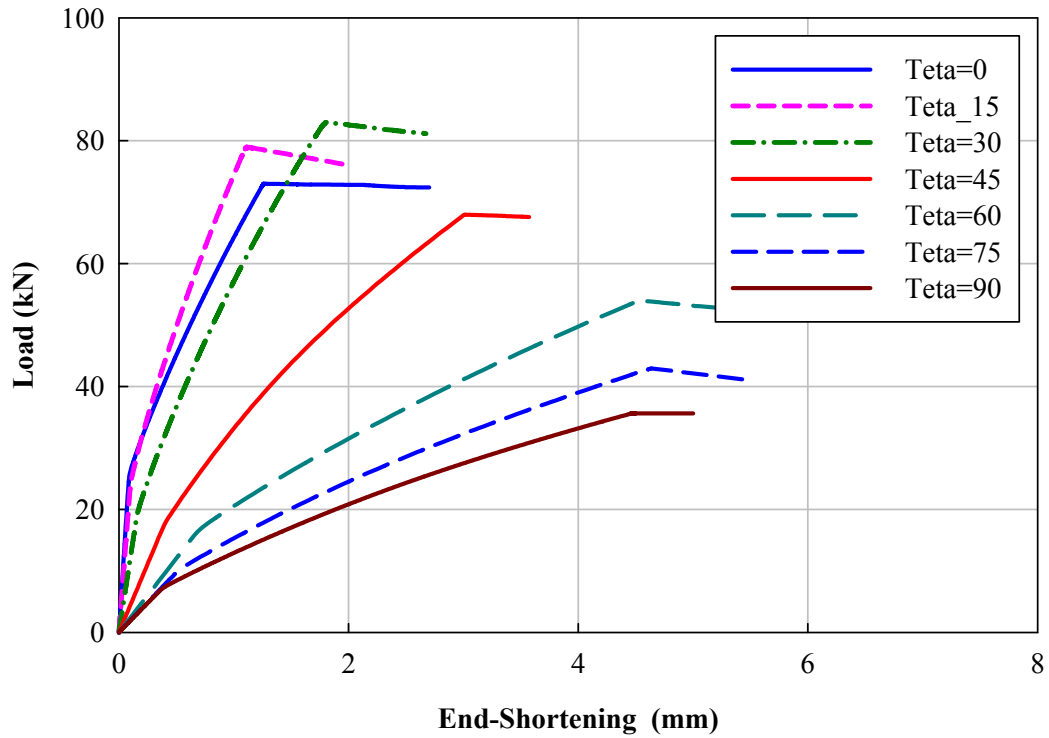


Figure 79. Load versus end-shortening displacements of angle ply $[\theta/-\theta]_{4S}$ UD laminates

Table 13. Buckling and failure loads of angle ply $[\theta/-\theta]_{4S}$ UD laminates and specimens

Laminate / Specimen	Buckling Load [kN]	Failure Load [kN]
[0/-0]_{4S}	26.0	73.0
[15/-15]_{4S}	24.7	78.9
[30/-30]_{4S}	19.7	83.0
[45/-45]_{4S}	18.0	68.0
[60/-60]_{4S}	17.1	54.0
[75/-75]_{4S}	10.4	43.0
[90/-90]_{4S}	7.4	35.6
UD-1(FE Result)	22.2	82.9
UD-1(Experiment)	22.2	84.4

7.3 Effects of Thickness and Ply Angle Variation on Buckling Load and Post-buckling Behavior for Fabric Laminates

Figure 80 shows that angle variation does not affect significantly the critical buckling loads of Fabric laminates and buckling loads increase with increasing laminate thickness. Buckling mode shapes have one longitudinal half wave for each thicknesses and stacking sequences.

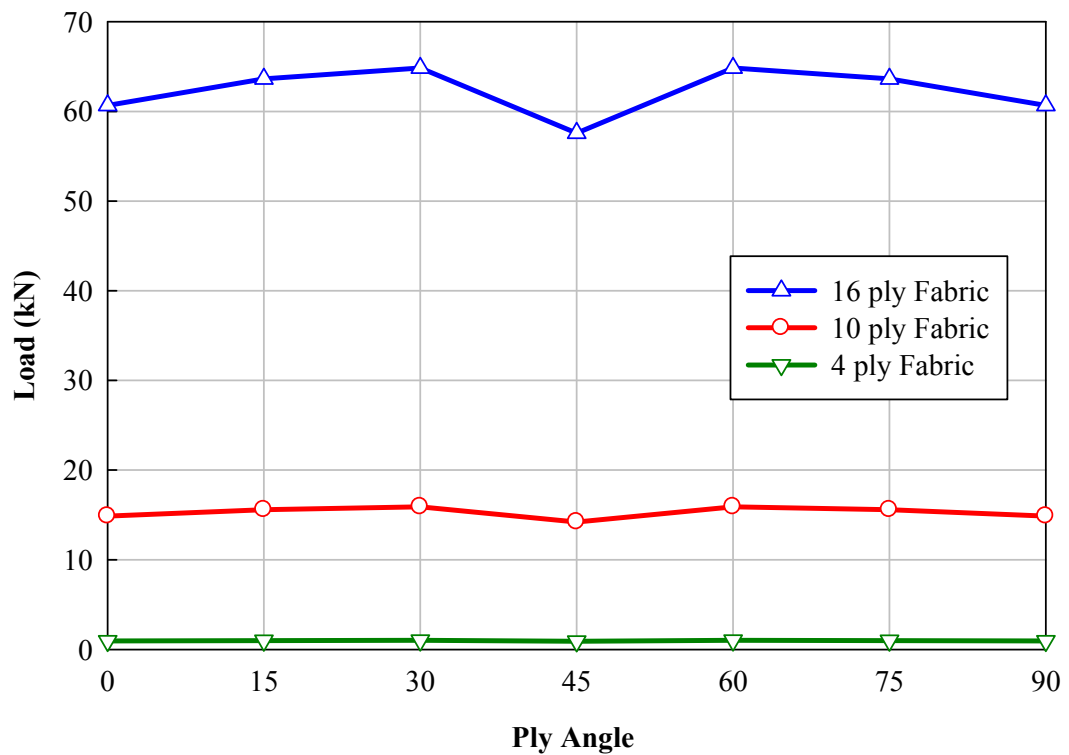


Figure 80. Variation of critical buckling loads of angle ply $[\theta/-\theta]_s$, $[\theta/-\theta/\theta/-\theta/\theta]_s$, $[\theta/-\theta]_{4s}$ Fabric laminates

As shown in Figure 81, angle variation on the stacking sequences does not affect significantly the critical buckling loads of Fabric laminates. Post-buckling behavior and failure load of $[45/-45]_s$ laminate is lower than the other laminates. On the other hand, the $[0/-0]_s$ laminate was observed to buckle in one half wave at the loading 0.95 kN and a mode-jump to two half-waves occurred at the loading 4.7 kN.

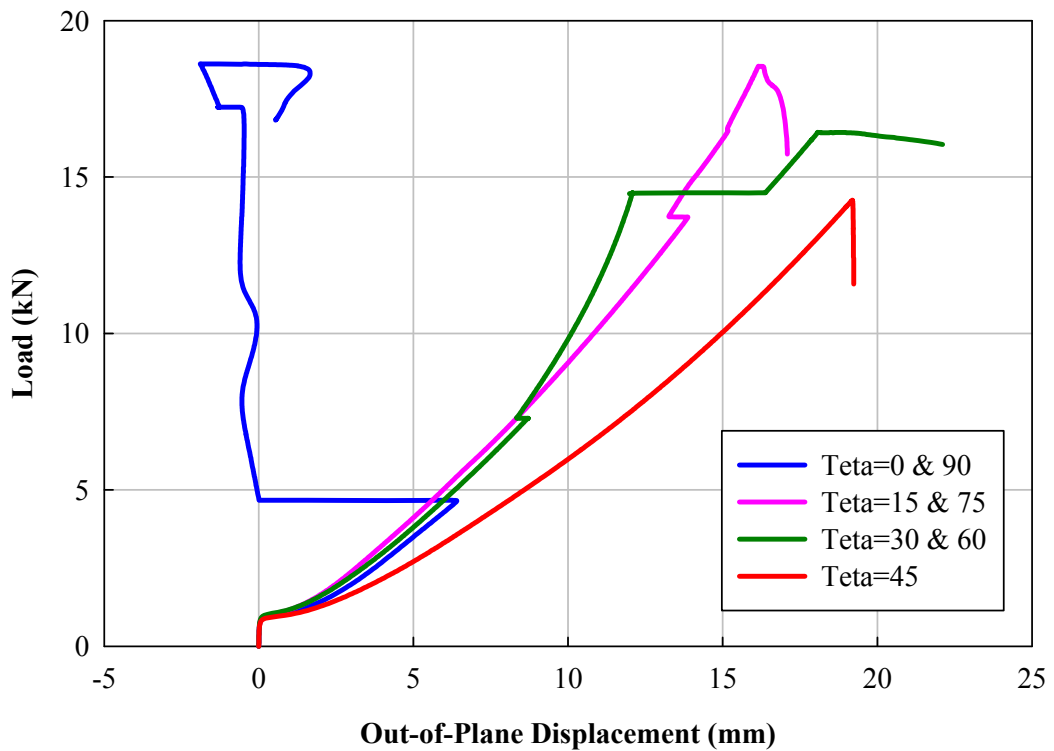


Figure 81. Load versus out-of-plane displacements of angle ply $[\theta/-\theta]_s$ Fabric laminates

Mechanical stiffness of $[45/-45]_S$ laminate is lower than the other laminates in longitudinal direction of plates (Figure 82). Mode-jump from one to two half-waves in $[0/-0]_S$ laminate is observed. Table 14 lists the critical buckling loads and failure loads of $[\theta/-\theta]_S$ Fabric laminates.

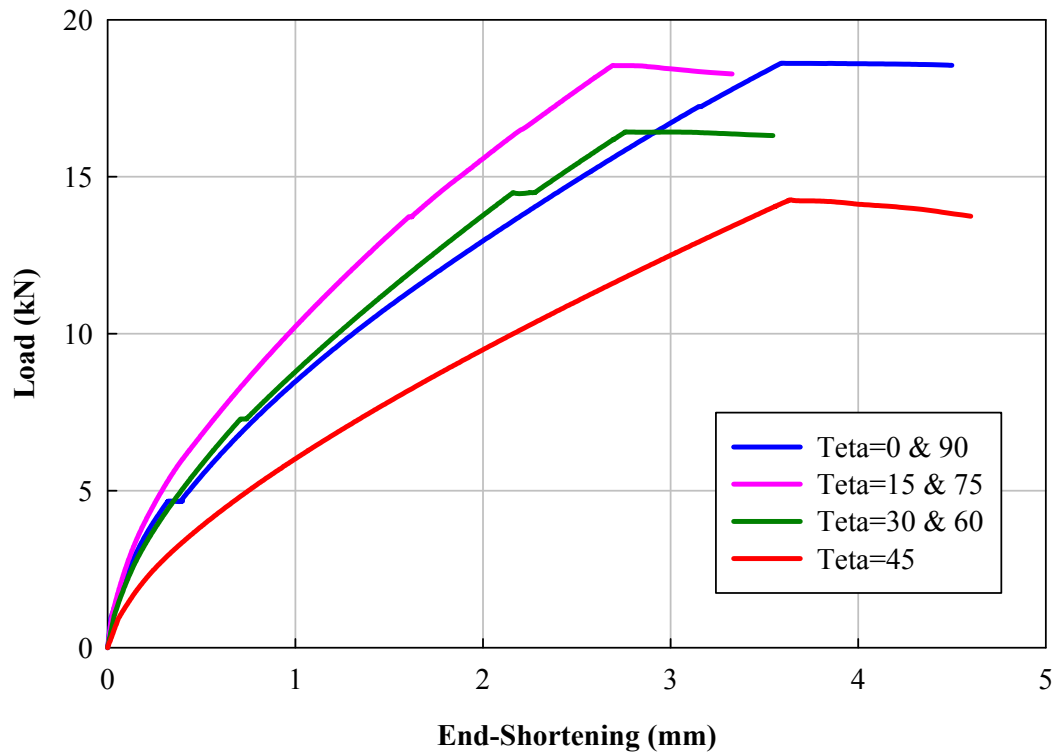


Figure 82. Load versus end-shortening displacements of angle ply $[\theta/-\theta]_S$ Fabric laminates

Table 14. Buckling and failure loads of angle ply $[\theta/-\theta]_s$ Fabric laminates

Laminate	Buckling Load [kN]	Failure Load [kN]
$[0/-0]_s$	0.95	18.6
$[15/-15]_s$	1.00	18.5
$[30/-30]_s$	1.02	16.4
$[45/-45]_s$	0.92	14.3
$[60/-60]_s$	1.02	16.4
$[75/-75]_s$	1.00	18.5
$[90/-90]_s$	0.95	18.6

Angle variation on the stacking sequences does not affect significantly the critical buckling loads of Fabric laminates (Figure 83). Post-buckling behavior and failure load of $[45/-45/45/-45/45]_S$ laminate is lower than the other laminates. As shown in Figure 84 and Figure 85, the first buckling mode shapes of all Fabric laminates have one longitudinal half wave pattern. On the other hand, the $[0/-0/0/-0/0]_S$ laminate was observed to buckle in one half wave at the loading 15 kN and a mode-jump to two half-waves occurred at the loading 65 kN.

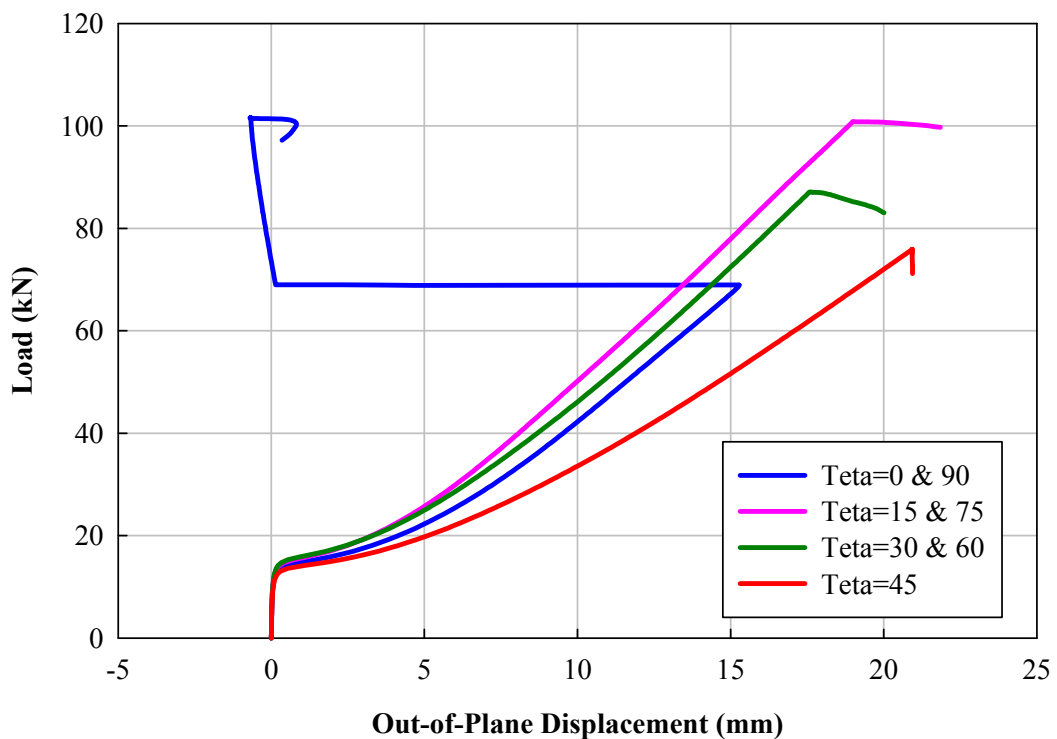


Figure 83. Load versus out-of-plane displacements of angle ply $[0/-\theta/\theta/-\theta/\theta]_S$ Fabric laminates

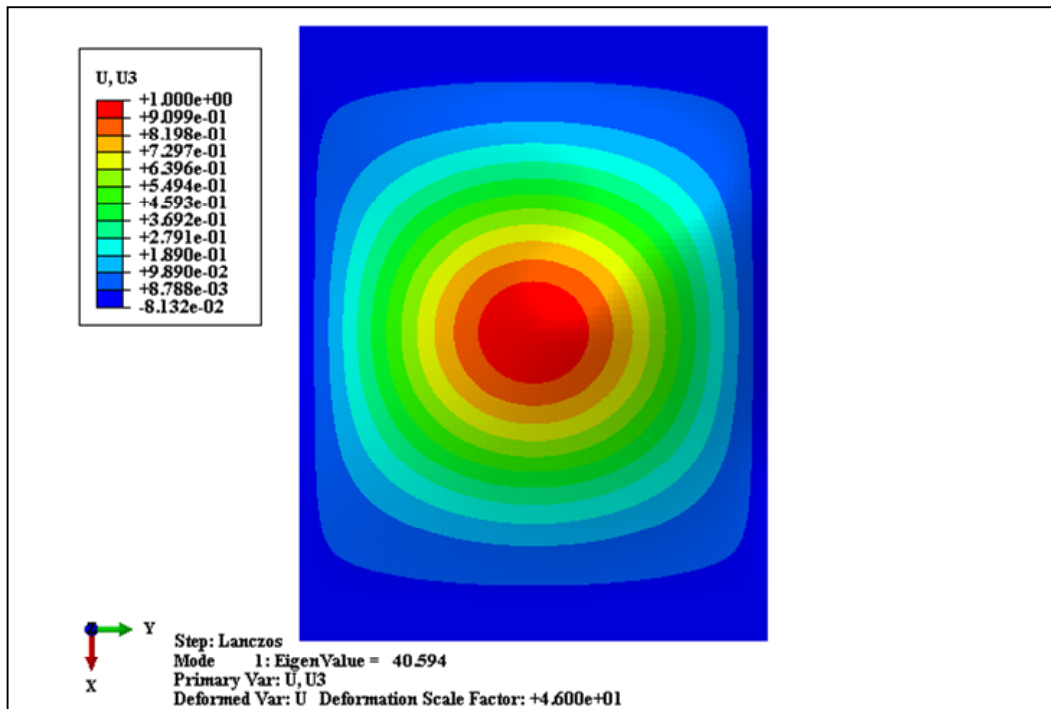


Figure 84. Out-of-plane displacement shape of $[45/-45/45/-45/45]_s$ Fabric laminate

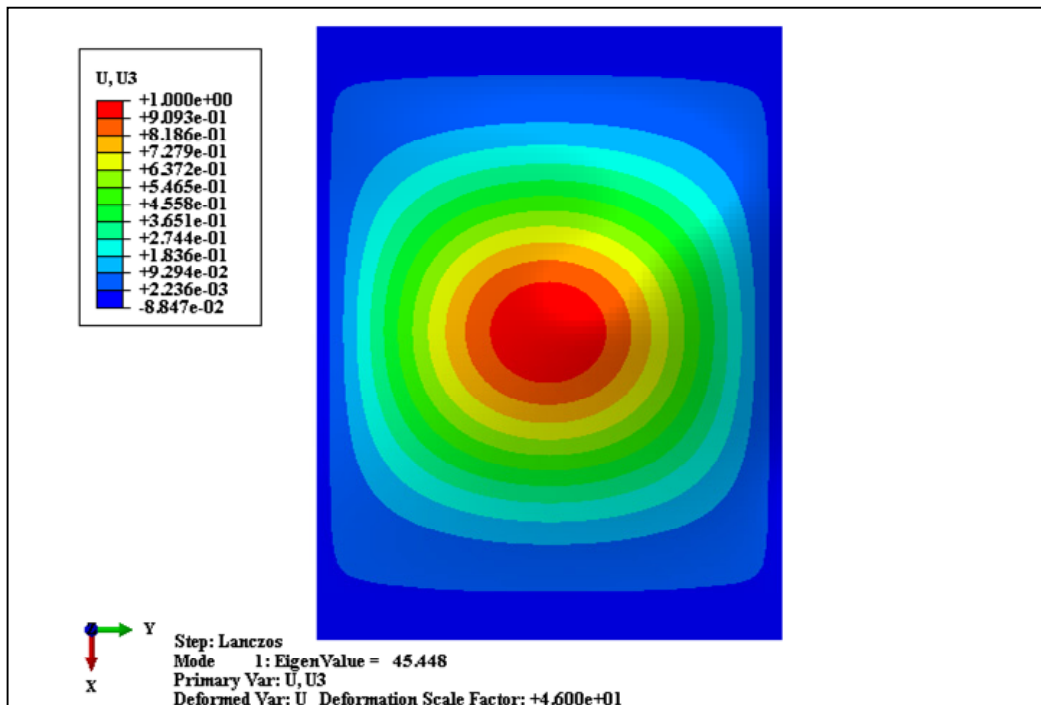


Figure 85. Out-of-plane displacement shape of $[60/-60/60/-60/60]_s$ Fabric laminate

As shown in Figure 86, mechanical stiffness of $[45/-45/45/-45/45]_S$ laminate is lower than the other laminates in longitudinal direction of plates. Mode-jump from one to two half-waves in $[0/-0/0/-0/0]_S$ laminate is observed. Table 15 lists the critical buckling loads and failure loads of $[\theta/-\theta/\theta/-\theta/\theta]_S$ Fabric laminates.

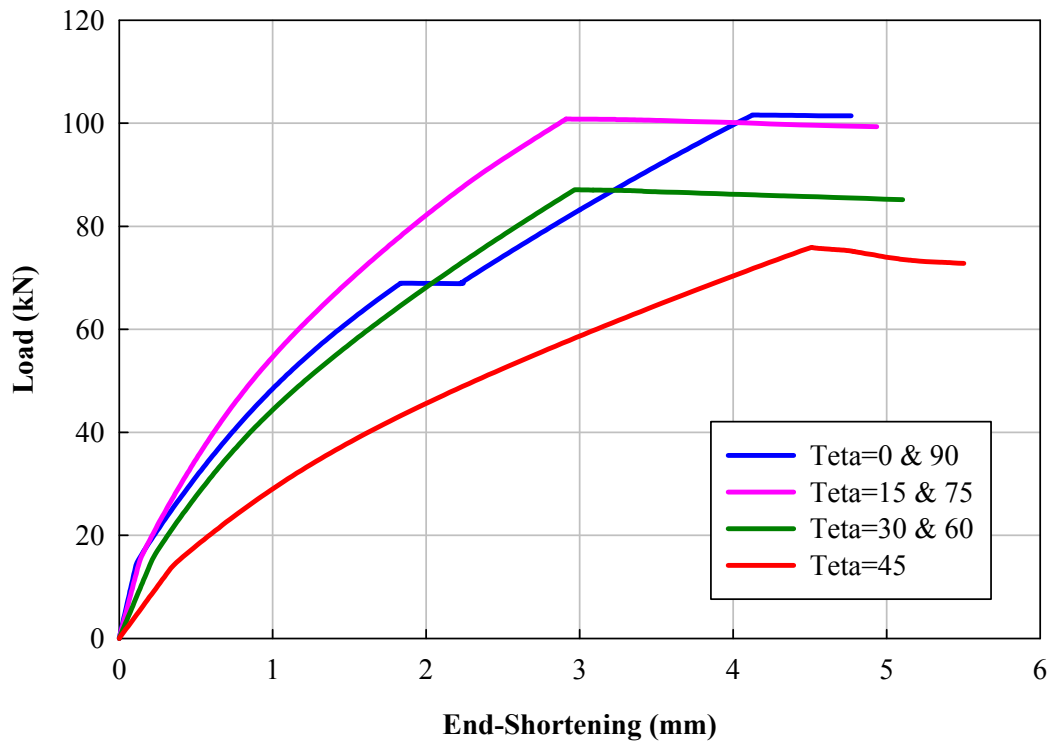


Figure 86. Load versus end-shortening displacements of angle ply $[\theta/-\theta/\theta/-\theta/\theta]_S$ Fabric laminates

Table 15. Buckling and failure loads of angle ply $[\theta/-\theta/\theta/-\theta/\theta]_s$ Fabric laminates and specimens

Laminate / Specimen	Buckling Load [kN]	Failure Load [kN]
$[0/-0/0/-0/0]_s$	14.9	101.6
$[15/-15/15/-15/15]_s$	15.6	100.8
$[30/-30/30/-30/30]_s$	15.9	87.1
$[45/-45/45/-45/45]_s$	14.2	75.9
$[60/-60/60/-60/60]_s$	15.9	87.1
$[75/-75/75/-75/75]_s$	15.6	99.3
$[90/-90/90/-90/90]_s$	14.9	99.5
FABRIC-1(FE Result)	16.3	91.8
FABRIC-1(Experiment)	16.3	77.8

Figure 87 shows that angle variation on the stacking sequences does not affect significantly the critical buckling loads of Fabric laminates. Post-buckling behavior and failure load of $[45/-45]_{4S}$ laminate is lower than the other laminates. First buckling mode shapes of all Fabric laminates have one longitudinal half wave pattern. Mode jump is not observed in any stacking sequence of 16 plied fabric laminates.

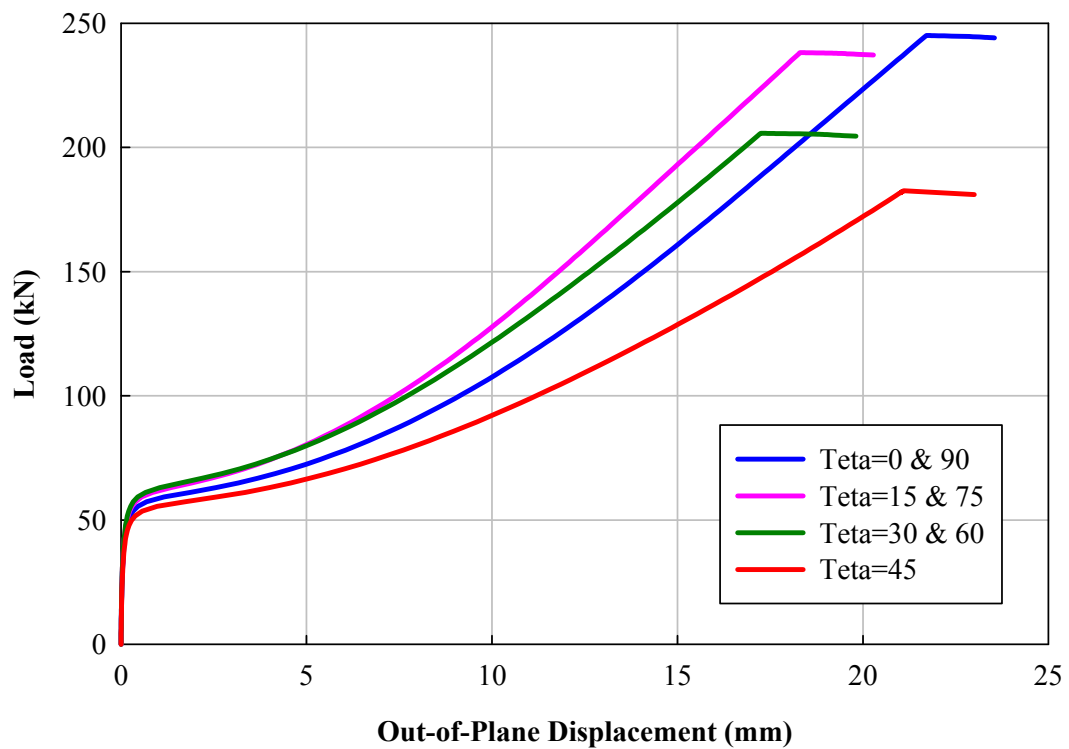


Figure 87. Load versus out-of-plane displacements of angle ply $[\theta/-\theta]_{4S}$ Fabric laminates

Mechanical stiffness of $[45/-45]_{4S}$ laminate is lower than the other laminates in longitudinal direction of plates (Figure 88). Table 16 lists the critical buckling loads and failure loads of $[\theta/-\theta]_{4S}$ Fabric laminates.

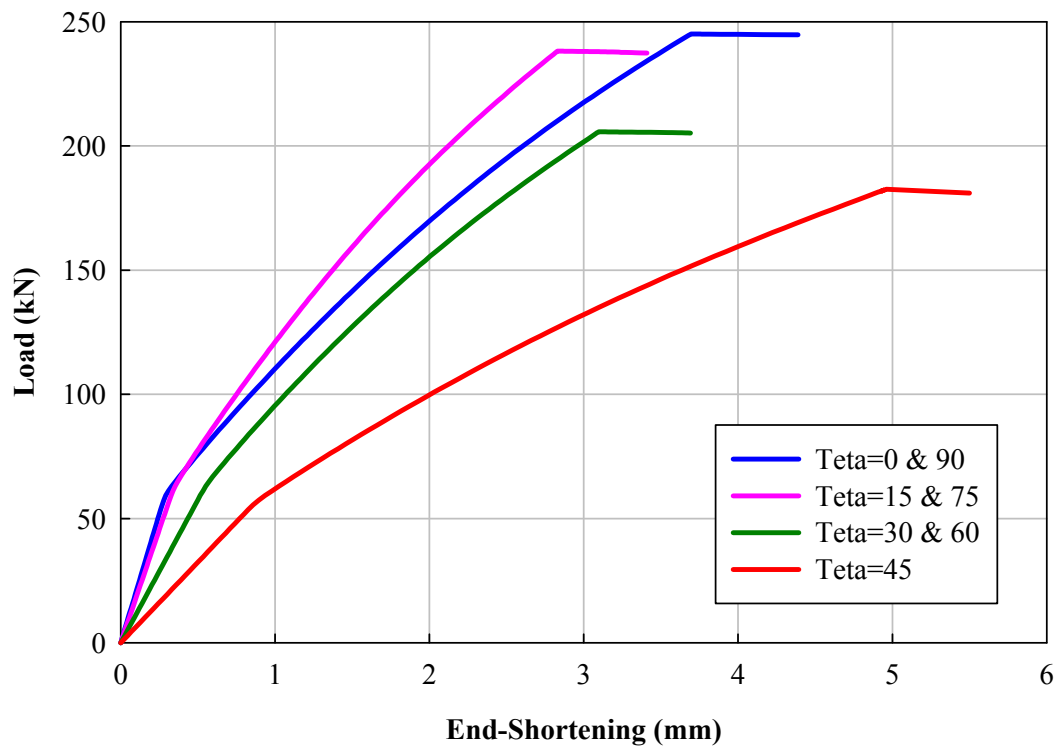


Figure 88. Load versus end-shortening displacements of angle ply $[\theta/-\theta]_{4S}$ Fabric laminates

Table 16. Buckling and failure loads of angle ply $[\theta/-\theta]_{4S}$ Fabric laminates

Laminate	Buckling Load [kN]	Failure Load [kN]
$[0/-0]_{4S}$	60.7	245.1
$[15/-15]_{4S}$	63.6	238.2
$[30/-30]_{4S}$	64.8	205.7
$[45/-45]_{4S}$	57.6	182.6
$[60/-60]_{4S}$	64.8	205.7
$[75/-75]_{4S}$	63.6	238.2
$[90/-90]_{4S}$	60.7	245.1

7.4 Comparisons of Critical Buckling Loads

In this section, the critical buckling loads of laminate examples which have similar stacking sequences are compared with each other. As shown in Figure 89-Figure 91, the critical buckling loads of Fabric laminates are exceedingly greater than the UD laminates. The critical buckling loads of UD laminates decrease with increasing ply angle. However, angle variation does not affect the critical buckling loads of Fabric laminates.

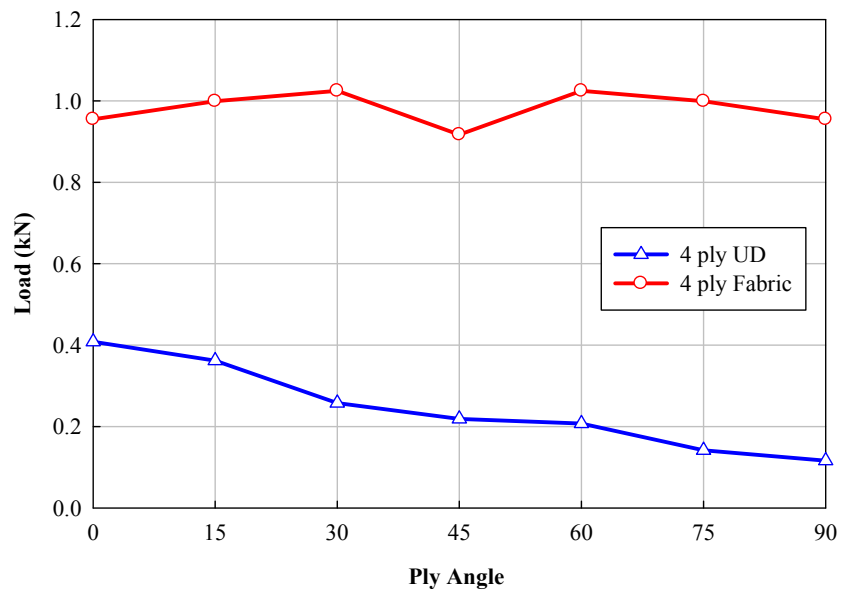


Figure 89. Variation of critical buckling loads of angle ply $[\theta/-\theta]_S$ UD laminates and $[\theta/-\theta]_S$ Fabric laminates

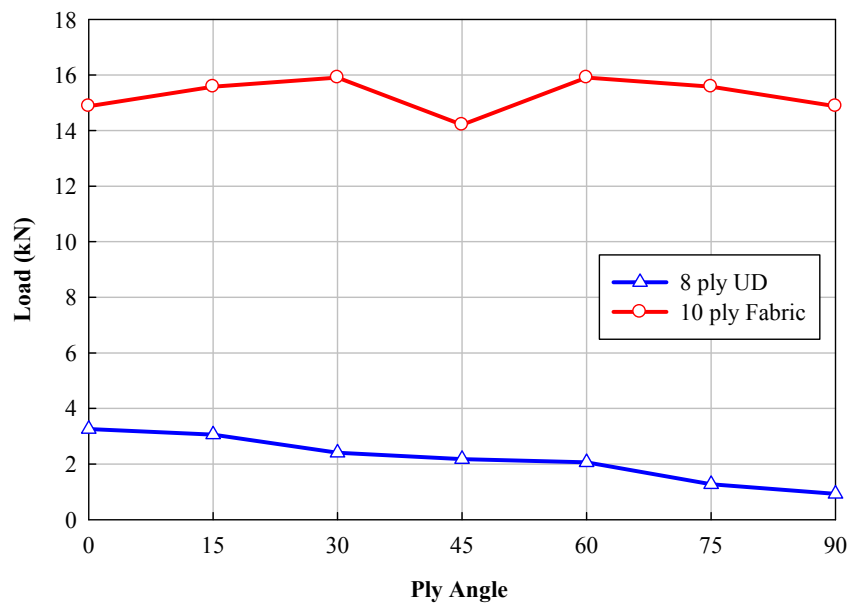


Figure 90. Variation of critical buckling loads of angle ply $[\theta/-\theta]_{2S}$ UD laminates and $[\theta/-\theta/\theta/-\theta/\theta]_S$ Fabric laminates

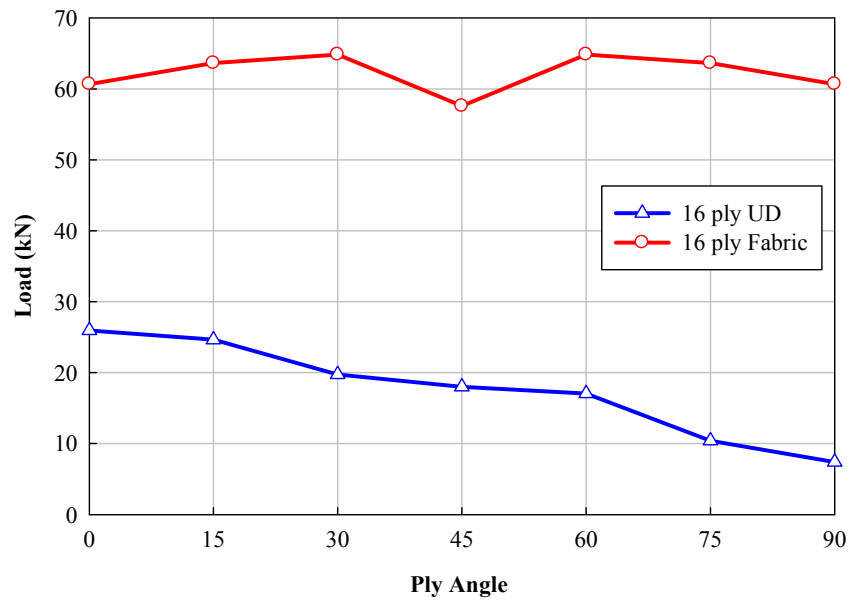


Figure 91. Variation of critical buckling loads of angle ply $[\theta/-\theta]_{4S}$ UD laminates and $[\theta/-\theta]_{4S}$ Fabric laminates

CHAPTER 8

CONCLUSIONS

This study presents numerical analyses of buckling, post-buckling and damage of composite laminated plates built with different carbon-epoxy laminates and stacking sequences. Three types of methods; eigen value extraction, non-linear Riks, Newton-Raphson are used in the finite element analyses. The numerical analyses are validated by experimental results. The following conclusions have been acquired by the current study:

1. Analyses showed that the buckling loads obtained eigenvalue extraction, non-linear Riks, Newton-Raphson methods are in good agreement with each other.
2. Results show that increasing imperfection amplitude does not affect the post-buckling behavior of the plates. However, imperfection amplitude varies the location of bifurcation point.
3. The buckling behavior of plates which were determined experimentally are similar with the FE results that were obtained by using %5 initial geometric imperfection amplitude. This can be attributed to assembly tolerance, quality of test mechanism, geometric perfectness of fixture and specimens, co-linearity between load actuator and specimens, manufacturing defects on the specimens (initial delaminations, curing problems, etc.).
4. The critical buckling loads obtained from numerical analyses are similar with the experimental results. However, UD-2 buckled earlier than the load level which was obtained from finite element analysis. On the other hand, first specimens of each UD and Fabric plate buckled at loads which were greater than the FE analyses but critical buckling load of second specimens were lower. This can be

attributed to disruptions on the test fixture due to high loading in the first experiments.

5. Experimental results obtained for UD and Fabric specimens were compared with the ones obtained numerically. Comparisons showed that there are good agreements between out-of-plane displacements. Post-buckling behaviors of specimens were identical with the numerical analyses except UD-2. However, out-of-plane displacements of specimens were greater than the analyses after a particular load level.
6. The end shortening of UD specimens have less accuracy as compared to out-of-plane deflections due to shifting of test mechanism. On the other hand, load versus end-shortening displacement results of fabric specimens agreed well with the experimental data.
7. The first damage initiation was observed at the outer layers of specimens in the analyses since buckling created higher bending strains and stresses on the outer layers as compared to inner ones. In the numerical analyses of UD and fabric plates, matrix compression failure was observed firstly. Then matrix tension and fiber compression occurred in the models.
8. In the experiments, the damage initiation is first observed at the upper end of the knife edges and then propagated towards to center of specimens. In the analyses, failure started at the region close to the upper end of the knife and propagated towards center of plate and upper end of the knife edges. However, failure locations of experiments and FE analyses are found close to each other. In the experiments, after the damage initiation, a sudden decrease was observed on the stiffness of specimens.
9. Failure load levels of UD specimens showed good agreement with the numerical analyses but Fabric specimens failed at load levels which were 15%-22% lower than analyses. As seen in the out of plane deflections, the displacement

increasing rate is more than the analyses. This means that the test fixture started to deform together with specimens after a particular load level. Therefore, stress concentrations occurred on the corner of knife edges and specimens failed at a lower load level. On the other hand, the mechanical strengths of fabrics may be lower than values which are used in the numerical analyses due to manufacturing defects.

10. Damage initiation occurred at a load which is 3.8 times higher than critical buckling load for UD-1 specimen and 4.8 times higher than critical buckling load of FABRIC-1 specimen. Although UD has higher buckling load fabrics have higher ratios.
11. Numerical results showed that angle variation did not affect the critical buckling load values of Fabric laminates significantly for all thicknesses; however the critical buckling loads of UD laminates decreased considerably with increasing ply angle.
12. Different buckling mode shapes were obtained from 60, 75 and 90 degree oriented UD laminates in the linear Eigen value analyses.
13. Maximum post buckling stiffness of UD laminates is observed for $[15/-15]_{4S}$ plates. The stiffness decreased with increasing ply angle giving then minimum stiffness for 90 degree oriented laminates. Mode-jumps are observed in the load-deformation behaviors of $[45/-45]_S$ and $[75/-75]_{2S}$ laminates.
14. Post buckling stiffness of fabric laminates decreased with increasing ply angle. Furthermore, mode-jumps are observed in the load-deformation behavior of 0 degree oriented laminates with four and eight plies. On the other hand, critical buckling loads of fabric specimens are greater than the numerical examples.
15. Failure loads of fabric specimens are lower than the several of numerical examples of fabric laminates. On the other hand, buckling and failure loads of

UD specimens which were validated with the experiments are greater than the buckling and failure loads of numerical examples of UD laminates except buckling loads of $[0/-0]_{4S}$ and $[15/-15]_{4S}$ laminates.

16. Stiffness of UD and Fabric laminates increase exponentially with increasing laminate thickness.
17. Mode-jump is observed for the laminates which have small thicknesses as compared to laminates with 16 plies for both of UD and Fabric.

REFERENCES

- [1] M. C. Y. Niu, *Composite Airframe Structures: Practical Design Information and Data*, Conmilit Press, 1992.
- [2] L. Tong, A. Mouritz and M. Bannister, *3D Fibre Reinforced Polymer Composites*, Elsevier, 2002.
- [3] B. G. Falzon and D. Hitchings, *An Introduction to Modelling Buckling and Collapse*, NAFEMS, 2006.
- [4] S. Singh and A. Kumar, "Postbuckling Response and Failure of Symmetric Laminates Under In-plane Shear," *Composites Science and Technology*, vol. 58, pp. 1949-1960, 1998.
- [5] C. W. Kong, I. C. Lee, C. G. Kim and C. S. Hong, "Postbuckling and Failure of Stiffened Composite Panels Under Axial Compression," *Composite Structures*, vol. 42, pp. 13-21, 1998.
- [6] B. G. Falzon, K. A. Stevens and G. O. Davies, "Postbuckling Behaviour of A Blade-stiffened Composite Panel Loaded in Uniaxial Compression," *Composites*, vol. 31, pp. 459-468, 2000.
- [7] A. K. Soh, L. C. Bian and J. Chakrabarty, "Elastic/plastic Buckling of A Composite Flat Plate Subjected to Uniform Edge Compression," *Thin-Walled Structures*, vol. 38, pp. 247-265, 2000.
- [8] C. Bisagni, "Numerical Analysis and Experimental Correlation of Composite Shell Buckling and Post-buckling," *Composites*, vol. 31, pp. 655-667, 2000.
- [9] J. Loughlan, "The Influence of Mechanical Couplings on the Compressive Stability of Anti-symmetric Angle-ply Laminates," *Composite Structures*, vol. 57, pp. 473-482, 2002.
- [10] F. Caputo, R. Esposito, P. Perugini and D. Santoro, "Numerical-experimental Investigation on Post-buckled Stiffened Composite Panels," *Composite Structures*, vol. 55, pp. 347-357, 2002.

- [11] C. Bisagni and P. Cordisco, "An Experimental Investigation into the Buckling and Post-buckling of CFRP Shells under Combined Axial and Torsion Loading," *Composite Structures*, vol. 60, pp. 391-402, 2003.
- [12] D. Xie and S. B. Biggers Jr., "Postbuckling Analysis with Progressive Damage Modeling in Tailored Laminated Plates and Shells with A Cutout," *Composite Structures*, vol. 59, pp. 199-216, 2003.
- [13] P. P. Camanho, C. G. Davila and M. F. De Moura, "Numerical Simulation of Mixed-mode Progressive Delamination in Composite Materials," *Journal of Composite Materials*, vol. 37, pp. 1415-1437, 2003.
- [14] B. G. Falzon and D. Hitchings, "Capturing Mode-switching in Postbuckling Composite Panels using A Modified Explicit Procedure," *Composite Structures*, vol. 60, pp. 447-453, 2003.
- [15] M. W. Hilburger and J. H. Starnes Jr., "Effects of Imperfections of the Buckling Response of Composite Shells," *Thin-Walled Structures*, vol. 42, p. 2004, 369-397.
- [16] C. A. Featherston and A. Watson, "Buckling of Optimised Flat Composite Plates under Shear and In-plane Bending," *Composites Science and Technology*, vol. 65, pp. 839-853, 2005.
- [17] C. G. Diaconu and P. M. Weaver, "Postbuckling of Long Unsymmetrically Laminated Composite Plates under Axial Compression," *International Journal of Solids and Structures*, vol. 43, pp. 6978-6997, 2006.
- [18] B. G. Falzon and M. Cerini, "An Automated Hybrid Procedure for Capturing Mode-jumping in Postbuckling Composite Stiffened Structures," *Composite Structures*, vol. 73, pp. 186-195, 2006.
- [19] E. Gal, R. Levy, H. Abramovich and P. Pavsner, "Buckling Analysis of Composite Panels," *Composite Structures*, vol. 73, pp. 179-185, 2006.
- [20] F. Laurin, N. Carrere and J.-F. Maire, "Laminated Composite Structures Subjected to Compressive Loading: A Material and Structural Buckling Analysis," *Composite Structures*, vol. 80, pp. 172-182, 2007.
- [21] C. S. Lopes, P. P. Camanho, Z. Gürdal and B. F. Tatting, "Progressive Failure

- Analysis of Tow-placed, Variable-stiffness Composite Panels," *International Journal of Solids and Structures*, vol. 44, pp. 8493-8516, 2007.
- [22] P. P. Camanho, P. Maimi and C. G. Davila, "Prediction of Size Effects in Notched Laminates using Continuum Damage Mechanics," *Composites Science and Technology*, vol. 67, pp. 2715-2727, 2007.
- [23] P. Pevzner, H. Abramovich and T. Weller, "Calculation of the Collapse Load of An Axially Compressed Laminated Composite Stringer-stiffened Curved Panel—An Engineering Approach," *Composite Structures*, vol. 83, pp. 341-353, 2008.
- [24] C. Kassapoglou, "Composite Plates with Two Concentric Layups under Compression," *Composites*, vol. 39, pp. 104-112, 2008.
- [25] P. Kere and M. Lyly, "On Post-buckling Analysis and Experimental Correlation of Cylindrical Composite Shells with Reissner–Mindlin–Von Karman Type Facet Model," *Computers and Structures*, vol. 86, pp. 1006-1013, 2008.
- [26] S. Basu, A. M. Waas and D. R. Ambur, "Prediction of Progressive Failure in Multidirectional Composite Laminated Panels," *International Journal of Solids and Structures*, vol. 44, pp. 2648-2676, 2007.
- [27] C. Bisagni and C. Walters, "Experimental Investigation of the Damage Propagation in Composite Specimens under Biaxial Loading," *Composite Structures*, vol. 85, pp. 293-310, 2008.
- [28] P. F. Liu and J. Y. Zheng, "Progressive Failure Analysis of Carbon Fiber/epoxy Composite Laminates using Continuum Damage Mechanics," *Materials Science and Engineering*, vol. 485, pp. 711-717, 2008.
- [29] E. J. Pineda, A. M. Waas, B. A. Bednarczyk, C. S. Collier and P. W. Yarrington, "Progressive Damage and Failure Modeling in Notched Laminated Fiber Reinforced Composites," *Int J Fract*, vol. 158, pp. 125-143, 2009.
- [30] F. P. Van Der Meer and L. J. Sluys, "Continuum Models for the Analysis of Progressive Failure in Composite Laminates," *Journal of Composite Materials*, vol. 43, pp. 2131-2156, 2009.
- [31] W. Wagner and C. Balzani, "Prediction of the Postbuckling Response of Composite Airframe Panels Including Ply Failure," *Engineering Fracture*

- Mechanics*, vol. 77, pp. 3648-3657, 2010.
- [32] R. Vescovini and C. Bisagni, "Single-mode Solution for Post-buckling Analysis of Composite Panels with Elastic Restraints Loaded in Compression," *Composites: Part B*, 2011.
- [33] M. Romanowicz, "A Numerical Approach for Predicting the Failure Locus of Fiber Reinforced Composites under Combined Transverse Compression and Axial Tension," *Computational Materials Science*, vol. 51, pp. 7-12, 2012.
- [34] R. M. Jones, *Mechanics of Composite Materials*, Taylor & Francis, 1998.
- [35] J. N. Reddy, *Mechanics of Composite Laminated Plates and Shells*, CRC Press, 2004.
- [36] *Abaqus Analysis User's Manual Version 6.10*, SIMULIA, 2010.
- [37] Z. Hashin, "Failure Criteria for Unidirectional Composites," *Journal of Applied Mechanics*, vol. 47, pp. 329-334, 1980.
- [38] A. Matzenmiller, J. Lubliner and R. L. Taylor, "A Constitutive Model for Anisotropic Damage in Fiber-composites," *Mechanics of Materials*, vol. 20, pp. 125-152, 1995.
- [39] D. W. Sleight, "Progressive Failure Analysis Methodology for Laminated Composite Structures," *NASA/TP-1999-209107*, pp. 1-67, 1999.
- [40] "Composite Materials," in *MIL-HDBK-17*, US Department of Defense, 1990.
- [41] "Statistical Methods," in *MIL-HDBK-17-1F*, US Department of Defense, 1990.
- [42] *Abaqus Theory Manual*, SIMULIA, 2010.